An investigation into the anti-tumour properties of resveratrol against ovarian cancer using the CAM model

Melanie Gabrielle Singh

Master of Science in Biochemistry

School of Biological Sciences

University of Canterbury

2019

Table of Contents

List of figures

Acknowledgments

I would like to express my gratitude for my supervisors Ashley Garrill, Kenny Chitcholtan, and Peter Sykes, for their guidance and support throughout this project.

I am also incredibly grateful to my peers in the lab, especially Alex Tino, for teaching me lab techniques, helping me when I needed it, and providing a comfortable and enjoyable working environment.

Finally, I would not have been able to complete this project without the help and support of my family. I would like to thank my mum, for helping me proofread everything; my dad, for helping me with all the maths; and my sister, Angela, for emotional support and guidance.

Abstract

Ovarian cancer is one of the deadliest gynaecological cancers. A key contributing factor to its high mortality rate is its non-specific symptoms and lack of early detection, which results in most patients being diagnosed with advanced stage cancer. Ovarian cancer is highly metastatic, with a unique route of dissemination that is facilitated by the movement of cancer cells through ascitic fluid, which accumulates in the peritoneal cavities of patients with advanced ovarian cancer. Cancer cells can then adhere to the peritoneum, or the surfaces of other organs, and form tumour nodules. This mode of metastasis is poorly understood, and therefore warrants further investigation.

Acquired resistance to currently available anticancer compounds is a common feature of advanced ovarian cancer, making the need for the development of alternative treatment options urgent. Resveratrol is a naturally-occurring food compound that has been shown to have some anti-cancer properties, including inhibition of angiogenesis, proliferation, and invasion, as well as induction of apoptosis. This study investigated the effects of resveratrol on several cellular processes known to contribute to cancer growth and survival using ovarian cancer tumour implants grown on chicken chorioallantoic membranes (CAMs) to mimic the growth of tumour nodules on the surface of the peritoneum during the early stages of metastasis.

This study demonstrated that using the CAM model as a proxy for the peritoneum is an appropriate model for investigation into the early stages of metastasis in the context of advanced ovarian cancer. Results also showed that treatment with 91 μg resveratrol inhibited invasion of OVCAR-8 and SKOV-3 cells into the CAM. This dose of resveratrol also led to a reduction in the number of red blood cells in SKOV-3 tumour implants, whereas 46 μg was sufficient to have a similar effect in OVCAR-8 tumour implants. Resveratrol may therefore be capable of slowing the progression of advanced ovarian cancer and warrants further *in vivo* study.

Abbreviations

AEC	3-Amino-9-ethyl-carbazole
AIF	Apoptosis-inducing factor
Akt	Protein kinase B
BSA	Bovine serum albumin
CAD	Caspase-activated DNase
CAM	Chorioallantoic membrane
CD31	Cluster of differentiation 31
	(see also: PECAM-1)
Cdk	Cyclin-dependent kinase
CKI	Cdk inhibitor
DAB	3,3'-Diaminobenzidine
DISC	Death-inducing signalling complex
ECM	Extracellular matrix
EDTA	Ethylenediaminetetraacetic acid
EMT	Epithelial-mesenchymal transition
Erk	Extracellular signal-regulated kinase
Fas	Apoptosis antigen 1
	(also called: CD95)
FasL	Fas ligand
FADD	Fas-associated protein with death domain
FBS	Foetal bovine serum
FGF	Fibroblast growth factor
HRP	Horseradish peroxidase
HtrA2/Omi	High temperature requiring protein A serine peptidase 2
IL	Interleukin
Ki67	Proliferation marker encoded by *MKI67* gene
OCT	Optimal cutting temperature [compound]
MEM	Modified Eagle medium
MMP	Matrix metalloproteinase
pI	Isoelectric point

PBS	Phosphate-buffered saline
PDGF	Platelet-derived growth factor
PECAM-1	Platelet endothelial cell adhesion molecule (see also: CD31)
PI3K	Phosphoinositide 3-kinase
Resveratrol	*Trans*-resveratrol
Rho	A GTPase (binds to ROCK)
ROCK	Rho-associated protein kinase
rpm	Revolutions per minute
SEM	Standard error of the mean
Smac/DIABLO	Second mitochondria-derived activator of caspase/direct inhibitor of apoptosis binding protein with low pI
TBS	Tris-buffered saline
TdT	Terminal deoxynucleotidyl transferase
TGF	Transforming growth factor
TNF	Tumour necrosis factor
TNFR	TNF receptor
TP53	Tumour protein p53
TRADD	TNFR with associated death domain
TUNEL	TdT dUTP nick-end labelling
VEGF	Vascular endothelial growth factor

Cancer cell lines mentioned

A2780	Human ovarian endometrioid adenocarcinoma
A498	Human renal cell carcinoma
A549	Human lung adenocarcinoma
ACHN	Human papillary renal cell carcinoma
Caov-3	Human high grade ovarian serous adenocarcinoma
HeLa	Human papillomavirus-related endocervical adenocarcinoma
MCF-7	Human breast adenocarcinoma
MIA PaCa-2	Human pancreatic ductal adenocarcinoma
NuTu-19	Rat ovarian adenocarcinoma
OVCAR-3	Human high grade ovarian serous adenocarcinoma
OVCAR-8	Human high grade ovarian serous adenocarcinoma
PA-1	Human ovarian mixed germ cell tumour
RT-2	Rat malignant glioma
SKOV-3	Human ovarian serous cystadenocarcinoma
T24	Human bladder carcinoma
U20S	Human osteosarcoma

1 Introduction

1.1 Cancer

Cancer is one of the leading causes of mortality worldwide, especially in developed countries such as the United States where it is the second leading cause of death after heart disease, as well as Australia and New Zealand, where it is the leading cause of death (Bray et al., 2018; Disney, 2016; Rebecca L. Siegel, Miller, & Jemal, 2018). In 2018, there were an estimated 18 million new cancer cases and more than 9.5 million deaths caused by cancer worldwide (Bray et al., 2018). Cancer therefore represents a major public health problem on a global scale.

While many different types and subtypes of cancer exist, almost all cancer cells share several common characteristics, which are generally considered the 'hallmarks' of cancer (Hanahan & Weinberg, 2000). An important underlying characteristic shared by all cancers is genomic instability or increased mutability, as this is what allows mutations to accumulate, thus supporting the growth and progression of tumours (Hanahan & Weinberg, 2000; Hanahan & Weinberg, 2011).

Of these common characteristics, several involve separating the growth of cancer cells from environmental signals (Hanahan & Weinberg, 2000). Whereas normal cells require the presence of growth signals in order to proliferate, cancer cells do not, possibly because they are able to produce their own proliferative signals (Evan & Vousden, 2001; Hanahan & Weinberg, 2000). Cancer cells are also typically insensitive to anti-proliferative signalling and will continue to proliferate, even in the presence of anti-growth signals or growth inhibition (Hanahan & Weinberg, 2000; Hanahan & Weinberg, 2011). Normal cells can only progress through the cell cycle a given number of times before dying or becoming senescent, but cancer cells often have infinite replicative potential (Hanahan & Weinberg, 2000; Hanahan & Weinberg, 2011). In addition, cancer cells can develop mechanisms of evading programmed cell death (Bold, Termuhlen, & McConkey, 1997; Hanahan & Weinberg, 2000). Other hallmarks of cancer include sustained angiogenesis to provide tumours with all the nutrients they require to continue growing, and tissue invasion and metastasis, an often-deadly characteristic of many late-stage malignancies (Fouad & Aanei, 2017; Hanahan & Weinberg, 2000; Yang & Weinberg, 2008; Ziyad & Iruela-Arispe, 2011).

1.2 Ovarian cancer

Ovarian cancer is a major cause of mortality among women with gynaecological cancers (R. L. Siegel, Miller, & Jemal, 2016). Cancer death rates in general are slowly beginning to decline; however, statistics describing ovarian cancer have remained reasonably stable over the past two decades (Greenlee, Murray, Bolden, & Wingo, 2000; Jemal et al., 2006; Rebecca L. Siegel et al., 2018; Rebecca L. Siegel, Naishadham, & Jemal, 2012). In 2018, there were an estimated 295,000 new cases of ovarian cancer, and 140,000 deaths caused by ovarian cancer worldwide (Bray et al., 2018). The relative five-year survival of epithelial ovarian cancer is less than 50% (Torre et al., 2018).

During its early stages, ovarian cancer is typically mostly asymptomatic, which makes early detection of the disease very difficult (Cannistra, 2004; R. L. Siegel et al., 2016). Consequently, patients are often only diagnosed with ovarian cancer after the disease has reached an advanced stage, and by this point chances of survival are typically quite low (Hassan, Chitcholtan, Sykes, & Garrill, 2016, 2018). Furthermore, late-stage disease is often difficult to treat effectively, particularly because commonly used chemotherapeutics are generally of limited efficacy with respect to ovarian cancer, as patients with recurring disease are likely to develop resistance to conventional chemotherapeutics (Cannistra, 2004; Huang et al., 2012; Kipps, Tan, & Kaye, 2013). Patients with advanced ovarian cancer also often suffer a poor quality of life due to a combination of the symptoms of the cancer itself, such as an accumulation of ascitic fluid in the peritoneal cavity, which is common among such patients and often causes considerable discomfort, and the harsh side effects of the treatment strategies employed to combat ovarian cancer (Cannistra, 2004).

In general, ovarian tumours arise in the lining of the ovary, and spreading throughout the abdominal cavity and other internal organs is relatively straightforward from this site (Fagotti et al., 2010). The peritoneal membrane covers the visceral organs, along with the abdominal and pelvic cavities, and consists of an interstitial or stromal space between a layer of endothelial cells on one side and a layer of mesothelial cells on the other (Kipps et al., 2013). As tumours develop, malignant cells can shed and then float in the peritoneal fluid, which allows cancer cells to spread and develop into tumours in locations other than the ovary (Fagotti et al., 2010; Weidle, Birzele, Kollmorgen, & Rueger, 2016). Free-floating tumour cells in the peritoneal fluid can also interact with the mesothelial layer of the peritoneal

membrane, adhere to this layer of cells, and eventually grow on the surface of the peritoneal membrane as tumour nodules (Weidle et al., 2016).

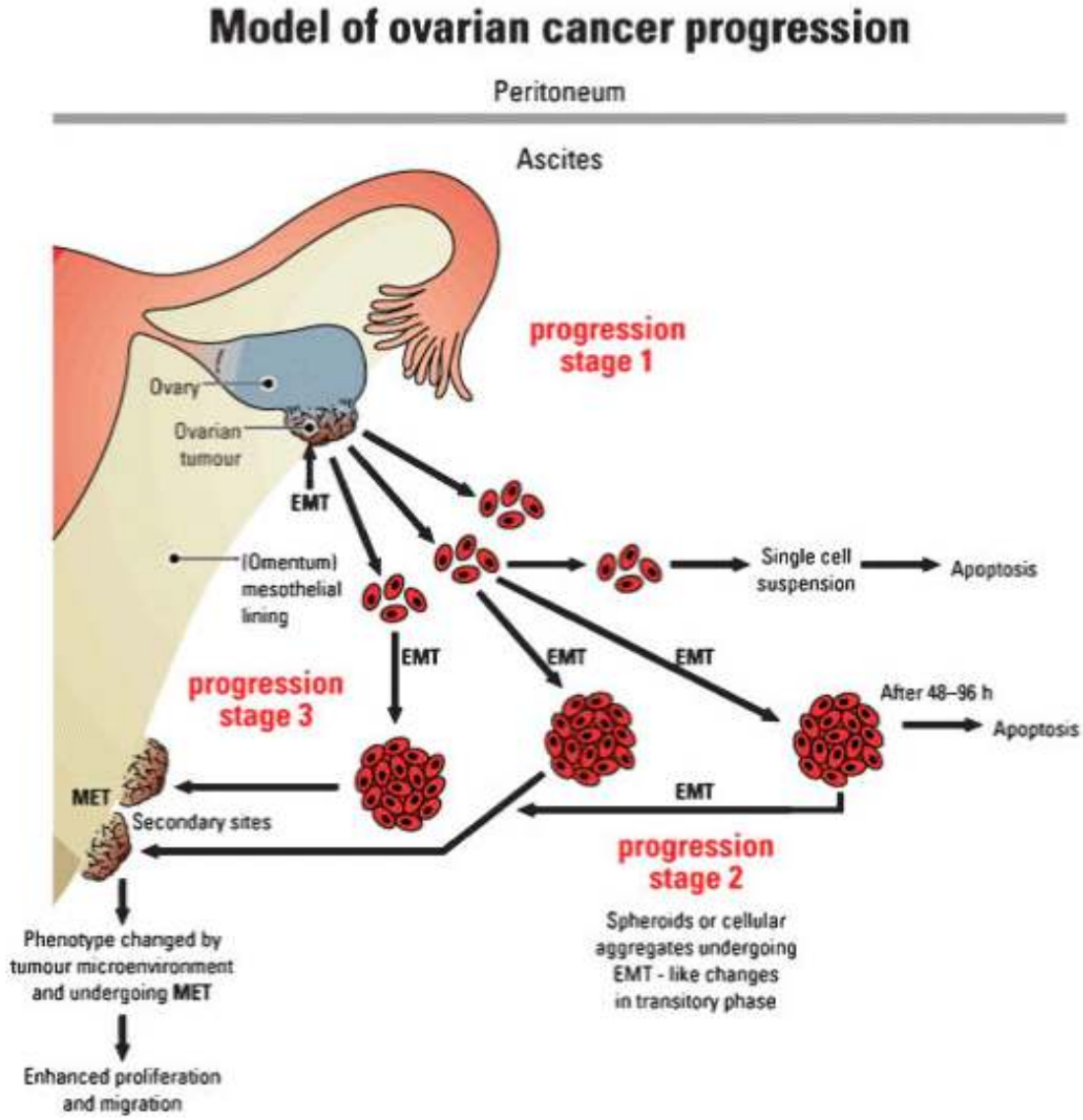

Figure 1.1 Proposed model of early metastasis of ovarian cancer. *Malignant cells on the surface of the ovary undergo EMT, and then shed from the ovary into the peritoneal cavity. Cells then form aggregates, which secrete growth factors and cytokines to encourage the accumulation of ascitic fluid in the peritoneal cavity, which allows cellular aggregates to survive until they reach a secondary attachment site. Image reproduced with permission (Ahmed, Thompson, & Quinn, 2007).*

The clinical progression of ovarian cancer is divided into four main stages: at stage I, the disease is restricted to the ovaries alone; at stage II, cancer cells have migrated into pelvic organs and tissues; at stage III, the cancer has spread to the abdominal cavity or invaded the lymph nodes, or both; and at stage IV, distant metastases have been established (Jayson, Kohn, Kitchener, & Ledermann, 2014). As ovarian cancer progresses through these stages, survival rates decrease dramatically; for patients diagnosed with stage I disease, the five-year survival rate is approximately 80%, but this drops to 30% and 20% for stage III and IV disease respectively (Torre et al., 2018).

Approximately 90% of ovarian cancers are epithelial in origin, and tumour cell morphology and molecular pathology can be used to further classify these as serous (high- or low-grade), endometrioid (high- or low-grade), clear cell, or mucinous (Cho & Shih, 2009; Jayson et al., 2014). Whether the cancer is high- or low-grade depends primarily on the amount of solid tumour growth, and typically reflects the aggressiveness of the cancer (Cho & Shih, 2009).

Serous carcinoma is the most common type of epithelial ovarian cancer (Cho & Shih, 2009). Mutations in the tumour suppressor gene *TP53* are very common in high-grade serous ovarian cancer, whereas mutations in *KRAS* or *BRAF* are common in low-grade serous cancer (Cho & Shih, 2009; Jayson et al., 2014). Clinically, high-grade serous ovarian cancer is typically aggressive and affects mostly older women, whereas low-grade cancer is slower to develop and affects mainly younger women (Ayhan et al., 2009). Most ovarian cancer deaths occur in patients with advanced, high-grade serous ovarian cancer as this is the most common subtype (The Cancer Genome Atlas Research et al., 2011). The endometrioid and clear cell subtypes are the next most common, although they are both quite rare compared to the serous subtype, and the mucinous subtype is the least common (Cho & Shih, 2009).

Treatment of advanced ovarian cancer typically involves surgery to remove as much of the cancer as possible; ‘optimal’ surgery refers to the removal of all tumours except nodules that are less than 1 cm in diameter, which can be very difficult to surgically remove (Pomel et al., 2007). However, individual cancer cells can penetrate the layer of mesothelial cells on the peritoneal membrane, invade the interstitial space, and can then spread to other internal organs in the abdominal cavity (Weidle et al., 2016). Therefore, an *in vivo* model that mimics the development of small tumour nodules on the surface of the peritoneal membrane and their subsequent invasion further into the stromal area of this membrane may provide information needed for the development of more effective treatments for ovarian cancer.

1.3 The chicken chorioallantoic membrane (CAM) model

The ability of ovarian tumour cells to detach from the ovary, adhere to, and invade the peritoneal membrane is often the basis of metastasis in ovarian cancer (Lokman, Elder, Ricciardelli, & Oehler, 2012). As such, research involving advanced ovarian cancer requires an *in vivo* model that can imitate this process. One method that can be used to replicate the natural environment of ovarian tumours and the spread of cancerous cells to the peritoneum is to use an animal cell model. The chicken chorioallantoic membrane (CAM) model is an example of such a system.

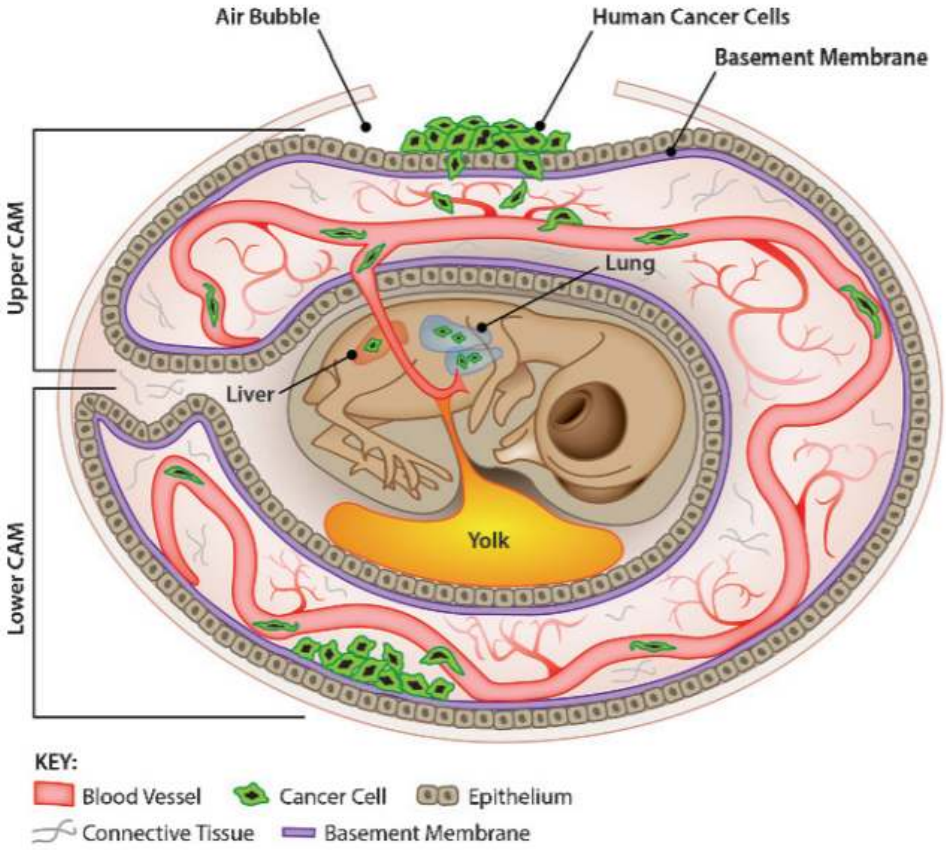

Figure 1.2 Overview of the CAM model*. Cancer cells are implanted on the surface of the upper CAM, and can then invade the epithelial layer and basement membrane. Cancer cells can then move into the vascular network and metastasise to distal portions of the CAM or organs in the developing embryo. Image reproduced with permission (M. Liu et al., 2013).*

The CAM is a very thin, highly vascularised membrane that surrounds developing chicken embryos (Durupt, Koppers-Lalic, et al., 2012). The membrane consists of an endoderm, mesoderm or stromal region, and an ectoderm, which is very similar to the peritoneal membrane (Lokman et al., 2012). Developing chicken embryos have immature immune systems and so can host tumour cells from various origins, including cancer cell lines derived from human patients, which are used in the present research (Durupt, Koppes-Lalic, et al., 2012). The highly vascularised nature of the membrane also helps to enhance the efficiency of tumour cell grafting (Lokman et al., 2012).

The CAM model has been widely used to study tumour invasion *in vivo* in different cancer types, including ovarian cancer (Lokman et al., 2012). Studies have shown that tumour cells grafted onto the CAM can develop into sizeable tumours and escape from the primary site by invading the mesodermal layer of the CAM, and eventually reach distal portions of the CAM (Deryugina & Quigley, 2008; Lokman et al., 2012). In this way, the CAM model can be used to replicate the process of metastasis in ovarian cancer (Deryugina & Quigley, 2008).

Use of the CAM model, compared with the use of mammalian models, is also appealing as the requirements of this model are much more basic (Taizi, Deutsch, Leitner, Ohana, & Goldstein, 2006). The CAM model is cost-effective and simple, whereas mammalian models are often expensive, complex, and entail large space requirements and time-consuming studies, all of which can make them impractical (Durupt, Koppes-Lalic, et al., 2012; Taizi et al., 2006). Furthermore, using the CAM model as opposed to mammalian models minimises the amount of testing carried out on sentient animals (Taizi et al., 2006). The key limitations of the CAM model are that it already contains a well-developed vascular network, which can make it difficult to determine the true extent of angiogenesis, and that non-specific inflammatory reactions may occur as a consequence of the implantation of tumour cells (D. Ribatti, 2010). In this case, these drawbacks are outweighed by the significant advantages of using the CAM model.

1.4 Angiogenesis

Early during the formation of an embryo, a primary vascular plexus is formed via a process called vasculogenesis (Risau, 1997). After this original network has been formed, angiogenesis, or the formation of new blood vessels from existing ones, can occur to expand this network and increase its complexity (Karamysheva, 2008).

Under normal circumstances, angiogenesis is tightly regulated, and will only occur under specific conditions (Karamysheva, 2008). It is an important process, but dysfunctional angiogenesis can have serious repercussions (Karamysheva, 2008; Nishida, Yano, Nishida, Kamura, & Kojiro, 2006). Excessive formation of new blood vessels and insufficient development of blood vessels can both contribute to severe human conditions including ischemic and inflammatory diseases, as well as cancer (Karamysheva, 2008; Potente, Gerhardt, & Carmeliet, 2011). Angiogenesis is necessary for the development of tumours; without adequate blood supply, tumour nodules cannot grow beyond approximately 100 to 200 μm^2, as hypoxia will lead to the death of the tumour cells that are too distant from any blood vessels (Folkman, 2006; Nishida et al., 2006; Schmitt & Matei, 2012; Ziyad & Iruela-Arispe, 2011).

The general pathways of angiogenesis are largely the same whether it is occurring during normal vascular growth or in tumours (Ziyad & Iruela-Arispe, 2011). However, tumour angiogenesis lacks feedback regulatory control. Where normal blood vessels are evenly distributed and highly ordered, tumour vasculature tends to be unevenly distributed, with irregular branching patterns and chaotic networks (Ziyad & Iruela-Arispe, 2011). Tumour vasculature is generally unstructured, fragile, and hyper-permeable (Ziyad & Iruela-Arispe, 2011). This can reduce the efficacy of chemotherapeutics, as the efficiency of distribution of chemotherapeutic agents around tumours is likely to be impaired (Schmitt & Matei, 2012; Ziyad & Iruela-Arispe, 2011).

There are essentially two main mechanisms of angiogenesis: sprouting and non-sprouting angiogenesis, which are discussed below (Risau, 1997).

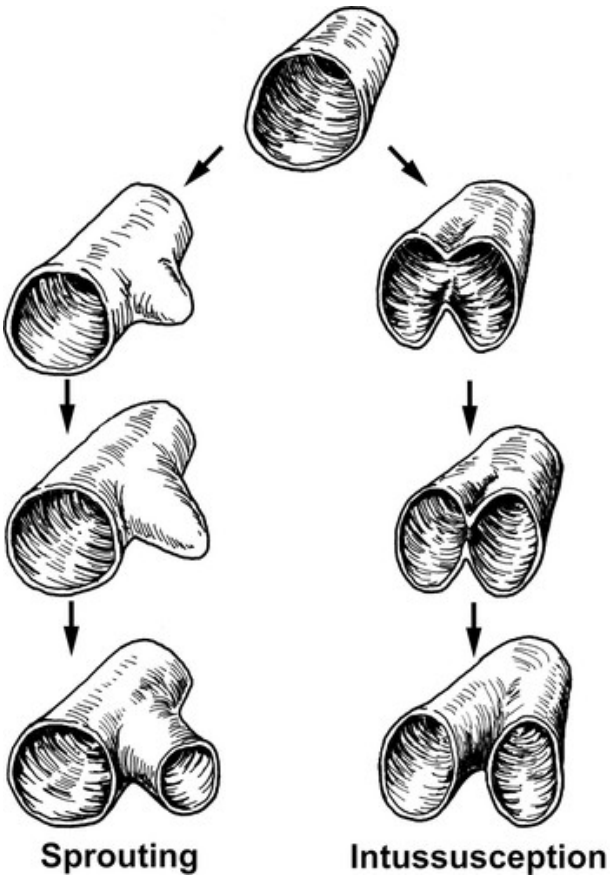

Figure 1.3 Angiogenesis may occur via sprouting or intussusception. *Image reproduced with permission (Prior, Yang, & Terjung, 2004).*

1.4.1 Sprouting angiogenesis

As its name suggests, sprouting angiogenesis is characterised by endothelial cells sprouting out from an existing blood vessel and growing towards an angiogenic signal (Adair & Montani, 2010). Angiogenic stimuli, such as hypoxia or inflammation, can trigger the release of angiogenic signalling molecules, including vascular growth factors and angiogenic chemokines (Carmeliet & Jain, 2011; Karamysheva, 2008). These molecules then bind to their cognate receptors, which are typically expressed on the surface of endothelial cells (Semenza, 2007). This leads to activation of signal transduction pathways that stimulate angiogenesis.

In response to angiogenic signalling, matrix metalloproteinases (MMPs), along with other proteinases, locally degrade the basement membrane and extracellular matrix (ECM) close to the angiogenic stimulus (Carmeliet, 2000; Domenico Ribatti & Crivellato, 2012). This leads to the destabilisation of the existing, mature blood vessels, which is compounded by the weakening of interactions between endothelial cells (Carmeliet, 2000; Domenico Ribatti & Crivellato, 2012). The consequent increased permeability of the existing vasculature allows for the migration of plasma proteins through the endothelial cell layer, where they form a provisional ECM scaffold (Carmeliet & Jain, 2011).

Endothelial cells can then migrate to this newly formed ECM, where they begin to assemble into a solid cord (Carmeliet, 2000; Carmeliet & Jain, 2011; Domenico Ribatti & Crivellato, 2012). A subset of endothelial cells become ‘tip cells’, which are highly migratory and respond to angiogenic signals, but undergo minimal proliferation (Domenico Ribatti & Crivellato, 2012; Rice, Gerwins, & Kilarski, 2012). Other endothelial cells proliferate actively to form the ‘stalk’ (Carmeliet & Jain, 2011). These stalk cells also form a vascular lumen, synthesise a new basement membrane, and associate with pericytes (Carmeliet & Jain, 2011; Domenico Ribatti & Crivellato, 2012). Finally, stalk cells stop proliferating and functional contacts between these endothelial cells are re-established in the newly formed blood vessel (Domenico Ribatti & Crivellato, 2012).

Key proteins involved in this type of angiogenesis include vascular growth factors such as the vascular endothelial growth factor (VEGF) family of proteins, transforming growth factors (TGF), fibroblast growth factors (FGF), and angiopoietin, along with all of their associated receptor proteins (Karamysheva, 2008). Cytokines, including tumour necrosis factor (TNF)-α

and some interleukins – particularly IL-1, IL-6, and IL-8, are also involved in this process (Karamysheva, 2008).

1.4.2 Intussusceptive angiogenesis

Non-sprouting angiogenesis, also called intussusceptive angiogenesis or intussusceptive microvascular growth, is the process of forming new blood vessels by splitting pre-existing vessels into two functional vessels using trans-capillary pillars (Rice et al., 2012; Risau, 1997). This method of blood vessel formation is significantly faster and less metabolically demanding than sprouting angiogenesis (Domenico Ribatti & Djonov, 2012; Rice et al., 2012). Furthermore, normal levels of vascular permeability are maintained, and the proliferation of endothelial cells is not an immediate requirement, as this type of angiogenesis simply involves the migration and remodelling of existing vasculature (Hillen & Griffioen, 2007; Rice et al., 2012). It is therefore an efficient means of expanding existing capillary networks, but in contrast to sprouting angiogenesis, intussusceptive angiogenesis is not an invasive process, and cannot be used to vascularise regions that were originally avascular (Burri, Hlushchuk, & Djonov, 2004; Paku et al., 2011). The exact molecular mechanism is incompletely understood, although it has been suggested that VEGF, angiopoietin, platelet-derived growth factor (PDGF), and erythropoietin may play a role (Domenico Ribatti & Djonov, 2012).

While the mechanistic details are still under investigation, the morphological changes involved in non-sprouting angiogenesis are well-described in the literature (Rice et al., 2012). Endothelial cells opposite one another, from the same blood vessel, are initially drawn together to form a 'transluminal bridge' (Burri et al., 2004). A small perforation, about 1 μm across, is then formed in the endothelial bilayer, resulting in a hollow, cylindrical bridge through the lumen (Burri et al., 2004; Rice et al., 2012). Pericytes migrate to this perforation, stabilising the junctions between endothelial cells and forming a new basement membrane (Rice et al., 2012). Extracellular matrix components such as collagen accumulate within the pillar, and the surrounding endothelial cells reorient themselves to continue elongating the pillar and splitting the vessel (Rice et al., 2012).

Intussusceptive angiogenesis can be induced by increased blood flow and shear stress, both of which are typical of tumour vasculature (Domenico Ribatti & Djonov, 2012). In addition, some research suggests that intussusceptive angiogenesis might be less dependent on VEGF signalling than sprouting angiogenesis, meaning that angiogenesis inhibitors designed to target this signalling pathway may have a limited effect on intussusceptive angiogenesis

(Rice et al., 2012). Switching from sprouting to intussusceptive angiogenesis may therefore represent an adaptive response to treatment with various anti-angiogenic compounds; that is, inhibition of sprouting angiogenesis may induce intussusceptive angiogenesis (Hillen & Griffioen, 2007; Domenico Ribatti & Djonov, 2012).

1.5 Invasion

Cancer cells at the primary tumour site can invade through the basement membrane of blood vessels and enter the circulation, allowing tumour cells to reach distant metastatic sites (Yeung et al., 2015). In addition, in patients with advanced ovarian cancer, passive dissemination of tumour cells is also possible. Cancer cells that become detached from the primary tumour may be carried throughout the peritoneal cavity by ascitic fluid to a metastatic site, where they adhere to the surface of an organ, tissue, or the peritoneum itself (Yeung et al., 2015). Once attached to the surface of the peritoneal membrane, tumour cells can proliferate and invade the mesothelium (Yeung et al., 2015). Ascitic fluid components can support this invasion of tumour cells by inducing secretion of matrix-degrading proteinases like MMPs (Yeung et al., 2015).

The process of invasion requires the conversion of stationary epithelial cells, which are connected securely to one another via specialised adhesion complexes, to mesenchymal cells, which do not have any such junctions and are motile (Nakayama, Nakayama, Katagiri, & Miyazaki, 2012; Yang & Weinberg, 2008). This mechanism for detachment of tumour cells from the epithelial cell layer and the gain of motility, known as epithelial-mesenchymal transition (EMT), enables tumour cell invasion and metastasis (Krakhmal, Zavyalova, Denisov, Vtorushin, & Perelmuter, 2015).

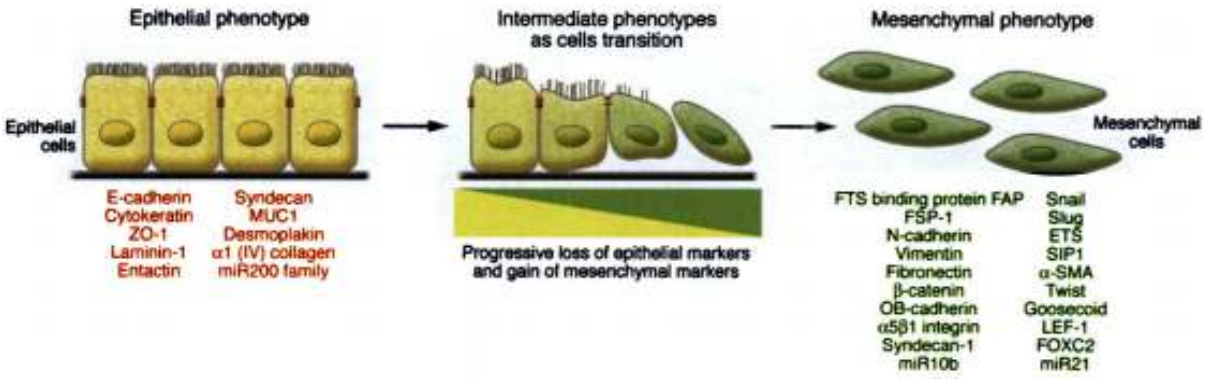

Figure 1.4 EMT involves the transition of epithelial cells into mobile mesenchymal cells. *Common markers of both epithelial and mesenchymal cells are listed. Image reproduced with permission (Kalluri & Weinberg, 2009).*

There are several crucial events that occur during EMT. One is a change in the cell's polarity; epithelial cells have apical-basal polarity as they are associated with a basement membrane, whereas mesenchymal cells have front-rear polarity and are not anchored to any substrate (Yang & Weinberg, 2008). Alongside this change in polarity is the dissolution of epithelial cell-cell junctions, allowing detachment of cells from the epithelial cell layer (Kalluri & Weinberg, 2009; Krakhmal et al., 2015; Lamouille, Xu, & Derynck, 2014). This involves the loss of cell-adhesion molecules such as E-cadherin, which may be mediated by various transcriptional repressors, such as Slug, Snail, or Twist (van Zijl, Krupitza, & Mikulits, 2011).

These changes are followed by reorganisation of the cytoskeleton and changes in cell shape, enabling cell elongation and motility (Lamouille et al., 2014). Mesenchymal cells are capable of projecting protrusions or lamellipodia and have increased contractility (Lamouille et al., 2014). Changes in gene expression then often occur to increase migratory and invasive properties, including downregulation of epithelial gene expression, increased expression of genes that define the mesenchymal phenotype, and increased formation of protrusions and motility (Krakhmal et al., 2015; Lamouille et al., 2014). The net result of these changes is the transition of an epithelial cell into a mesenchymal one, which has the ability to migrate and invade the ECM (Yang & Weinberg, 2008).

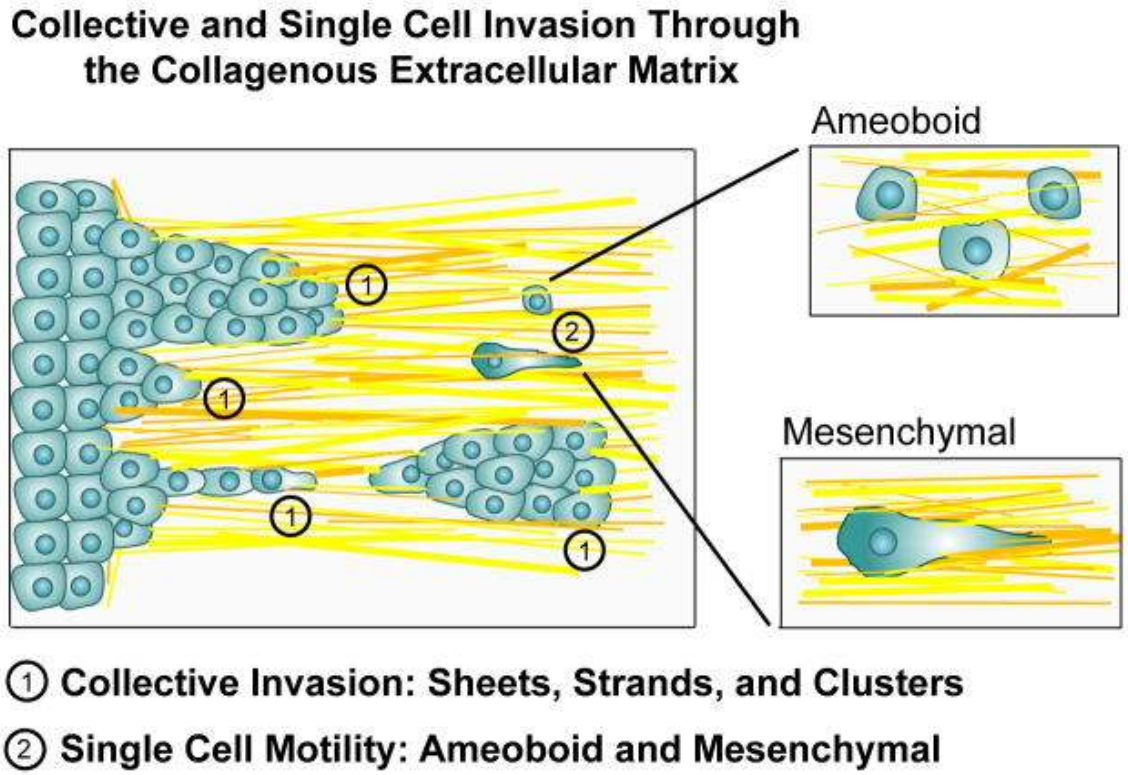

Figure 1.5 Cell phenotypes that are associated with invasion through the ECM. *Image reproduced with permission (Provenzano, Eliceiri, & Keely, 2009).*

Once tumour cells are capable of invasion, they may do this as individual cells or as a collection of cells simultaneously, and in each case invasion may occur via either a mesenchymal or amoeboid mechanism (Krakhmal et al., 2015). The mesenchymal, or fibroblast-like, mechanism of invasion is reasonably slow and inefficient, with cells only moving at a rate of about 0.1 – 1.0 µm per minute (van Zijl et al., 2011). This mechanism involves the formation of a protrusion from one of the poles of a cell, and then the formation of focal adhesions between the cell and ECM, which is dependent upon the activity of integrins (Krakhmal et al., 2015). Integrins then mediate the assembly of focal contacts, and proteolytic enzymes, including MMPs, locally degrade and remodel the ECM and basement membrane (Krakhmal et al., 2015; van Zijl et al., 2011). Contractions of the cell body, facilitated by myosin-mediated changes in the polarisation of the actin cytoskeleton, enable movement of the cell and the trailing edge is 'pulled' along through the region of degraded ECM (Krakhmal et al., 2015).

In contrast to the mesenchymal invasion mechanism, amoeboid invasion is much more rapid, with cells moving at speeds of up to 20 µm per minute (van Zijl et al., 2011). This type of

invasion is characterised by weak interactions between cells and the ECM (Krakhmal et al., 2015). Amoeboid invasion is not reliant on integrins, and does not require degradation of the ECM, so no proteolytic enzymes are involved in this mechanism of invasion (Krakhmal et al., 2015). Movement via this type of invasion is achieved through successive high-speed cycles of cell body expansion and contraction, mediated by the actomyosin cortex (Krakhmal et al., 2015; Panková, Rösel, Novotný, & Brábek, 2010). Activation of the Rho/ROCK signalling pathway, which is mainly involved in regulating the shape and movement of cells, enhances the contractility of these cells, allowing them to modify their shape so that they may squeeze through smalls gaps between components of the ECM (Panková et al., 2010).

1.6 Cell proliferation

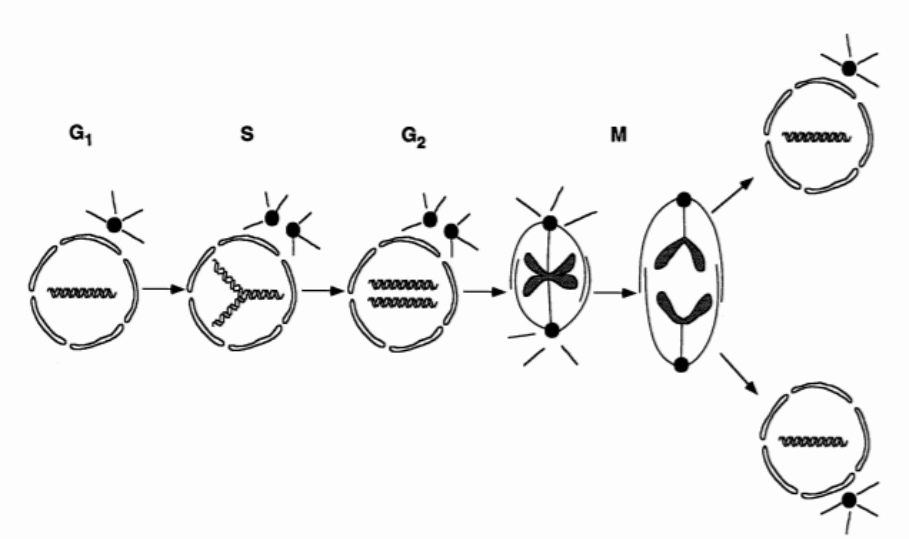

Figure 1.6 The cell cycle. *Image reproduced with permission (Hartwell & Kastan, 1994).*

The cell cycle consists of a cell growth phase (G1 phase), followed by the synthesis of DNA (S phase), followed by more growth (G2 phase), and finally mitosis and cytokinesis (M phase), ultimately producing two identical daughter cells. Cells which divide rapidly continually go through this cell cycle, producing more and more daughter cells (Cooper, 2000). In contrast, cells which divide more slowly, or not at all, may exit the cell cycle at G1 phase, before reaching S phase, and enter what is known as G0 phase, a resting state where cells are not actively preparing to divide (Cooper, 2000).

Progression through the cell cycle is mediated by cell cycle regulators, including cyclins, cyclin dependent kinase (Cdk) proteins, and Cdk inhibitor (CKI) proteins (Lim & Kaldis, 2013). These regulatory molecules respond to both intra- and extracellular cues; for example, the presence of growth factors will stimulate progression through the cell cycle, whereas DNA damage will halt the cell cycle (Lim & Kaldis, 2013). Cdk proteins are activated by the binding of relevant cyclins, and can then phosphorylate target proteins to either activate or inactivate them (Lim & Kaldis, 2013). Cyclins are regulatory proteins that control Cdk activity and substrate specificity (Lim & Kaldis, 2013). The activity of Cdk/cyclin complexes is carefully controlled by CKI proteins, which can halt progression through the cell cycle, when needed, by inhibiting Cdk activity (Lim & Kaldis, 2013).

There are several checkpoints in the cell cycle, of which two of the most important are the G1 and G2 checkpoints. At the G1/S transition, the cell is checked for appropriate size, nutrients, growth factors, and for any DNA damage, before DNA replication can proceed (Cooper, 2000). At the G2/M transition, the cell is, again, checked for DNA damage, along with a check of the completeness of DNA replication, before cell division occurs (Cooper, 2000).

Abnormal regulation of the cell cycle, caused primarily by the accumulation of mutations, can lead to cancer. Tumour cells can proliferate well beyond the constraints that normally limit growth in healthy cells (Evan & Vousden, 2001). In some cases, cancer cells no longer require mitogenic signals in order to proliferate – that is, they will continue to proliferate even in the absence of proliferative signals (Evan & Vousden, 2001). In other cases, cancer cells are able to bypass checkpoints in the cell cycle and divide even if they do not meet the usual criteria for progression through the cell cycle (Evan & Vousden, 2001). Loss of the tumour suppressor protein p53, which normally mediates the G2/S transition, allows cells to progress to S phase without undergoing the appropriate checks, and subsequently allows the formation of mutation-harbouring daughter cells (Alsina-Sanchís et al., 2017).

In healthy tissues, the production and release of signals that promote progression through the cell cycle are carefully controlled; however, cancer cells often proliferate independently of these growth factors as they are able to overexpress positive proliferative signals, or elevate the levels of receptors on cell surfaces to make those cells hyper-sensitive to proliferative signalling, which would limit cell growth under normal circumstances (Evan & Vousden, 2001; Hanahan & Weinberg, 2011). Disruption of negative feedback mechanisms and evasion of growth suppression mechanisms may also enable cells to continue to proliferate when, in a healthy system, proliferation would be inhibited (Hanahan & Weinberg, 2011). In addition, normal cells may only progress through the cell cycle a limited number of times before becoming senescent or dying, whereas cancer cells have essentially infinite replicative potential (Hanahan & Weinberg, 2011).

1.7 Cell death

Cell death is a critical to maintaining healthy tissues; it is a mechanism for eliminating cells that are no longer needed, or are potentially dangerous to the rest of the organism. There are many different pathways through which cells may die, but two of the most common are apoptosis and necrosis, which are described below.

1.7.1 Apoptosis

Apoptosis is a programmed, controlled form of cell death. It is an essential cellular process, critical to various developmental processes, the healing of wounds, and the removal of deteriorating or otherwise damaged cells (Elmore, 2007). Apoptosis also plays a crucial role in the proper development and functioning of the immune system as it is the process by which cells invaded by pathogens are eliminated (Elmore, 2007). There are two key pathways through which apoptosis usually occurs: the extrinsic pathway, and the intrinsic pathway (R. S. Y. Wong, 2011).

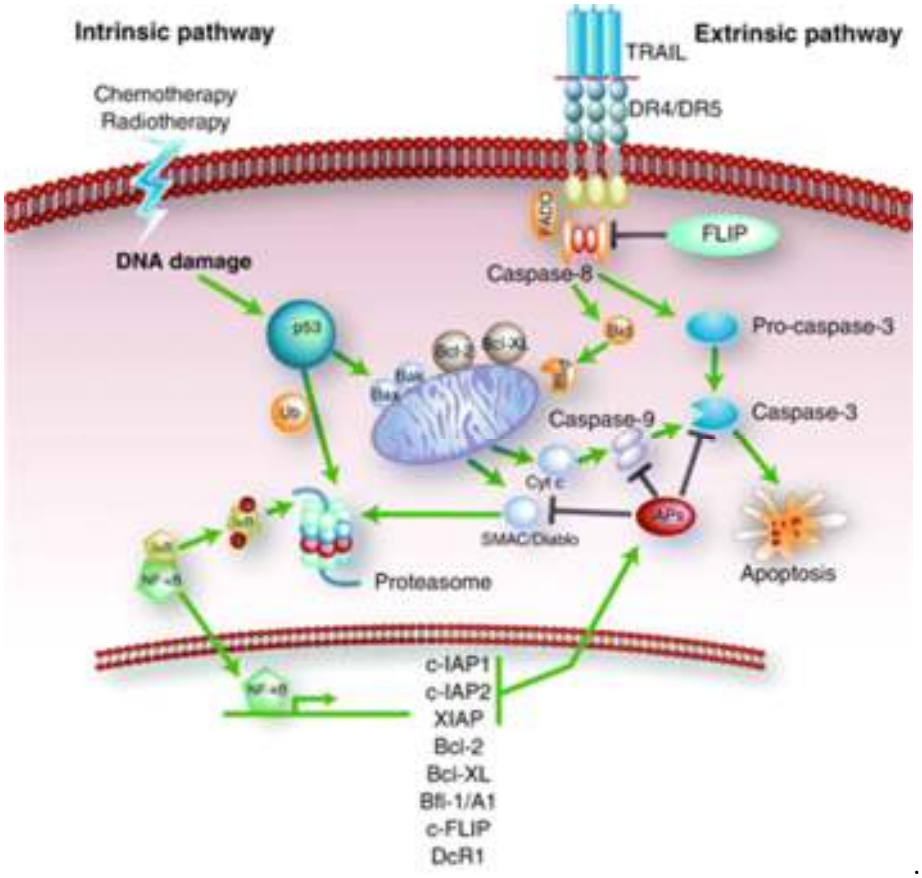

Figure 1.7 Schematic representation of both the intrinsic and extrinsic apoptotic pathways. *Image reproduced with permission (de Vries, Gietema, & de Jong, 2006).*

The extrinsic apoptotic pathway, or the 'death receptor pathway', is triggered by the binding of a ligand to its corresponding 'death receptor' (R. S. Y. Wong, 2011). One of the most commonly described examples of this is the binding of the Fas ligand (FasL) to its receptor

(Fas), and the subsequent binding of the adapter protein, Fas-associated death domain (FADD) (Bold et al., 1997; R. S. Y. Wong, 2011). Another common example is the binding of tumour necrosis factor (TNF) to its receptor (TNFR), and then the binding of TNFR-associated death domain (TRADD) (Bold et al., 1997; Elmore, 2007; R. S. Y. Wong, 2011). This whole complex of the ligand, receptor, and associated adapter protein form a death inducing signalling complex (DISC) (R. S. Y. Wong, 2011). The DISC then facilitates the assembly and activation of pro-caspase-8, which subsequently activates pro-caspase-3 (Elmore, 2007).

The intrinsic pathway of apoptosis, sometimes referred to as the mitochondrial apoptotic pathway, is typically triggered by an internal stimulus, such as the loss of apoptotic suppression or the presence of radiation, toxins, hypoxia, or free radicals (Elmore, 2007). Any of these events can lead to the loss of the mitochondrial transmembrane potential, which disrupts the integrity of the outer mitochondrial membrane (R. S. Y. Wong, 2011). Increased permeability of the mitochondrial membrane facilitates the release of pro-apoptotic molecules such as cytochrome c, Smac/DIABLO, and HtrA2/Omi into the cytosol (Elmore, 2007).

Cytochrome c, once it is present in the cytoplasm, activates pro-caspase 9, which then activates pro-caspase-3 (R. S. Y. Wong, 2011). When the pro-apoptotic mitochondrial protein, second mitochondria-derived activator of caspase/direct inhibitor of apoptosis binding protein with low pI (Smac/DIABLO), is present in the cytosol it can act as an antagonist of inhibitor of apoptosis proteins and thereby induce apoptosis (Martinez-Ruiz, Maldonado, Ceballos-Cancino, Grajeda, & Melendez-Zajgla, 2008). High-temperature requirement (HtrA) proteins are a family of serine proteases; HtrA2/Omi resides in the mitochondrial intermembrane space, and also facilitates apoptosis by binding and antagonising inhibitor of apoptosis proteins (Vande Walle, Lamkanfi, & Vandenabeele, 2008).

Both the extrinsic and intrinsic apoptotic pathways converge at a common step: the activation of pro-caspase-3 at the beginning of what is known as the ‘execution pathway’ (Elmore, 2007; R. S. Y. Wong, 2011). Caspase-3 activates various endonucleases, including apoptosis inducing factor (AIF), endonuclease G, and caspase-activated DNase (CAD), which then mediate the degradation of chromosomal DNA (Elmore, 2007). Caspase-3 also activates proteases, leading to the degradation of nuclear and cytoskeletal proteins and the reorganisation of cytoskeletal components (Elmore, 2007; R. S. Y. Wong, 2011). The

cytoplasm and nuclear chromatin are then condensed and the nucleus is broken down (R. S. Y. Wong, 2011). This all manifests morphologically as shrinkage of the cell, condensation of chromatin, and blebbing of the plasma membrane (Kerr, Winterford, & Harmon, 1994). 'Apoptotic bodies', composed of cytoplasm, organelles, and possibly nuclear fragments, all encased within a plasma membrane, are then formed (R. S. Y. Wong, 2011). These are then rapidly phagocytosed by macrophages, which are recruited to the site of the apoptotic cell by phosphatidylserine residues which usually line the inside of cell membranes, but which are exposed during apoptosis (Elmore, 2007).

When it occurs normally, apoptosis is a very useful cellular event. However, inappropriate levels of apoptosis – too much or too little – can have severe consequences (Bold et al., 1997; Elmore, 2007). Dysfunctional apoptosis is implicated in various human conditions, including many types of cancer, neurological disorders, cardiovascular disorders, and autoimmune disease (Elmore, 2007; Favaloro, Allocati, Graziano, Di Ilio, & De Laurenzi, 2012). An error in an apoptotic pathway could cause the survival of malignant cells, which would otherwise be eliminated by the cell under normal circumstances (R. S. Y. Wong, 2011). There are multiple possible apoptotic pathways, each of which is complex, with many different proteins and other molecules playing a role in the process, meaning that there are numerous opportunities for defects to arise in these pathways.

While there are many proteins involved in apoptosis, there are several key groups of proteins which play a critical role. One such group is the caspases, or cysteine-aspartic acid proteases (Bold et al., 1997; R. S. Y. Wong, 2011). These are enzymes that cleave proteins at specific amino acid residues during apoptosis (R. S. Y. Wong, 2011). Caspases 2, 8, 9, and 10 are known as 'initiator caspases', and they are closely coupled to pro-apoptotic signals (R. S. Y. Wong, 2011). For example, the binding of FasL to Fas leads to the activation of pro-caspase-8, and the binding of TNF to TNFR leads to the activation of pro-caspase-10 (Elmore, 2007). Once activated, these initiator caspases will cleave, thereby activating, a group of downstream caspases known as 'effector caspases', including caspases 3, 6, and 7 (R. S. Y. Wong, 2011).

Another key group of proteins is the Bcl-2 family of proteins. There are a large number of these proteins, and they are responsible for regulating the permeabilization of the mitochondrial membrane in the intrinsic apoptotic pathway (Elmore, 2007; R. S. Y. Wong, 2011). Some Bcl-2 family proteins are pro-apoptotic proteins (such as Bax and Bak), and so

disrupt the integrity of the mitochondrial membrane, allowing the release of cytochrome c into the cytosol and initiating the apoptotic signalling cascade (Bold et al., 1997; Elmore, 2007). However, some members of this family are pro-survival proteins (including Bcl-2 and Bcl-XL), which inhibit apoptosis (Bold et al., 1997; Elmore, 2007).

As detailed above, many cancer types, including ovarian cancer, often involve dysfunctional apoptosis. Inappropriate expression or activity of pro- and anti-apoptotic proteins can derail normal apoptosis; for example, increased expression of anti-apoptotic proteins such as Bcl-2, and decreased expression of pro-apoptotic proteins such as Bax, can lead to the inhibition of apoptosis (Bold et al., 1997). In addition, changes in the expression or activity of proteins which have a crucial role in apoptosis, such as caspases and death receptors, may also reduce the efficiency of apoptosis (Bold et al., 1997).

Ovarian cancer cells are often less sensitive to apoptotic stimuli than healthy cells (Bast Jr, Hennessy, & Mills, 2009; Bold et al., 1997; Glinsky, Glinsky, Ivanova, & Hueser, 1997). This is problematic, not only because reduced apoptosis allows malignant cells to survive, but also because disruptions to apoptosis are often linked with resistance to common modes of therapy (Bold et al., 1997; Elmore, 2007; R. S. Y. Wong, 2011). Some therapy strategies, including radiation therapy and some chemotherapeutic agents, work by triggering apoptosis (Bold et al., 1997). Where apoptosis is dysfunctional, these treatments may not be very effective, as cancer cells are able to resist programmed cell death (Bold et al., 1997; Kerr et al., 1994).

Disruption of apoptosis is also important for facilitating metastasis, as detachment of epithelial cells from the ECM is likely to induce apoptosis, unless apoptosis is dysfunctional (Bold et al., 1997; Glinsky et al., 1997). Therefore, it is unsurprising that highly metastatic cells tend to be more resistant to apoptosis than their less metastatic counterparts (Glinsky et al., 1997).

1.7.2 Necrosis

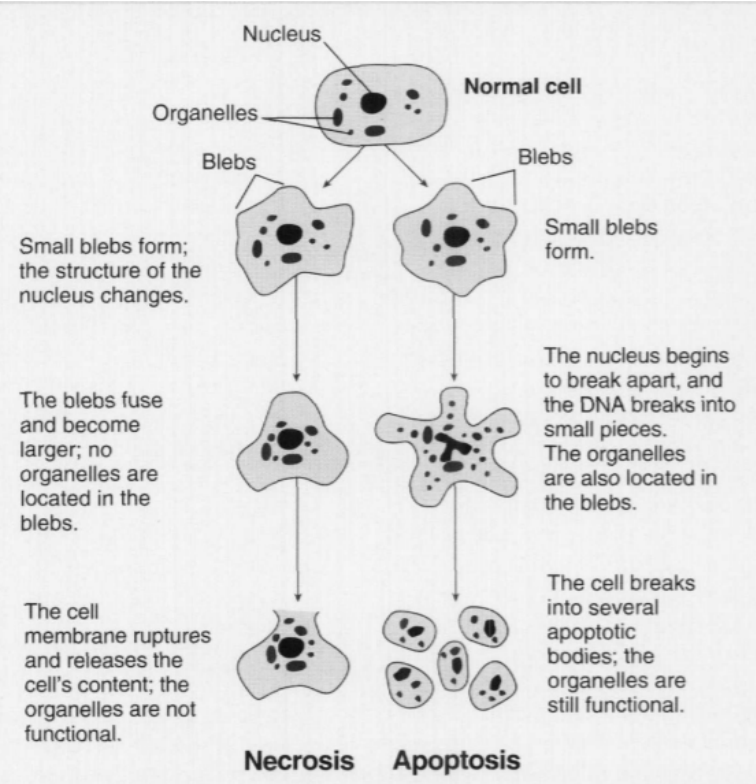

Figure 1.8 Structural changes occurring in cells as they undergo necrosis or apoptosis. *Image reproduced with permission (Goodlett & Horn, 2001).*

In contrast to apoptosis, necrosis is an uncontrolled mode of cell death, which usually occurs as a consequence of disruption to the cell's energy supply or direct damage to the cell membrane (Majno & Joris, 1995). Morphologically, necrosis is quite different from apoptosis. Necrosis typically involves the swelling of necrotic cells, the formation of cytoplasmic vacuoles and blebs, distension of the endoplasmic reticulum, and the swelling of cellular components such as the mitochondria and lysosomes (Elmore, 2007). This eventually leads to the disruption of the cell membrane and the release of the cell contents into the surrounding interstitial tissue, which often ultimately leads to the initiation of an inflammatory response (Bold et al., 1997).

The presence of necrosis is often associated with poor prognosis across a variety of tumour types (Bredholt et al., 2015). Rapidly proliferating tumour cells will eventually outgrow their blood supply, leading to local hypoxia (Dutta et al., 2012). Hypoxia induces cell death by

way of both apoptosis and necrosis (Shimizu et al., 1996). Necrotic cells release pro-inflammatory cytokines, which can stimulate angiogenesis by upregulating expression of angiogenic molecules, including VEGF, FGF, and MMPs (Bredholt et al., 2015). Thus, necrosis can support the progression of tumours, and it follows that necrosis is typically associated with aggressive tumour types, advanced stage disease, and decreased patient survival (Bredholt et al., 2015; Dutta et al., 2012; Vakkila & Lotze, 2004).

1.8 Resveratrol

Resveratrol was first isolated in 1940 from the roots of white hellebore, but it was not until 1992 that it began to gain attention, initially for its cardioprotective effects (Baur & Sinclair, 2006). Its anticancer properties were not identified until 1997, when it was observed that resveratrol inhibited cellular events that are involved in all three stages of carcinogenesis: initiation, promotion, and progression (Jang et al., 1997).

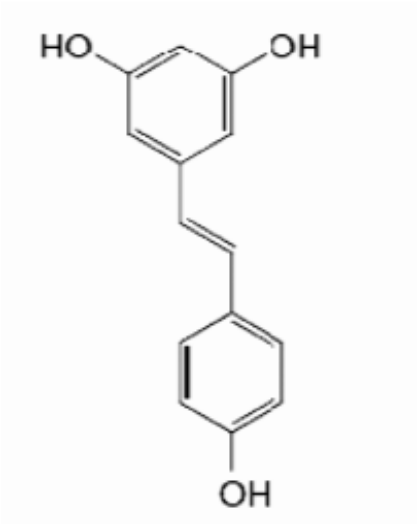

Figure 1.9* trans-*Resveratrol. *Image reproduced with permission (Kraft, Parisotto, Schempp, & Efferth, 2009).*

Resveratrol is a polyphenolic phytoalexin that occurs naturally in a range of plant species, including various grapes and berries, and is perhaps most widely known as a component of red wine (Bishayee, 2009; Hogg, Chitcholtan, Hassan, Sykes, & Garrill, 2015; Villa-Cuesta, Boylan, Tatar, & Gruppuso, 2011). It can exist as either in *cis* or *trans* conformations, but the *trans* conformation predominates in nature and this is the isomer which has been studied and found to have anti-tumour activity (Kraft et al., 2009).

Many *in vitro* studies to investigate the anticancer effects of resveratrol have thus far yielded promising results, suggesting that resveratrol may be able to slow tumour progression (Hogg et al., 2015). It has antioxidant properties, which means that it may prevent tumour initiation; it has also been shown to prevent angiogenesis and induce apoptosis (Kraft et al., 2009). In addition, resveratrol is not toxic to healthy cells, and has multiple molecular targets in various

pathways, so chemoresistance-inducing mutations may be overcome (Kraft et al., 2009). These factors make resveratrol a promising chemotherapeutic candidate.

However, the bioavailability of resveratrol is low, which could interfere with its successful application *in vivo* (Hogg et al., 2015; Kraft et al., 2009). The results of *in vivo* studies investigating the effects of resveratrol are somewhat inconsistent: in some experiments, a chemo-preventative effect is observed, while in others there is no observable benefit to treatment with resveratrol (Baur & Sinclair, 2006). It is therefore difficult to draw strong conclusions about the efficacy of resveratrol as an anti-tumour compound.

1.9 Cell line selection

In the present study, the effects of resveratrol on ovarian cancer growth and progression are investigated using two cell lines: OVCAR-8, and SKOV-3. Due to the highly heterogenous nature of ovarian cancer, it is important that appropriate cell lines are selected. Diversity among these cancer cell lines is important, as it is necessary to investigate a range of subtypes and cell lines in order to evaluate the efficacy of the treatment overall. The OVCAR-8 cell line has been reported to possibly represent the most common subtype of ovarian cancer: high-grade serous (Domcke, Sinha, Levine, Sander, & Schultz, 2013). The SKOV-3 cell line is still widely used in ovarian cancer research; however, is no longer believed to be representative of the high-grade serous subtype (Domcke et al., 2013). Nonetheless, it still presents a useful study tool, as results from this cell line can be compared with results from cell lines that are likely to be ovarian in origin.

1.10 Hypotheses and aims

The progression of advanced ovarian cancer is a complex process that is poorly understood, and this limits our understanding of the biology of this disease. To advance our understanding of the biology underlying advanced ovarian cancer, a pre-clinical model system that attempts to replicate the natural environment of tumours in the body, while still being reasonably simple, is essential.

In the context of advanced ovarian cancer, ideal anticancer compounds should be cost-effective, readily available, and have minimal to no adverse side effects, while still being effective at slowing the development of advanced ovarian tumours.

I hypothesise that resveratrol will inhibit the growth of ovarian tumours in the CAM model.

1.10.1 Aims

To study the effects of resveratrol on ovarian cancer growth and progression using the CAM model.

To study the effect of resveratrol on the number of red blood cells present in tumour implants.

To study the effect of resveratrol on secretion of VEGF.

To study the effect of resveratrol on invasion of tumour cells.

To study the effect of resveratrol on expression of Ki67.

To study the effect of resveratrol on apoptosis.

2 Materials and Methods

2.1 Materials

2.1.1 General solutions, buffers, and media

2.1.1.1 1x Phosphate-buffered saline (PBS)

1x PBS was prepared using 137 mM sodium chloride (NaCl), 10 mM disodium phosphate (Na_2HPO_4), 1.76 mM monopotassium phosphate (KH_2PO_4), 2.7 mM potassium chloride (KCl), hydrochloric acid (HCl) to adjust pH to 7.4 and Milli Q water to make a final volume of 1 L.

2.1.1.2 10x Trypsin-ethylenediaminetetraacetic acid (trypsin-EDTA)

10x Trypsin-EDTA was prepared by dissolving 1 mM Trypsin powder and 25.7 mM EDTA in 1x PBS. pH was adjusted to 8 using sodium hydroxide. Final volume was 200 mL.

2.1.1.3 Dulbecco's modified Eagle medium (DMEM)

DMEM base media prepared up using one packet of Alpha medium and 44 mM sodium bicarbonate ($NaHCO_3$) in 1 L Milli Q water. pH was adjusted to between 7.1 and 7.3 using sodium hydroxide (NaOH). This media was then filtered in a cell culture laminar flow cabinet.

This base media was supplemented with 100 mL D-FBS, PenStrep antibiotics at a concentration of 100 units/mL penicillin and 100 µg/mL (172 µM) streptomycin, 2 mM GlutaMAX, and 0.2 µM Fungizone. This solution is hereafter referred to as 'working media'.

2.1.1.4 Fixing solution

Fixing solution was prepared using 4 g paraformaldehyde and 100 mL 1x PBS.

2.1.2 H&E staining solutions and buffers

2.1.2.1 Scott's tap water

Scott's tap water was prepared by dissolving 41.7 mM sodium bicarbonate ($NaHCO_3$) and 166 mM magnesium sulphate ($MgSO_4$) in 1 L Milli Q water.

2.1.2.2 Differentiation buffer

Differentiation buffer was prepared using 70 mL 100% ethanol and 30 mL Milli Q water.

2.1.2.3 Eosin

Eosin solution was prepared using 3.8 mM eosin Y stock, 80 mL Milli Q water, 320 mL 95% ethanol, and 0.4 mL acetic acid.

2.1.3 Immunohistochemistry solutions and buffers

2.1.3.1 Antigen retrieval buffer

Antigen retrieval buffer was prepared by dissolving 20 mM Tris base in Milli Q water and adjusting pH to 9 using EDTA. Final volume was 2 L.

2.1.3.2 Membrane permeabilization buffer

Membrane permeabilization buffer was prepared using 100 mL 1x PBS and 0.1 mL Triton X-100.

2.1.3.3 Wash buffer

Wash buffer was prepared using 1 L 1x PBS and 1 mL Tween 20.

2.1.3.4 Kit (ab93705)

Mouse and Rabbit Specific HRP/AEC (ABC) Detection IHC Kit, purchased from ABCAM, contains:

- AEC Single Solution
- Biotinylated Goat Anti-Polyvalent
- Hydrogen Peroxide Block
- Protein Block
- Streptavidin-Peroxidase

2.1.3.5 Bovine serum albumin (BSA)

4% BSA was prepared using 100 mL 1x PBS and 4 g BSA

2.1.4 TUNEL assay solutions

2.1.4.1 2 M Tris-HCl (pH 7.8)

2 M Tris-HCl was prepared by dissolving 2 M Tris base in Milli Q water and adjusting pH to 7.8 using concentrated HCl. Final volume was 100mL.

2.1.4.2 1x Tris-buffered saline (TBS)

1x TBS was prepared using 10 mL 2 M Tris-HCl (pH 7.8), 140 mM NaCl and 1 L Milli Q water.

2.1.4.3 Kit (ab206386)

TUNEL assay kit – HRP-DAB, purchased from ABCAM, contains:

- 25x Conjugate
- Blocking Buffer
- DAB Solution 1 (DAB concentrate)
- DAB Solution 2 (substrate reaction buffer)
- Methyl green counterstain

- Proteinase K
- Stop Buffer
- TdT Enzyme
- TdT Equilibration Buffer
- TdT Labelling Reaction Mix

2.2 Methods

2.2.1 Frozen tissue sections

2.2.1.1 Preparation of frozen samples

Tumour implants, grown from OVCAR-8 or SKOV-3 cancer cells, and surrounding CAM were provided by my co-supervisor, Dr Chitcholtan. These were prepared using cancer cells (OVCAR-8, SKOV-3) encapsulated in collagen gels and fertilised chicken eggs. On day four of embryonic development, a hole was cut in the shells of the eggs. The shell was then resealed using sterile sticky tape and the eggs were returned to the incubator until day eight of embryonic development. On day eight, CAMs were inoculated with cancer cells. These were left to grow until day twelve of embryonic development, when treatment with resveratrol commenced. On embryonic development day eighteen, the tumour implants were excised from the surrounding CAMs and then fixed at 4ºC overnight.

Fixing solution was removed and replaced with approximately 2 mL 1x PBS. Samples were then gently shaken for five minutes to rinse the samples. This rinsing process was repeated twice with fresh 1x PBS.

The CAM around the tumour implants was carefully trimmed using a scalpel blade, then the sample was embedded vertically in optimal cutting temperature (OCT) compound (Tissue-Tek), ensuring that no air bubbles were present in the OCT compound. Samples were frozen at -80ºC for at least 30 minutes before being transferred to a -20ºC freezer for storage.

2.2.1.2 Frozen sectioning

SuperFrost Plus slides were appropriately labelled using pencil, and a chuck and block were placed on dry ice to bring down the temperature so that OCT compound would begin to freeze solid on contact. OCT compound was used to securely mount the frozen sample onto the chuck, and the sample and chuck were kept on dry ice for several minutes to ensure the OCT compound was completely frozen.

The sample and chuck were then loaded into a cryostat (Leica) set to -20ºC and sectioned. Three sections of the tumour implants, each 7 µm thick were placed on each slide, and seven slides were collected per frozen sample. Slides were stored at -20ºC until needed.

2.2.2 H&E staining

Frozen slides were allowed to dry at 37ºC for approximately ten minutes to remove any moisture before samples were outlined using a mini PAP pen containing hydrophobic ink (ABCAM).

After the ink had dried completely, samples were covered with approximately 300 µL Harris' haematoxylin and incubated at room temperature for 20 minutes. Slides were rinsed using Scott's tap water until the water ran clear (approximately five times). Slides were then rinsed using differentiation buffer five times. The samples were covered with 300 µL Scott's tap water and incubated at room temperature for two minutes. The samples were then covered with 300 µL eosin and incubated at room temperature for ten minutes. Slides were rinsed using Scott's tap water until the eosin stopped streaking (approximately three times).

The samples were then dehydrated by sequentially dipping the slides in 50% ethanol ten times, 70% ethanol ten times, then immersing in 95% ethanol for 30 seconds, 100% ethanol for one minute, and finally dipped in 100% xylene ten times. Slides were allowed to dry completely before a coverslip was mounted using DPX Mountant mounting media.

2.2.2.1 Counting red blood cells

A micrograph was taken near the centre of each implant using a 10x objective lens (Zeiss; numerical aperture: 0.25). The area of the implant visible in the photo was determined using Zen software. The red blood cells visible within this area were counted manually, and then expressed as a number of red blood cells per mm^2.

2.2.2.2 Counting invasive cells

Cancer cells located inside the mesodermal region of the CAM of each implant were manually counted by observation through a microscope using a 40x objective lens (Zeiss; numerical aperture: 0.65).

2.2.3 Immunohistochemical staining

2.2.3.1 Cell cultures

Human cancer cell lines derived from ovarian adenocarcinoma patients, OVCAR-8 and SKOV-3, were provided by Dr Chitcholtan. Both cell lines were maintained continuously in 5 mL working media in 25 mL culture flasks in a 5% CO_2 incubator at 37^{o}C. All subculturing and experimental procedures were carried out under sterile conditions in a cell culture laminar flow cabinet.

Working media was replaced with warmed, fresh working media every two to three days. Confluency was determined using a light microscope; when cells were 60 – 80% confluent, cells were subcultured.

To subculture, the media was discarded, and the flask was rinsed with sterile 1x PBS. 4 mL sterile 1x Trypsin-EDTA was added to the flasks, and flasks were incubated at 37^{o}C for approximately 15 – 20 minutes, until no cells remained adhered to the bottom of the flask. The contents of the flasks were transferred to centrifuge tubes, and the flasks were rinsed with approximately 2 mL sterile 1x PBS, which was also transferred to the centrifuge tubes. Cells were centrifuged at 2500 rpm for five minutes. The supernatant was discarded, and the cell pellets were resuspended in 5 mL warmed, fresh working media. 1 mL of the resulting cell suspension was added to a new culture flask along with 5 mL warmed, fresh working media.

2.2.3.2 Immunohistochemical analysis

The solution used to fix cells and tissue samples was paraformaldehyde, which is a cross-linking agent. Antibodies may not recognise cross-linked antigens, and so will not necessarily bind to their target proteins. This leads to a lack of staining, and so an antigen retrieval step was required prior to immunohistochemical analysis in this case.

Slides were submerged in approximately 500 mL antigen retrieval buffer, heated to 95ºC for 20 minutes. The temperature of the buffer was monitored during this time: the temperature was not allowed to exceed 95ºC while the slides were submerged, as rigorous boiling can damage samples, and if the temperature dropped below 90ºC the samples were temporarily removed until the temperature reached 95ºC again.

Slides were allowed to cool and dry completely and were then rinsed five times using wash buffer before samples were outlined using hydrophobic ink.

Membrane permeabilization was required for antibodies to gain access to their target antigens. After the ink had dried completely, samples were covered with 300 µL membrane permeabilization solution and incubated at room temperature for 20 minutes. Slides were then rinsed five times using wash buffer.

To block endogenous peroxidase activity, samples were covered with approximately 300 µL peroxide block. Slides were incubated at room temperature for ten minutes, then rinsed four times using wash buffer.

Samples were then covered with approximately 300 µL protein block. Then, slides were incubated at room temperature for ten minutes, and then rinsed twice using wash buffer.

After protein blocking, samples were covered with approximately 300 µL of the appropriate dilution of primary antibody in 4% BSA, and then were incubated at 4ºC overnight. To rinse samples, slides were submerged in wash buffer, which was agitated using a magnetic stirring bar, for 20 minutes.

Next, samples were covered with approximately 300 µL biotinylated goat anti-polyvalent. Slides were incubated at room temperature for ten minutes, then slides were submerged in wash buffer with a magnetic stirring bar for 20 minutes.

Samples were subsequently incubated with approximately 300 µL secondary antibody (streptavidin), conjugated to horseradish peroxidase for ten minutes at room temperature, then slides were submerged in wash buffer with a magnetic stirring bar for 20 minutes.

Finally, samples were covered with approximately 300 µL chromogenic AEC single solution. Slides were incubated at room temperature for ten minutes, then rinsed five times using wash buffer.

Samples were covered with approximately 300 μL haematoxylin. Slides were incubated at room temperature for 20 minutes, then rinsed using water until the water ran clear (approximately five times). Haematoxylin stains nuclei, and can sometimes overpower positive staining of nuclear antigens, including Ki67. For this reason, counterstaining with haematoxylin was omitted for this antibody.

Slides were allowed to dry completely before a coverslip was mounted. The mounting media DPX Mountant is suitable for slides stained with haematoxylin and eosin,

but it was found to be quite harsh and degraded the brown stain that indicated positive immunohistochemical staining, which caused the staining to be lost when the coverslip was mounted. For this reason, this process was repeated with a milder mounting media, ImmunoHistoMount, to facilitate retention of the visible positive stain for analysis. A micrograph was taken near the centre of each implant using a 10x objective lens (Zeiss; numerical aperture: 0.25) for analysis.

2.2.3.3 Controls (cell monolayers)

Slides with eight plastic wells affixed were used for controls and optimisation of antibodies. Cell monolayers (OVCAR-8, SKOV-3) were grown in each of these wells.

The protocol for immunohistochemical analysis was the same as described above (2.2.3.2), except a serial dilution of primary antibody was used (1/200, 1/400, 1/800), with two wells dedicated to each dilution factor to establish the optimum dilution factor of each antibody.

It was determined that the optimum dilution factor for both the VEGF and Ki67 antibodies was 1/200. The optimum dilution factor for the CD31 antibody used was determined by the manufacturer as being 1/50.

Negative controls were incubated overnight at 4ºC with 4% BSA only.

2.2.4 TUNEL assay

2.2.4.1 Frozen sections

Frozen slides were allowed to dry at 37ºC to remove any moisture before samples were outlined using a mini PAP pen. After the ink had dried completely, samples were covered with 300 µL 1x TBS and incubated at room temperature for 15 minutes.

1 µL Proteinase K solution was mixed with 99 µL water for each slide being analysed. Samples were covered with this solution and incubated at room temperature for no longer than ten minutes. Slides were then rinsed in 1x TBS for five minutes.

To block endogenous peroxidase activity, 10 µL 30% hydrogen peroxide was mixed with 90 µL 100% methanol for each slide being analysed. Samples were covered with this solution and incubated at room temperature for five minutes, and then slides were rinsed in 1x TBS for five minutes.

Next, samples were covered with 100 µL Equilibration Buffer and incubated at room temperature for 30 minutes.

To label cells containing fragmented DNA, 1 µL TdT Enzyme solution was mixed with 39 µL TdT Labelling Reaction Mix for each slide being analysed. Samples were covered with this solution and a coverslip was applied. Slides were incubated in a humidified chamber at 37ºC for 90 minutes, following which the coverslips were carefully removed by submerging slides in 1x TBS, and then slides were rinsed in 1x TBS for five minutes.

To stop the labelling reaction, samples were subsequently covered with 100 µL Stop Buffer and incubated at room temperature for ten minutes. Slides were then rinsed in 1x TBS for five minutes.

Next, samples were covered with 100 µL Blocking Buffer and incubated at room temperature for ten minutes, then slides were rinsed in 1x TBS for five minutes.

4 µL 25x Conjugate solution was mixed with 96 µL Blocking Buffer for each slide being analysed and samples were subsequently covered with this solution and incubated at room temperature for 30 minutes.

For chromogenic labelling of TUNEL-positive cells, 4 µL DAB Solution 1 was mixed with 116 µL DAB Solution 2 for each slide being analysed. Samples were covered with this solution and incubated at room temperature for 15 minutes and were then rinsed in water until the water ran clear (approximately three times).

Finally, samples were covered with 100 µL Methyl Green Counterstain and incubated at room temperature for 20 minutes. Slides were dipped in 100% ethanol four times, and then this was repeated with fresh ethanol. Slides were then dipped in 100% xylene four times and then allowed to dry completely before a coverslip was mounted using ImmunoHistoMount mounting media.

A micrograph was taken near the centre of each implant using a 10x objective lens (Zeiss; numerical aperture: 0.25) for analysis.

2.2.4.2 Controls (cell monolayers)

Samples were covered with 300 µL 1x TBS and incubated at room temperature for 15 minutes.

1 µL Proteinase K solution was mixed with 99 µL 10 mM Tris (pH 7.8) for each slide being analysed. Samples were covered with this solution and incubated at room temperature for no longer than five minutes. Slides were then dipped in 1x TBS three times.

The remainder of the protocol was the same as for the frozen sections (above, 2.2.4.1).

For positive controls, the working media was supplemented with 1 µM paclitaxel. Cells were incubated at 37ºC for two days to allow cells to grow, and then fixed at 4ºC overnight.

For negative controls, the protocol was the same as for positive controls, except treatment with paclitaxel was omitted.

2.2.5 Analysis of images (ImageJ)

2.2.5.1 Samples stained for VEGF

Brightness was adjusted to remove some of the background, then colours were deconvoluted to separate haematoxylin staining from AEC staining and noise. The image showing AEC staining was then converted to black and white. The region of interest was selected and measured, which provided the mean grey value for the selected area. Mean grey values were the sum of grey values of all pixels within the selection, divided by the number of pixels.

2.2.5.2 Samples stained for Ki67

Brightness was adjusted to remove some of the background, then the background was subtracted, and the remaining image was converted to black and white. The region of interest was selected and measured, which provided the mean grey value for the selected area.

2.2.5.3 Samples on which a TUNEL assay was performed

Brightness was adjusted to remove some of the background, then colours were deconvoluted to separate methyl green staining from DAB staining and noise. The image showing DAB staining was then converted to black and white. The region of interest was selected and measured, which provided the mean grey value for the selected area.

2.2.6 Statistical analysis

Statistical analyses were performed using GraphPad Prism software. Experimental results were assessed for significance using a two-tailed t-test and a one-way ANOVA. $p < 0.05$ was used as a measure of statistical significance.

3 Results and Discussion

3.1 Morphology of tumour implants grown on CAMs

In order to evaluate the growth of OVCAR-8 and SKOV-3 tumour cells implanted on CAMs, the morphology of these tumour implants and their associated vascular networks were investigated.

OVCAR-8 cells were encapsulated in collagen gels and placed on the surface of CAMs. Cancer cells were then allowed to grow for six days (Fig. 3.1 and 3.2). The vascular networks of the CAMs surrounding the tumour implants are visible (Fig. 3.1), although it is not possible to visually distinguish between the control implants (A) and implants treated with resveratrol (B – E). The vascular networks underneath the implants are more readily visible when the implants have been removed from the surrounding CAM and inverted (Fig. 3.2). Again, there are no apparent differences between the control implants (A) and those treated with resveratrol (B – F).

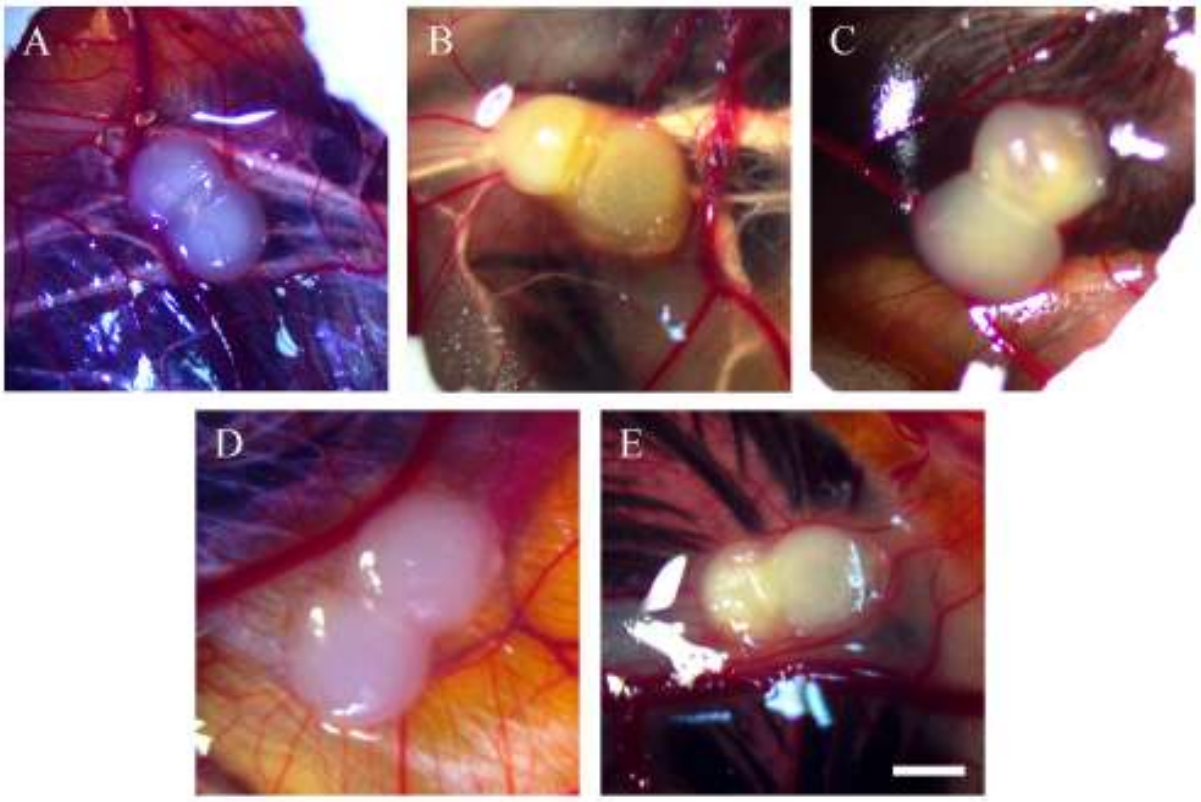

Figure 3.1 Stereomicroscopic images of OVCAR-8 tumour implants after 18 days growth on CAMs. *Tumour implants were treated with various doses of resveratrol for six days, starting at day 12 of embryonic development, and then images were taken. Control (A), 0.3 µg (B), 0.5 µg (C), 46 µg (D), 91 µg resveratrol (E). Scale bar, 1 mm.*

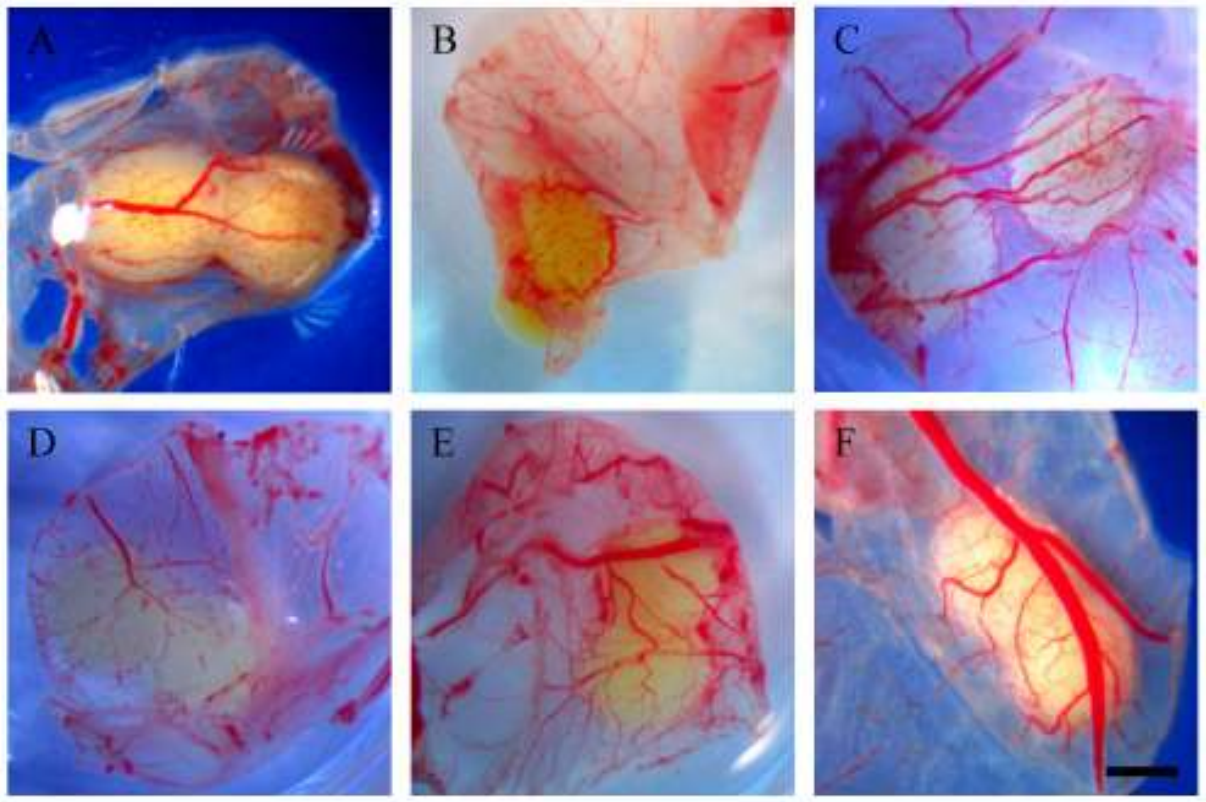

Figure 3.2 Stereomicroscopic images of excised and inverted OVCAR-8 tumour implants after 18 days growth on CAMs. *Tumour implants were excised from surrounding CAM and inverted so the vascular networks could be viewed from underneath. Control (A), 0.3 µg (B), 0.5 µg (C), 46 µg (D), 91 µg (E), 183 µg resveratrol (F). Scale bar, 1 mm.*

Using the same method utilised for OVCAR-8 cells, SKOV-3 cells captured in collagen gels were placed on CAMs and allowed to grow for six days (Fig. 3.3 and 3.4). The vascular networks of the CAMs are visible from above (Fig. 3.3), but the control implants (A) show no differences compared to those treated with resveratrol (B – E). Again, the vascular networks beneath implants are more easily observable when the implants are cut out from the surrounding CAM and viewed from underneath (Fig. 3.4). Again, there were no obvious differences between control implants (A) and resveratrol treated implants (B – D).

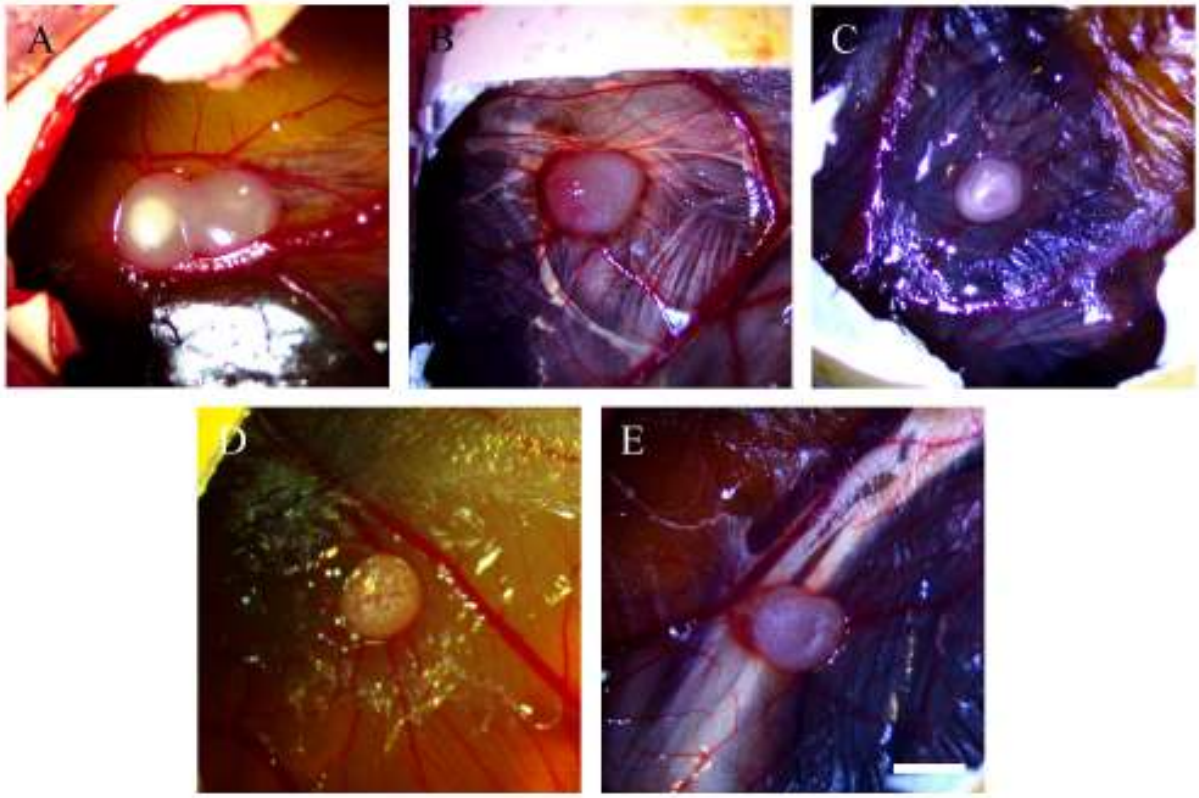

Figure 3.3 Stereomicroscopic images of SKOV-3 tumour implants after 18 days growth on CAMs. *Tumour implants were treated with various doses of resveratrol for six days, starting at day 12 of embryonic development, and then images were taken. Control (A), 0.3 µg (B), 0.5 µg (C), 46 µg (D), 91 µg resveratrol (E). Scale bar, 1 mm.*

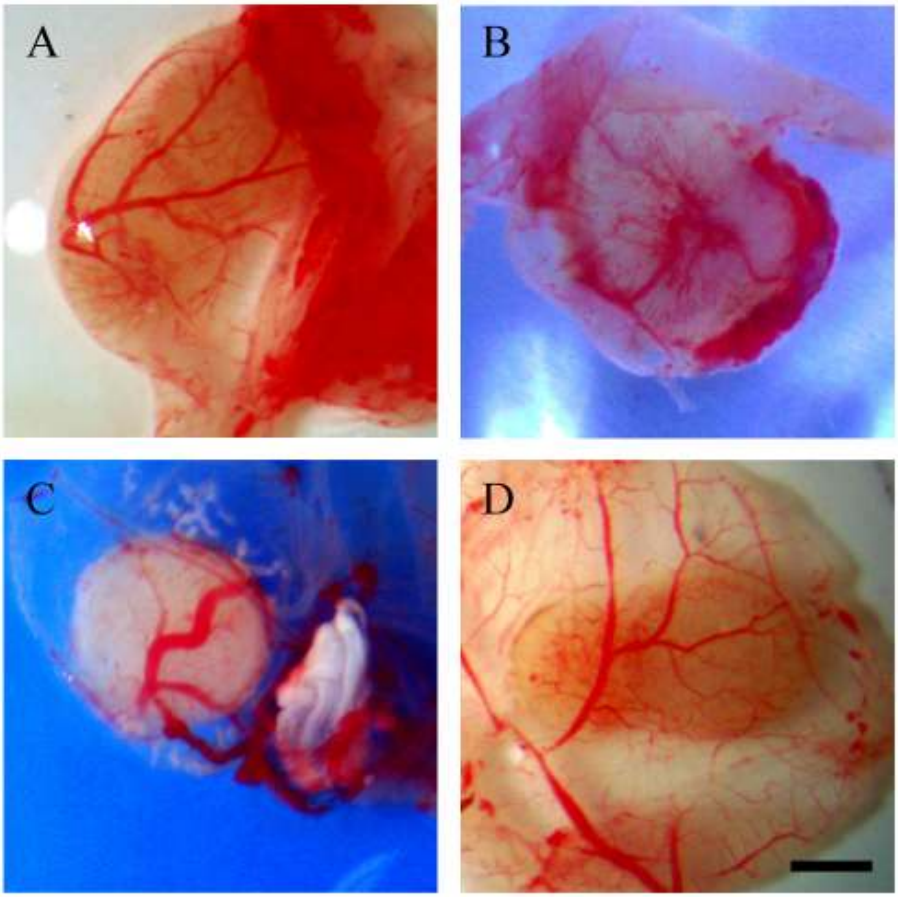

Figure 3.4 Stereomicroscopic images of excised and inverted OVCAR-8 tumour implants after 18 days growth on CAMs. *Tumour implants were excised from surrounding CAM and inverted so the vascular networks could be viewed from underneath. Control (A), 0.3 µg (B), 46 µg (C), 91 µg resveratrol (D). Scale bar, 1 mm.*

3.2 Number of red blood cells found in tumour implants

The number of red blood cells found in the tumour implants is indicative of the degree to which angiogenesis has occurred, as more extensive angiogenesis is likely to lead to the presence of a greater number of red blood cells. As a result, counting the red blood cells can provide an indirect measure of angiogenesis. Staining with haematoxylin and eosin makes red blood cells stand out from cancer cells, and so facilitates counting of red blood cells.

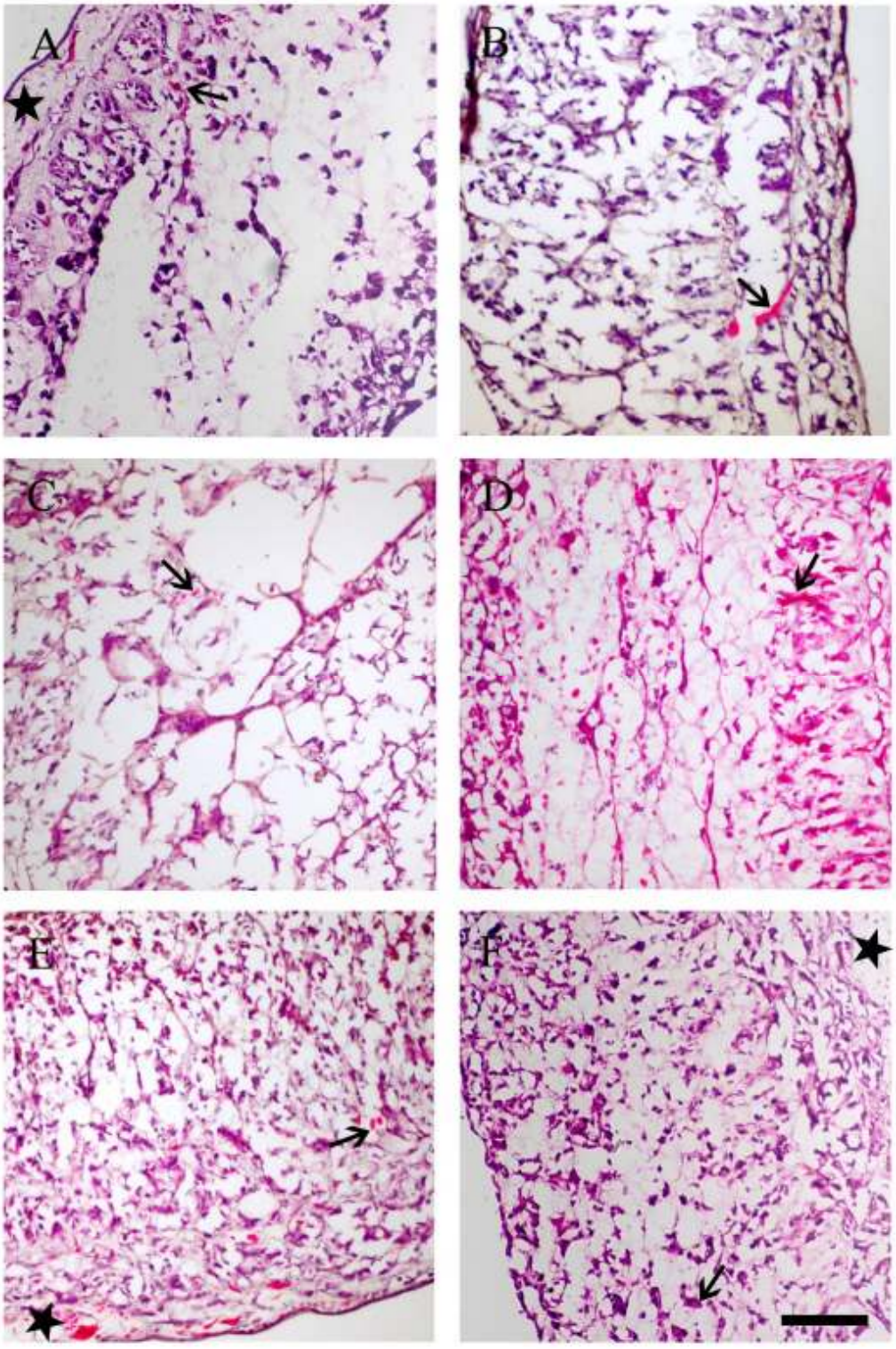

Figure 3.5 Microscopic images of tumour implants (OVCAR-8) after six days of treatment with varying doses of resveratrol showing red blood cells present in implants (arrows). *Treatment with 46 µg resveratrol led to reduced numbers of red blood cells in implants (see Fig. 3.7). Control (A), 0.3 µg (B), 0.5 µg (C), 46 µg (D), 91 µg (E), 183 µg (F) resveratrol. Stars indicate CAM area. Scale bar, 200 µm.*

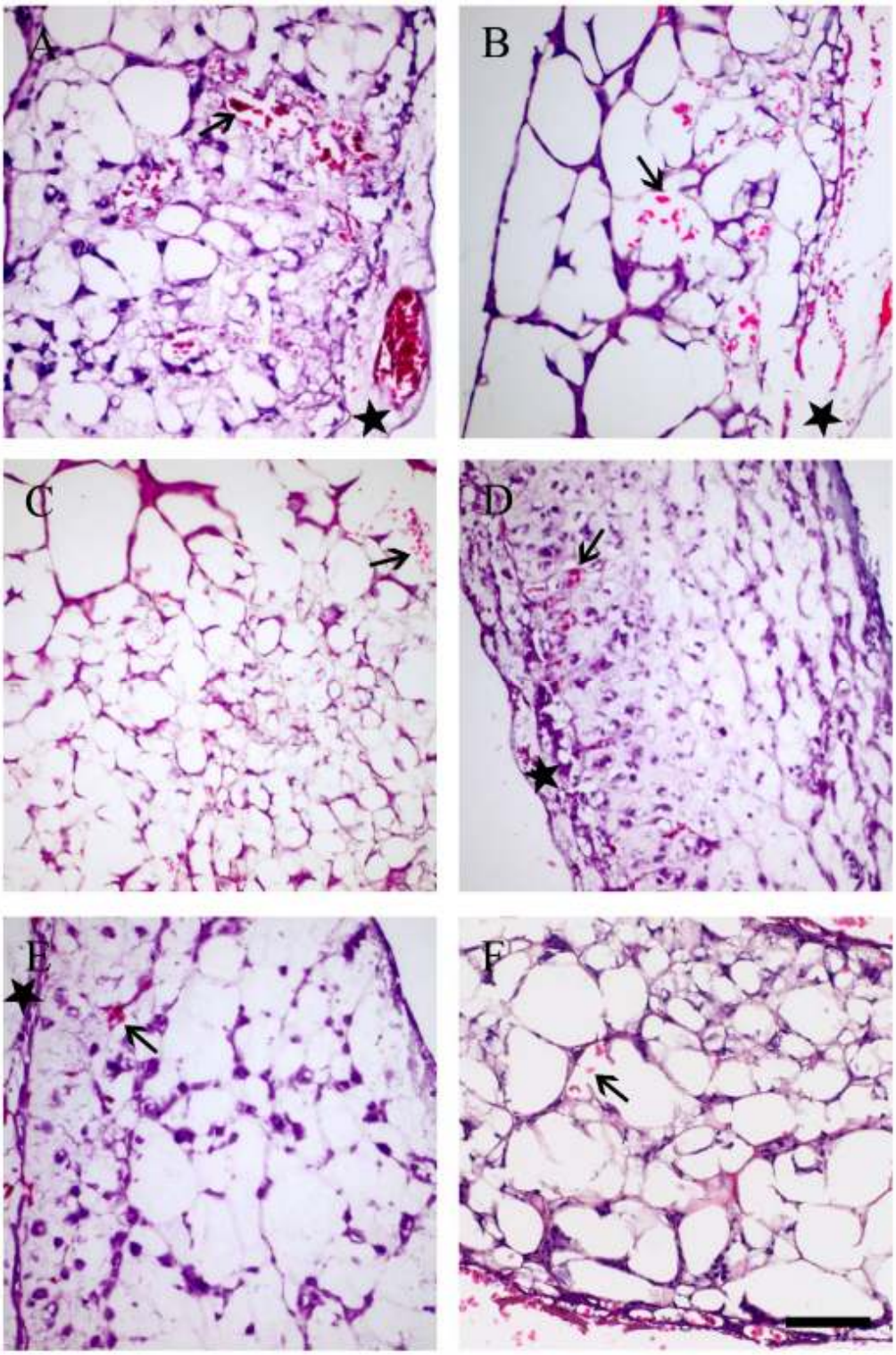

Figure 3.6 Microscopic images of tumour implants (SKOV-3) after six days of treatment with varying doses of resveratrol showing red blood cells present in implants (arrows). *Treatment with 91 µg resveratrol led to reduced numbers of red blood cells in implants (see Fig. 3.7). Control (A), 0.3 µg (B), 0.5 µg (C), 46 µg (D), 91 µg (E), 183 µg (F) resveratrol. Stars indicate CAM area. Scale bar, 200 µm.*

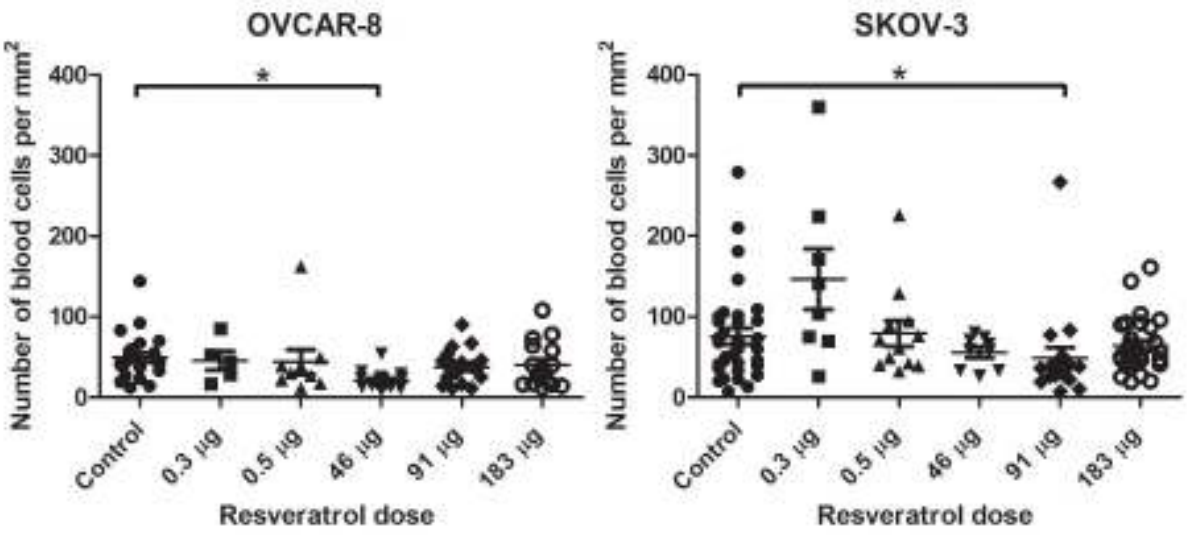

Figure 3.7 Number of red blood cells present in tumour implants (OVCAR-8 (n = 85) and SKOV-3 (n = 109)) after six days of treatment with varying doses of resveratrol. *Numbers of red blood cells were significantly reduced in OVCAR-8 implants treated with 46 µg resveratrol, and in SKOV-3 implants treated with 91 µg resveratrol. Data expressed as means ± SEM. Data considered statistically significantly compared to controls are indicated as $p < 0.05$ (*).*

In OVCAR-8 implants, a significant decrease in the number of red blood cells per mm^2 was observed when implants were treated with 46 µg resveratrol compared with control implants ($p < 0.0001$, t-test) (Fig. 3.7). In SKOV-3 implants, treatment with 91 µg resveratrol led to a significant decrease in the number of red blood cells present relative to controls ($p = 0.0131$, t-test) (Fig. 3.7).

These results suggest that, at certain concentrations, resveratrol can lead to the presence of significantly fewer red blood cells in tumour implants, possibly due to the inhibition of angiogenesis. For both cell lines tested, there seems to be an optimum dose of resveratrol, at which a statistically significant reduction in the number of red blood cells present in the tumour implants is observed. Doses above or below this optimum dose may have no effect on the number of red blood cells present in implants or may increase the number of red blood cells. This suggests that while some doses of resveratrol may suppress angiogenesis in these tumour implants, some doses of resveratrol may actually support angiogenesis.

In the literature, multiple studies describe resveratrol as having an anti-angiogenic effect, particularly when it is administered at high doses (Chen & Tseng, 2007). One study using rat malignant glioma cells (RT-2) found that treatment with 40 mg/kg/day of resveratrol led to reduced micro-vessel density after 21 days of treatment, but not after 14 days of treatment (Tseng et al., 2004). This is in contrast to treatment with 10 mg/kg/day of resveratrol, for which they observed had no effect on micro-vessel density (Tseng et al., 2004). Another study investigating the effect of resveratrol on angiogenesis in human umbilical vein endothelial cells found that treatment with 100 or 500 µM resveratrol for 24 hours inhibited tube formation, whereas treatment with 10 or 50 µM had no effect (J. C. Wong & Fiscus, 2015). These results suggest that both dose and exposure time are factors which can impact the anti-angiogenic effect of resveratrol.

An *in vivo* study using pancreatic cancer (MIA PaCa-2) xenografts in a mouse model observed reduced micro-vessel density in mice that had been treated with 40 mg/kg/day resveratrol for 28 days compared with controls (Harikumar et al., 2010). A similar study using ovarian cancer (PA-1) xenografts in a mouse model found that treatment with 50 or 100 mg/kg/day resveratrol for 28 days led to a dose-dependent reduction in micro-vessel density (Lee et al., 2009). A different research group used the CAM model to investigate the effects of resveratrol on angiogenesis and found that the addition of discs containing 25, 50, or 100 µg resveratrol for 48 to 72 hours induced the formation of avascular zones in the developing CAMs (Brakenhielm, Cao, & Cao, 2001).

The data from the present study are generally in agreement with the literature, as low resveratrol doses have varied effects on the number of red blood cells present, whereas the optimum dose, which leads to a decrease in red blood cell counts, is a higher dose. However, it is not clear why doses higher than the optimum do not lead to reduced red blood cell counts. Some research suggests that under some circumstances, resveratrol may actually have a pro-angiogenic effect, although this effect is not typically observed in the context of tumour angiogenesis (Chen & Tseng, 2007).

It is worth noting that the number of red blood cells present in tumour implants provides only an indirect measure of angiogenesis. Therefore, these data may not provide an accurate representation of the true extent of angiogenesis in these implants.

3.2.1 Immunostaining of CD31 in tumour implants

Immunostaining for proteins that are known to have a role in angiogenesis represents an alternative method of quantifying angiogenesis in tumour implants. CD31, or platelet endothelial cell adhesion molecule (PECAM)-1, is highly expressed on the surface of endothelial cells and its involvement in monitoring vessel density in tumour tissue is well established (DeLisser et al., 1997; Schlüter et al., 2018). It is an endothelial cell-cell adhesion molecule, and, as angiogenesis involves the destruction and formation of endothelial cell-cell interactions and the migration of endothelial cells, CD31 can be used as a marker of angiogenesis (DeLisser et al., 1997; Schlüter et al., 2018).

It is possible that resveratrol exerts its effect on angiogenesis via restriction of the growth and migration of endothelial cells. If this were the case, antibody staining for CD31 might have provided useful information about the effect of resveratrol on angiogenesis. However, this experiment was unsuccessful, perhaps due to improper optimisation of the antibody, insufficient affinity of the antibody for CD31, or an error in the experimental protocol, but time constraints did not permit further investigation.

Other studies suggest that CD31 staining can be a good indicator of angiogenesis. A study using pancreatic cancer (MIA PaCa-2) xenografts in a mouse model observed downregulation of CD31 in mice treated with 40 mg/kg/day resveratrol for 28 days compared with controls (Harikumar et al., 2010). It has also been shown that 28 days of treatment with 50 or 100 mg/kg/day resveratrol reduced CD31 expression in ovarian cancer (PA-1) xenografts in a mouse model (Lee et al., 2009).

3.3 Immunostaining of vascular endothelial growth factor (VEGF) in tumour implants

VEGF is a key mediator of angiogenesis, and cells that express VEGF are therefore likely to be actively involved in angiogenesis. An increase in positive staining indicates more VEGF is present in the tumour implant, which in turn suggests that more angiogenesis is occurring in that implant. VEGF, stained brown, is clearly prevalent in the tumour region of these implants (Fig. 3.8 and 3.9).

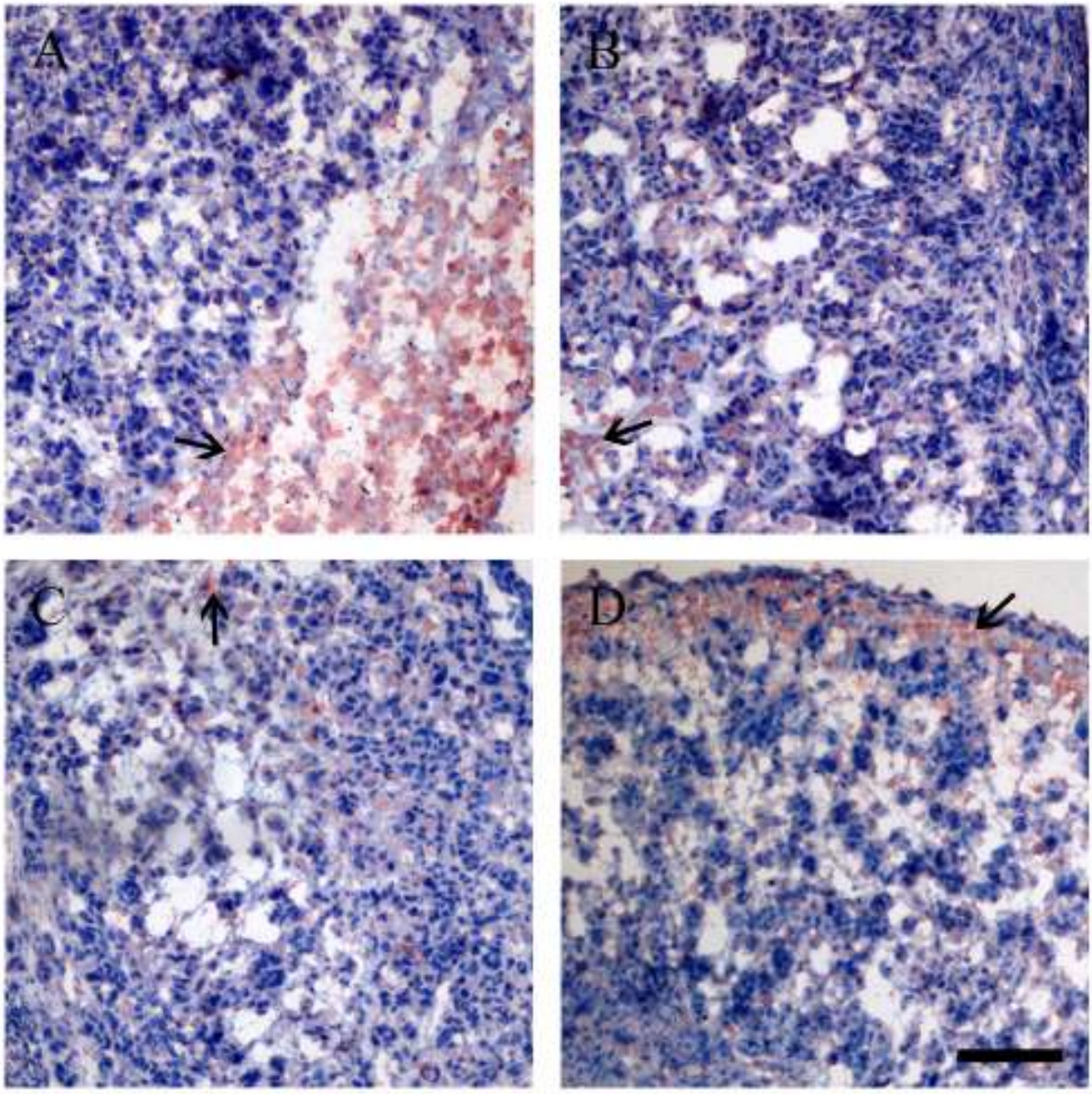

Figure 3.8 Microscopic images of tumour implants (OVCAR-8) after six days treatment with various doses of resveratrol showing staining of VEGF (arrows). *Treatment with resveratrol did not significantly alter VEGF expression in tumour implants (see Fig. 3.10). Control (A), 0.3 µg (B), 46 µg (C), 183 µg (D) resveratrol. Scale bar, 200 µm.*

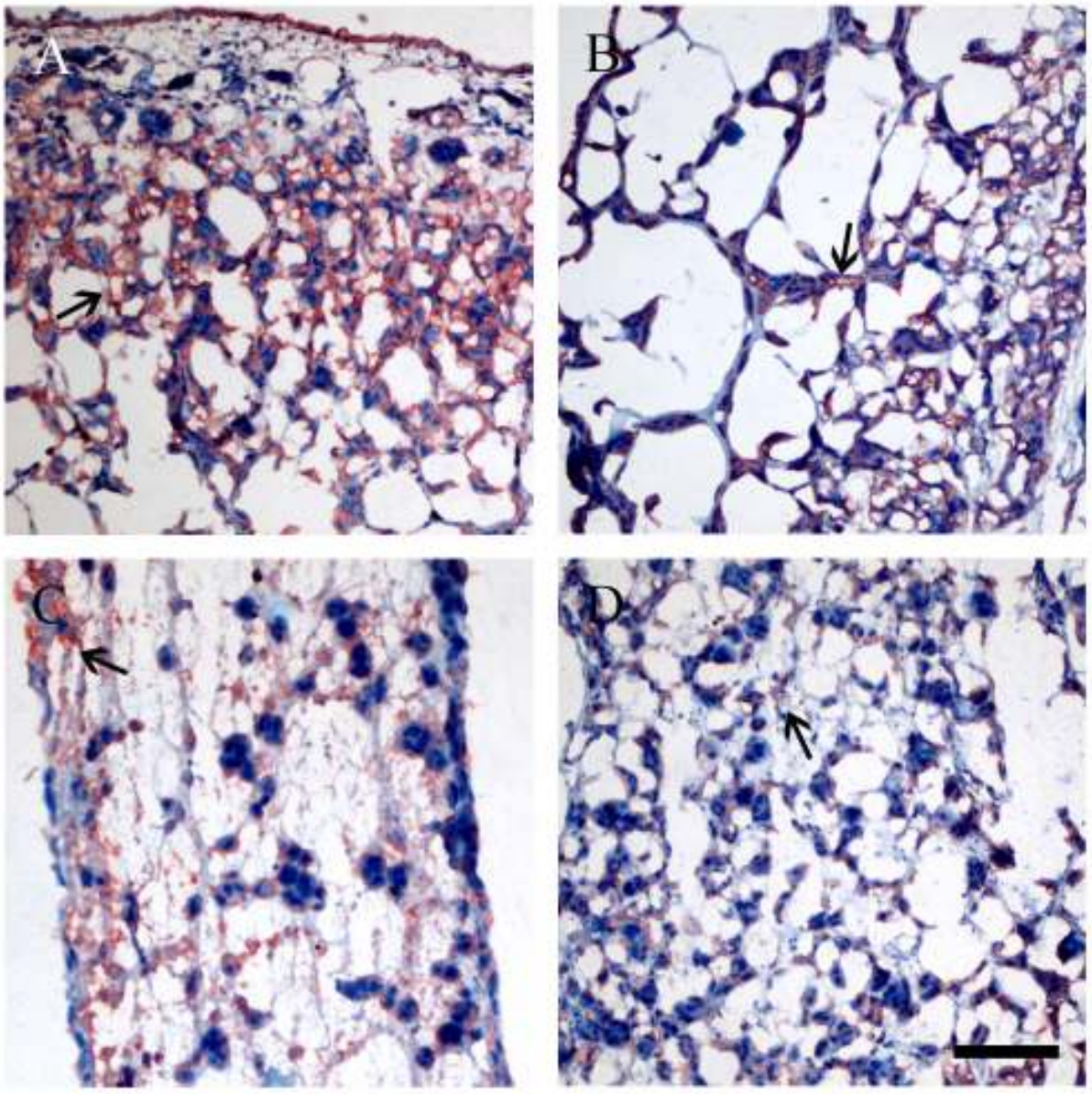

Figure 3.9 Microscopic images of tumour implants (SKOV-3) after six days treatment with different doses of resveratrol showing staining of VEGF (arrows). *Treatment with resveratrol did not significantly alter VEGF expression in tumour implants (see Fig. 3.10). Control (A), 0.3 µg (B), 91 µg (C), 183 µg (D) resveratrol. Scale bar, 200 µm.*

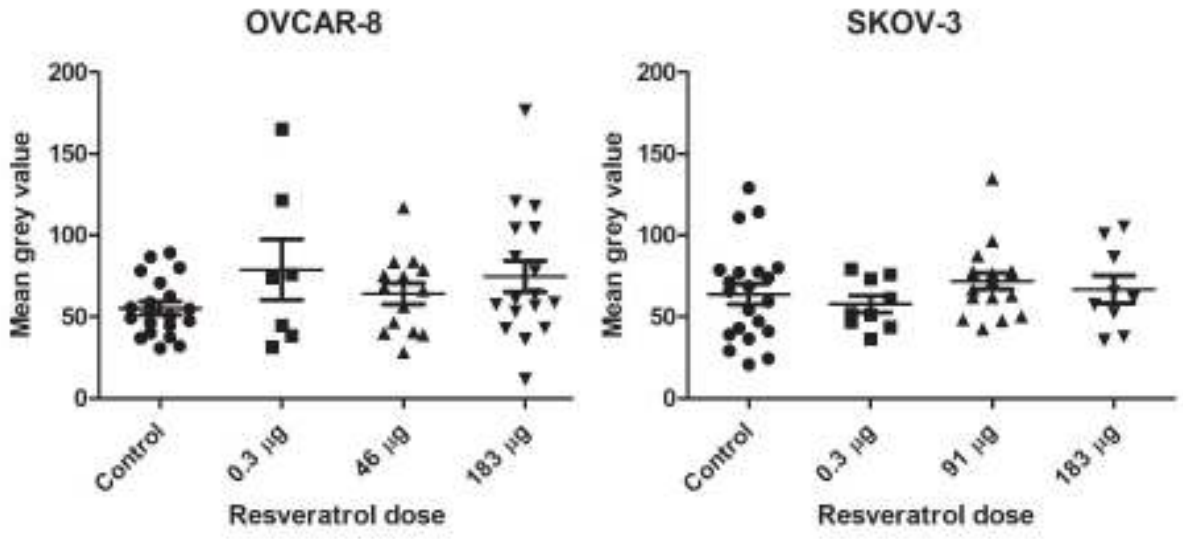

Figure 3.10 Intensity of immunohistochemical staining of VEGF in tumour implants (OVCAR-8 (n = 58) and SKOV-3 (n = 56)) after six days of treatment with various doses of resveratrol. *There is no statistically significant difference between control implants and implants treated with resveratrol ($p > 0.05$). Data expressed as means ± SEM.*

These data suggest that treatment with resveratrol did not lead to a significant effect on expression of VEGF in tumour implants, irrespective of cell line or resveratrol dose (Fig. 3.10). Many previous studies have shown that resveratrol is capable of reducing expression of VEGF and thereby inhibiting angiogenesis, so it is surprising that the present experiment showed no effect of resveratrol on VEGF expression. For example, a study investigating VEGF expression in rat glioma cells (RT-2) in response to resveratrol treatment observed that treatment with 10, 25, or 100 µM resveratrol for six, 24, or 48 hours led to suppression of VEGF expression (Tseng et al., 2004). VEGF expression in the human osteosarcoma cell line U20S was also shown to be suppressed when cells were treated with 10, 20, or 40 µM resveratrol for 24, 48, or 72 hours (Z. Liu, Li, & Yang, 2012). That study found that suppression of VEGF expression increased with increasing doses or resveratrol and increasing exposure times (Z. Liu et al., 2012).

Human retinal pigment epithelial cells treated with 10, 20, or 50 µM resveratrol for 48 hours displayed a dose-dependent reduction in VEGF secretion, whereas treatment with 2 µM resveratrol for the same time period had no effect (Nagineni et al., 2014). A similar study investigated the effects of a wider range of resveratrol doses on human gingival fibroblast cells over 48 hours (Núñez et al., 2010). Results showed that 10, 20, 40, 80, or 160 µM resveratrol suppressed VEGF in a dose-dependent manner (Núñez et al., 2010). In addition,

an *in vivo* study using human bladder cancer (T24) xenografts in a mouse model observed suppression of VEGF expression in mice treated with 20 mg/kg/day resveratrol for 28 days compared with controls (Bai et al., 2010).

Several *in vitro* experiments have used ovarian cancer cells to study the effects of resveratrol on VEGF expression. One treated A2780/CIP and OVCAR-3 cells with 12.5 – 150 μM resveratrol for six hours and observed dose-dependent inhibition of VEGF (Cao, Fang, Xia, Shi, & Jiang, 2004). Another tested the effects of treatment of OVCAR-3 and Caov-3 cells with 10, 25, or 50 μM resveratrol for 24 hours, and also found that resveratrol suppressed VEGF in a dose-dependent fashion (Park et al., 2007). Furthermore, an *in vivo* study using mice bearing Ehrlich ascites carcinoma found that treatment with 10 mg/kg/day resveratrol for seven days led to a significant inhibition of VEGF (El-Azab, Hishe, Moustafa, & El-Awady, 2011)

The results of the present study may suggest that these doses of resveratrol have no significant effect on angiogenesis in tumour implants grown using the CAM model. However, this is inconsistent with the results of the above experiment in which the number of red blood cells were reduced by some doses of resveratrol. It also seems unlikely that resveratrol has no effect on angiogenesis given the wealth of previous research indicating that resveratrol can inhibit VEGF expression and angiogenesis. It is possible that the mechanism of angiogenesis occurs somewhat differently in the CAM model with respect to VEGF expression. While VEGF is typically known to be important with respect to angiogenesis, it is not the only protein to play role in this process. (Hu et al., 2018).

Previous research has suggested that the effect of resveratrol on angiogenesis – whether it exerts a pro- or anti-angiogenic effect – may be determined by the situation (Chen & Tseng, 2007). Generally, in the context of tumour angiogenesis, resveratrol has been shown to have an anti-angiogenic effect; however, in some situations, resveratrol may support angiogenesis (Chen & Tseng, 2007; Trapp, Parmakhtiar, Papazian, Willmott, & Fruehauf, 2010). The exact reasons why resveratrol can behave differently under different circumstances are not understood, however dosage, pharmacokinetics, events, and cell types are factors that are worth considering (Chen & Tseng, 2007).

In the literature, data from experiments involving low doses (up to approximately 1.5 mg/kg/day) of resveratrol are inconsistent (Chen & Tseng, 2007; J. C. Wong & Fiscus, 2015). It is therefore possible that the doses of resveratrol administered in this experiment may not

be sufficient to exert an anti-angiogenic effect. In addition, a well-described clinical shortcoming of resveratrol is its poor bioavailability (Berman, Motechin, Wiesenfeld, & Holz, 2017; Tino, Chitcholtan, Sykes, & Garrill, 2016). Resveratrol is rapidly metabolised, primarily via glucuronidation and sulphation, giving it a short initial half-life, and the extent to which metabolites retain the activity of the parent molecule is currently unclear (Berman et al., 2017; Chen & Tseng, 2007). Resveratrol metabolites may not have as pronounced an effect, if they have any effect at all, on tumour angiogenesis as un-metabolised resveratrol.

3.4 Invasion of tumour cells into the CAM

Tumour cell invasion is indicative of the aggressiveness of tumour cells. Ovarian cancer cells often grow on the surface of the peritoneal membrane in the form of tumour nodules early during metastasis, and some cancer cells can invade through this membrane and into distant tissues. Consequently, patients with invasive tumour cells typically have poor prognoses.

The CAM model facilitates investigation into the invasiveness of tumour cells and assessment of the effect of resveratrol on this invasiveness. The number of cancer cells found inside the mesodermal layer of the CAM is reflective of the invasiveness of those cancer cells. Staining with haematoxylin and eosin colours cancer cells intensely purple, making them easily identifiable inside the CAM area.

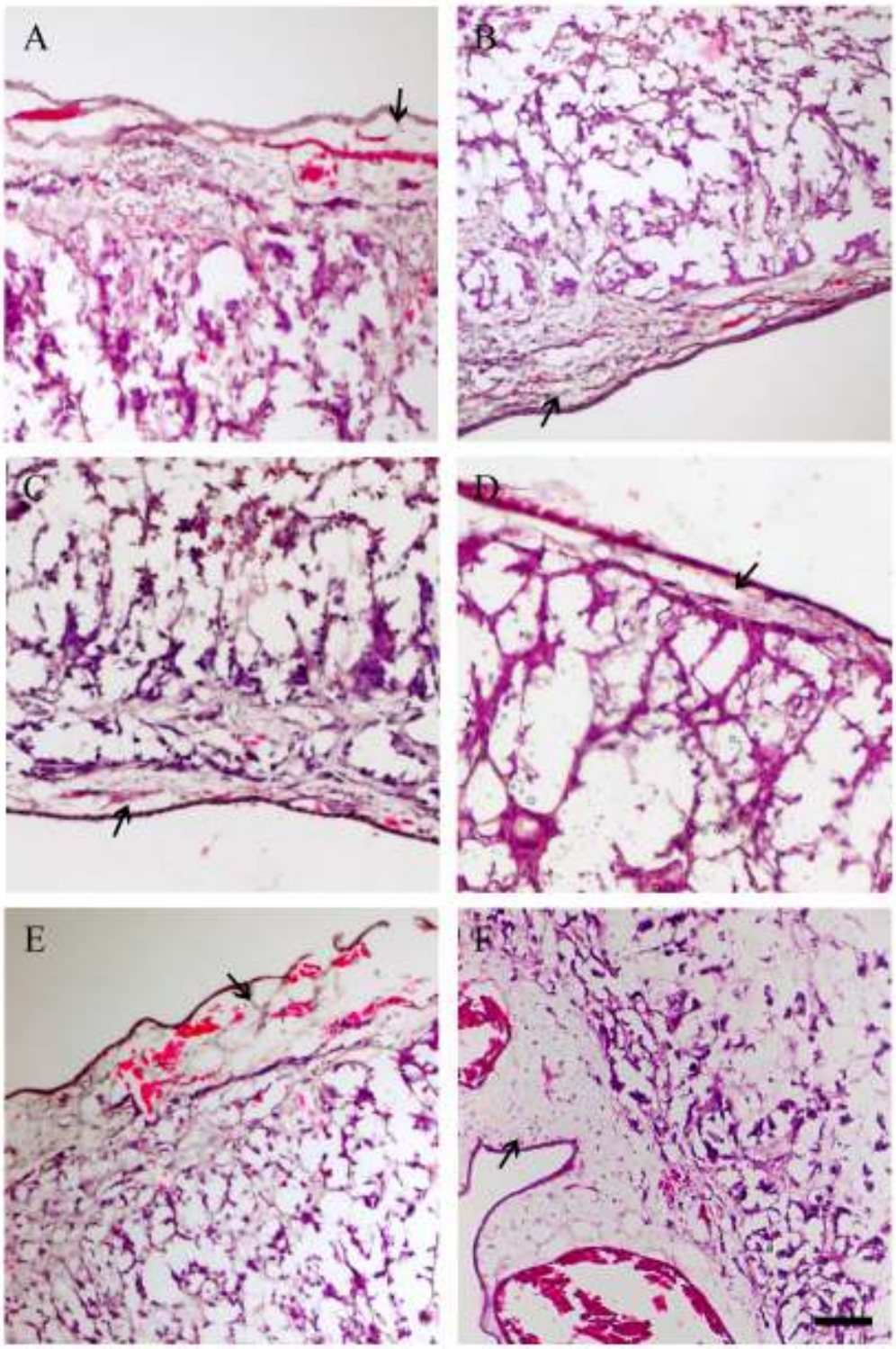

Figure 3.11 Microscopic images of tumour implants (OVCAR-8) after six days treatment with varying doses of resveratrol showing invasion of cancer cells into the mesodermal layer of CAMs (CAM area is indicated by arrows). *Treatment with 91 µg resveratrol led to reduced invasion of tumour cells into the CAM (see Fig. 3.13). Control (A), 0.3 µg (B), 0.5 µg (C), 46 µg (D), 91 µg (E), 183 µg (F) resveratrol. Scale bar, 200 µm.*

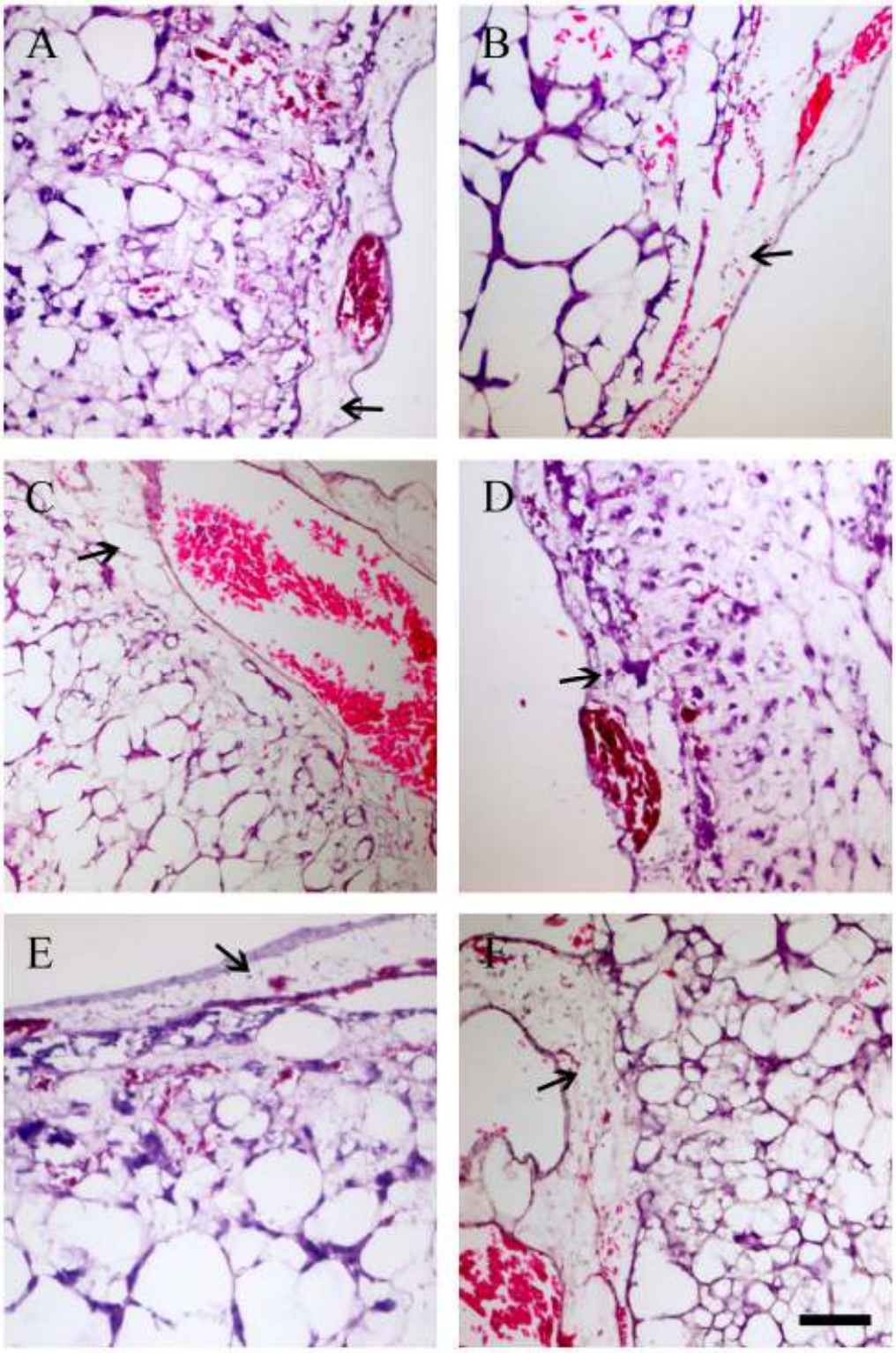

Figure 3.12 Microscopic images of tumour implants (SKOV-3) after six days treatment with varying doses of resveratrol showing invasion of cancer cells into the mesodermal layer of CAMs (arrows). *Treatment with 91 µg resveratrol led to reduced invasion of tumour cells into the CAM (see Fig. 3.13). Control (A), 0.3 µg (B), 0.5 µg (C), 46 µg (D), 91 µg (E), 183 µg (F) resveratrol. Scale bar, 200 µm.*

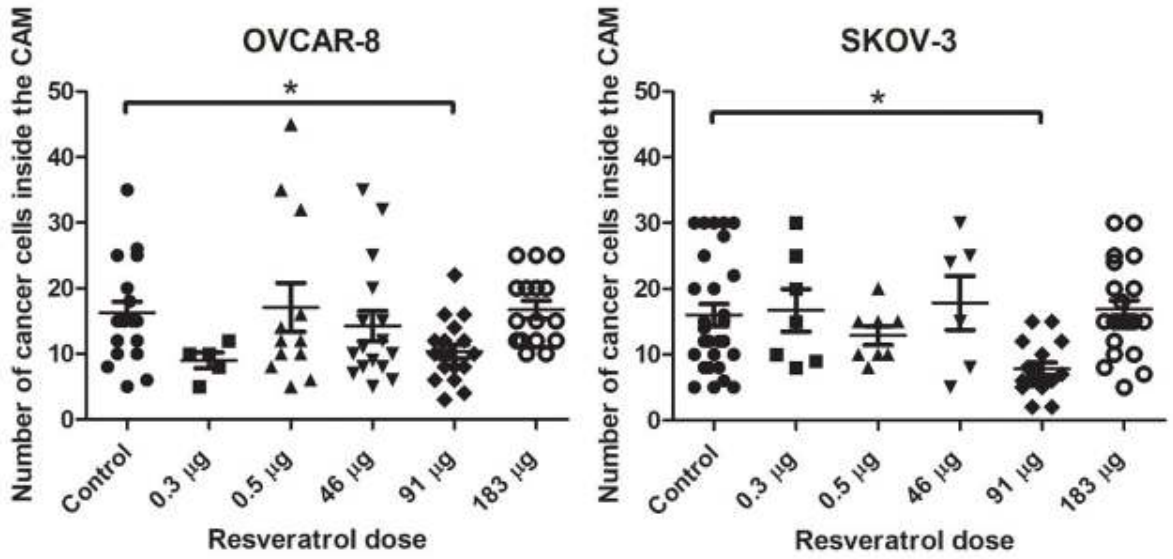

Figure 3.13 Number of invasive cancer cells present inside the CAM tissue from the tumour implants (OVCAR-8 (n = 83) and SKOV-3 (n = 92)), which were treated with various doses of resveratrol for six days. *Numbers of invasive cancer cells were significantly reduced in both OVCAR-8 and SKOV-3 implants treated with 91 µg resveratrol. Data expressed as means ± SEM. Data considered statistically significantly compared to controls are indicated as $p < 0.05$ (*).*

In both OVCAR-8 and SKOV-3 implants, treatment with 91 µg resveratrol led to significantly fewer cancer cells inside the mesodermal region of the CAM compared with control implants ($p = 0.0066$ and 0.0014 respectively, t-test) (Fig. 3.13). These results suggest that, at certain concentrations, resveratrol can lead to the inhibition of cancer cell migration and invasion. For both OVCAR-8 and SKOV-3, 91 µg resveratrol appears to be the optimum dose, and doses above or below this do not affect the invasive capability of tumour cells.

In the literature, it has been reported that resveratrol can inhibit migration and invasion of tumour cells and inhibit metastasis. One research group that carried out wound healing assays using human renal cell carcinoma cells (ACHN, A498) observed a reduction in movement of cells treated with 100 µM resveratrol for 24 hours compared with controls (Zhao, Tang, Zeng, Ye, & Liu, 2018). Another group carried out a similar wound healing assay, this time using cervical cancer (HeLa) and lung adenocarcinoma (A549) cells; this study found that treatment with 30 µM resveratrol for 24 hours led to reduced cell migration (Y. S. Kim, Sull, & Sung, 2012).

Treatment with 25, 50, 100, 200, 400, or 800 μM resveratrol for 72 hours also resulted in less migration in wound healing assays performed on ovarian cancer cells (A2780, SKOV-3) (Y. Liu et al., 2018). Invasion of ovarian cancer cells (NuTu-19) across a Matrigel membrane was shown to be inhibited in cells treated with 100 μM resveratrol for 48 hours compared with controls (Stakleff et al., 2012). Furthermore, an *in vivo* study using ovarian cancer (SKOV-3) xenografts in a mouse model resulted in a reduced metastatic index in mice treated with 100 mg/kg/day resveratrol for 18 days compared with control mice (Y. Liu et al., 2018).

Inhibition of cell migration and invasion by resveratrol could be mediated by a wide variety of proteins. MMPs including MMP-2, 7, and 9 are involved in degradation of the ECM, which is required for EMT and migration, and so are possible targets. Treatment of HeLa and A549 cancer cells with 10 or 30 μM resveratrol for 24 hours led to reduced expression of MMP-9 (Y. S. Kim et al., 2012). 15, 30, or 50 μM resveratrol suppressed MMP-7 expression in human colorectal cancer cells (LoVo, HCT116) in a dose-dependent manner over a time period of 24 or 48 hours (Ji et al., 2013). Expression of both MMP-2 and MMP-9 was shown to decrease in renal cell carcinoma cells (ACHN, A498) in response to treatment with 10, 20, 50, 100, and 200 μM resveratrol for 24 hours, and, again, this effect was dose-dependent (Zhao et al., 2018).

Cell adhesion molecules also represent a possible target as the dissolution and reformation of endothelial cell-cell interactions is involved in cell migration (Lamouille et al., 2014). An investigation into the effects of 24 hours of treatment with 10, 20, 50, 100, and 200 μM resveratrol on renal cell carcinoma cells (ACHN, A498) demonstrated a reduction in expression of N-cadherin as well as the transcriptional repressor Snail, along with a corresponding increase in E-cadherin expression (Zhao et al., 2018).

Signal transduction pathways, such as the PI-3K/Akt and ERK1/2 pathway, are involved in regulating cell migration and invasion, among other things, and so represent another potential target of cell invasion inhibitors; this is supported by the decreased expression of p-Akt and p-ERK1/2 observed in ACHN and A498 cells treated with between 10 and 200 μM resveratrol for 24 hours (Zhao et al., 2018).

3.5 Immunostaining of Ki67 in tumour implants

Ki67 is present during all active phases of the cell cycle (G1, S, G2, M) but is absent from senescent cells (G0), which makes it a useful marker of cellular proliferation (Scholzen & Gerdes, 2000). Increased staining, leading to higher mean grey values, is indicative of higher levels of Ki67 expression and therefore more cellular proliferation.

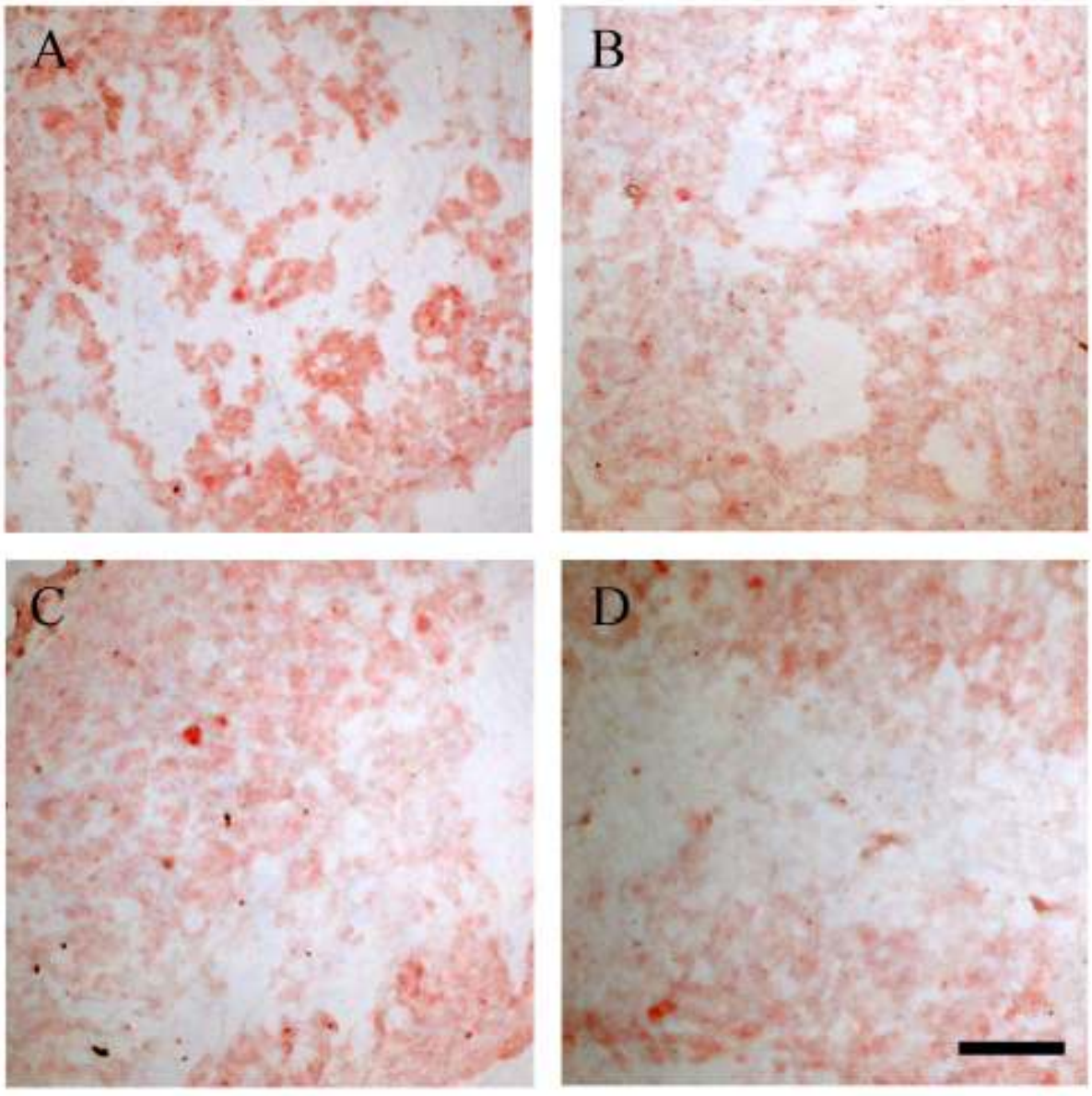

Figure 3.14 Microscopic images of tumour implants (OVCAR-8) after six days treatment with different doses of resveratrol showing staining of Ki67. *Treatment with resveratrol did not significantly alter Ki67 expression in tumour implants (see Fig. 3.16). Control (A), 0.3 µg (B), 46 µg (C), 183 µg (D) resveratrol. Scale bar, 200 µm.*

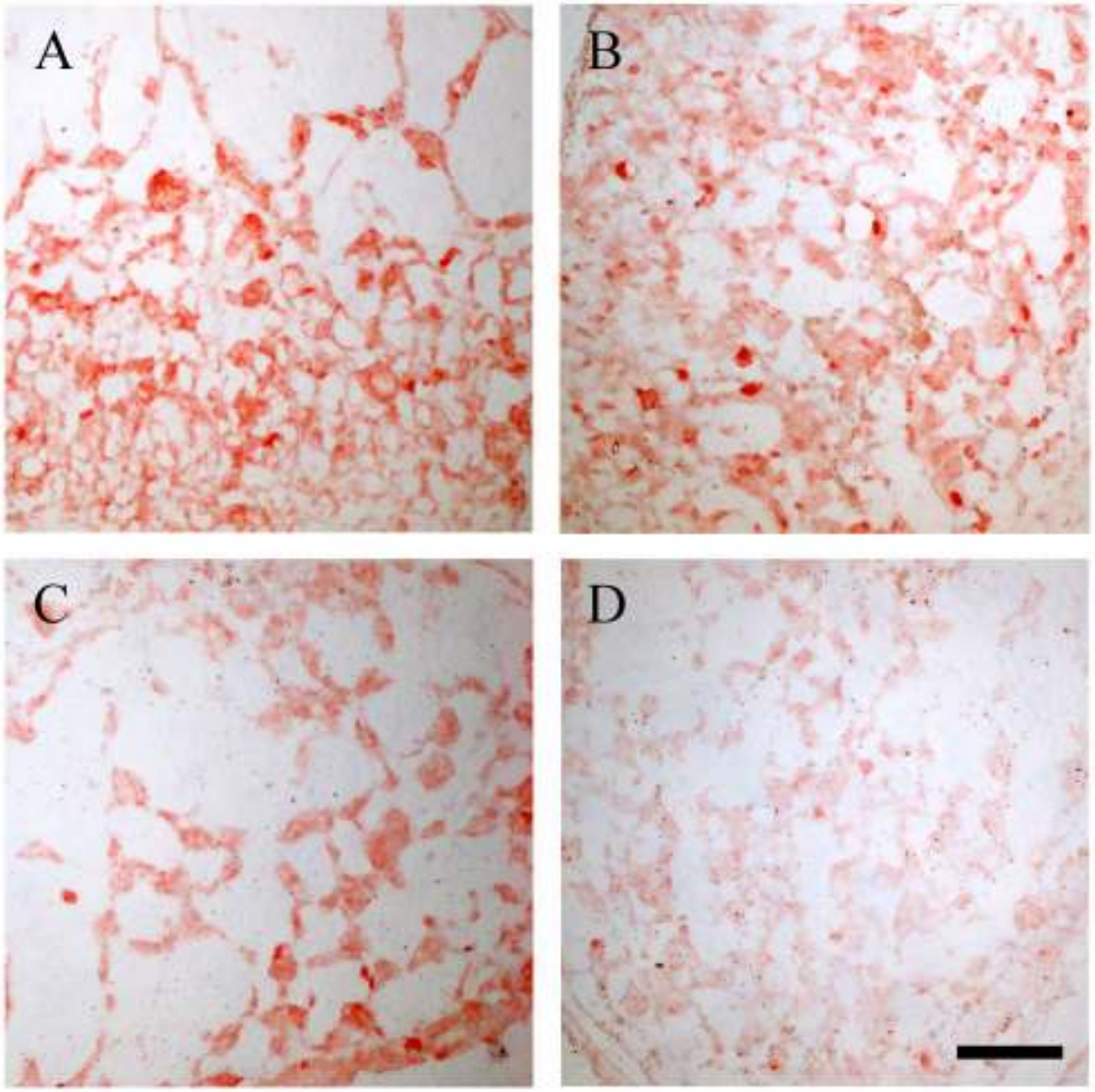

Figure 3.15 Microscopic images of tumour implants (SKOV-3) after six days treatment with various doses of resveratrol showing staining of Ki67. *Treatment with resveratrol did not significantly alter Ki67 expression in tumour implants (see Fig. 3.16). Control (A), 0.3 µg (B), 91 µg (C), 183 µg (D) resveratrol. Scale bar, 200 µm.*

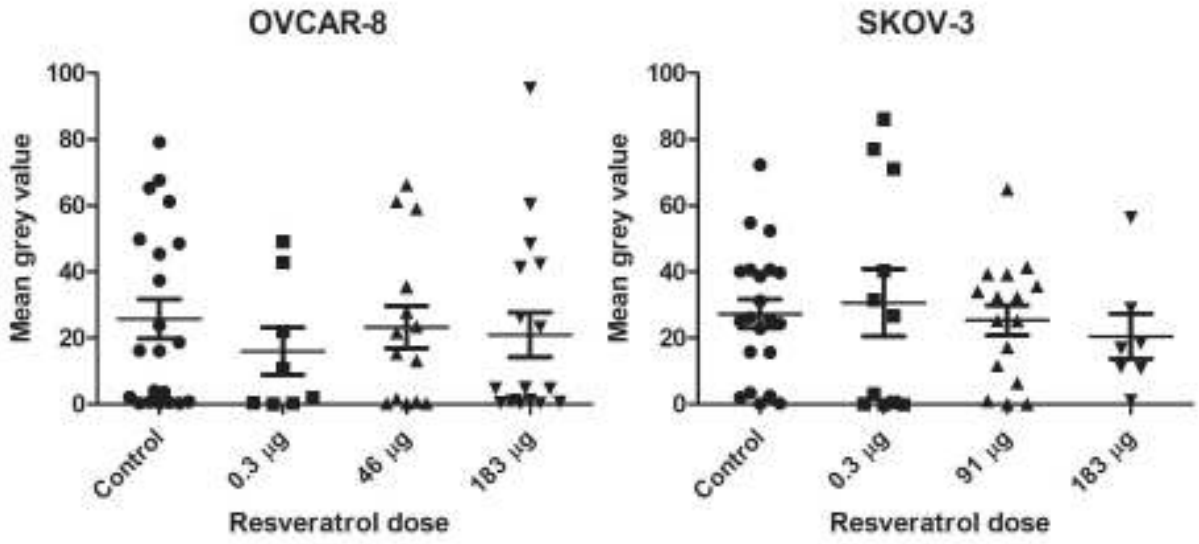

Figure 3.16 Intensity of immunohistochemical staining of Ki67 in tumour implants (OVCAR-8 (n = 60) and SKOV-3 (n = 55)) after six days of treatment with various doses of resveratrol. *There is no statistically significant difference between control implants and implants treated with resveratrol ($p > 0.05$). Data expressed as means ± SEM.*

These data suggest that the treatment of tumour implants with various doses of resveratrol does not affect the expression of Ki67 in OVCAR-8 or SKOV-3 tumour implants ($p > 0.05$, t-test) (Fig. 3.16). These results may suggest that these cancer cells are not actively proliferating. However, in contrast with the findings of the present study, existing research typically shows that resveratrol is able to inhibit proliferation and decrease expression of Ki67 (Harikumar et al., 2010; Zhai et al., 2016).

One study used human breast cancer cells (MCF-7) to investigate the effects of resveratrol on cell growth and proliferation, focusing specifically on regulators of the cell cycle (Y. A. Kim et al., 2004). That study demonstrated a dose-dependent inhibition of cell growth by resveratrol, which was likely a consequence of the inhibition of cyclin D and the associated Cdk 4, as well as the induction of p53 and a Cdk inhibitor protein (p21WAF1/CIP) causing cells to stall at the G1/S phase transition (Y. A. Kim et al., 2004).

Pancreatic cancer (MIA PaCa-2) xenografts in a mouse model treated with 40 mg/kg/day resveratrol for 28 days showed reduced tumour growth and inhibition of Ki67 expression compared with controls (Harikumar et al., 2010). Treatment of ovarian cancer (SKOV-3) xenografts in mice with 100 mg/kg/day resveratrol for 18 days was also shown to result in smaller tumours and lower Ki67 indices compared with controls (Y. Liu et al., 2018).

Given the existing evidence that resveratrol can disrupt proliferation of cancer, it seems unlikely that resveratrol has no effect on proliferation; it is more likely that in this particular experiment, the lack of effect of resveratrol on proliferation may be due to technical or experimental difficulties. It is possible, for example, that the antibody used to detect Ki67 was not sufficiently specific or was not appropriately optimised for this experiment. Another possibility is that the Ki67 antibody used was no longer fully functional, and therefore needed to be replaced with fresh stock.

3.6 TUNEL assay of tumour implants

Extensive DNA damage can be used as a surrogate marker for apoptosis. More DNA damage leads to increased dark brown staining, which is indicative of more apoptosis occurring in tumour implants.

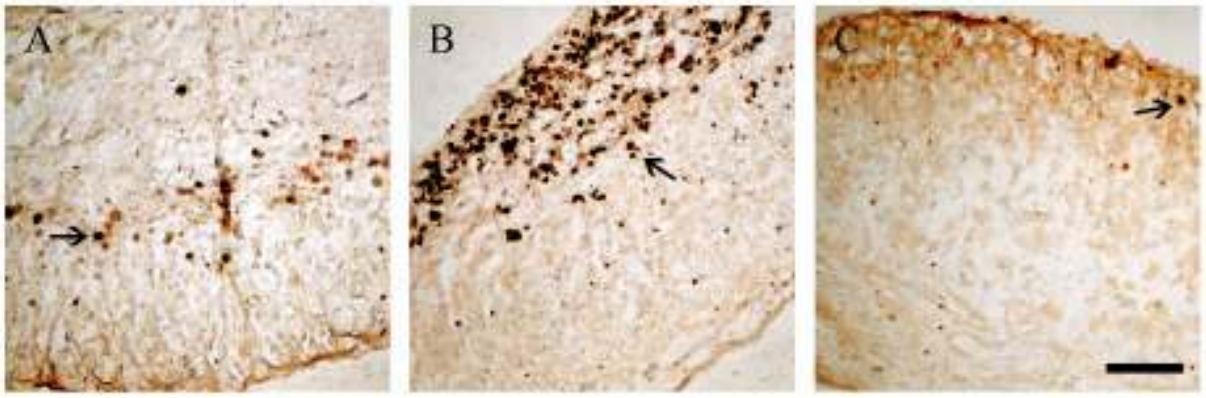

Figure 3.17 Microscopic images of tumour implants (OVCAR-8) after six days treatment with various doses of resveratrol showing staining of cells containing extensive DNA damage (arrows), indicative of apoptosis. *Treatment with resveratrol did not increase levels of apoptosis occurring in tumour implants (see Fig. 3.19). Control (A), 46 µg (B), 183 µg (C) resveratrol. Scale bar, 200 µm.*

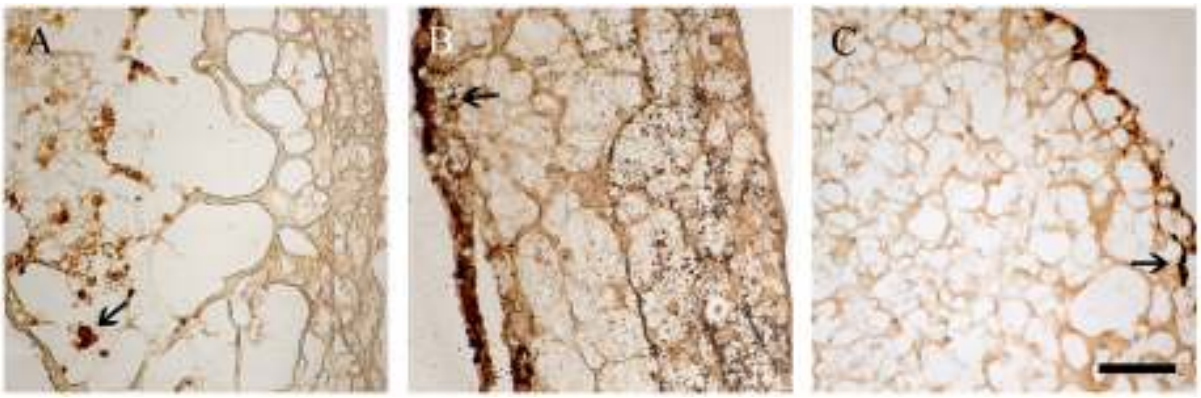

Figure 3.18 Microscopic images of tumour implants (SKOV-3) after six days treatment with varying doses of resveratrol showing staining of cells containing extensive DNA damage (arrows), indicative of apoptosis. *Treatment with resveratrol did not increase levels of apoptosis occurring in tumour implants (see Fig. 3.19). Control (A), 91 µg (B), 183 µg (C) resveratrol. Scale bar, 200 µm.*

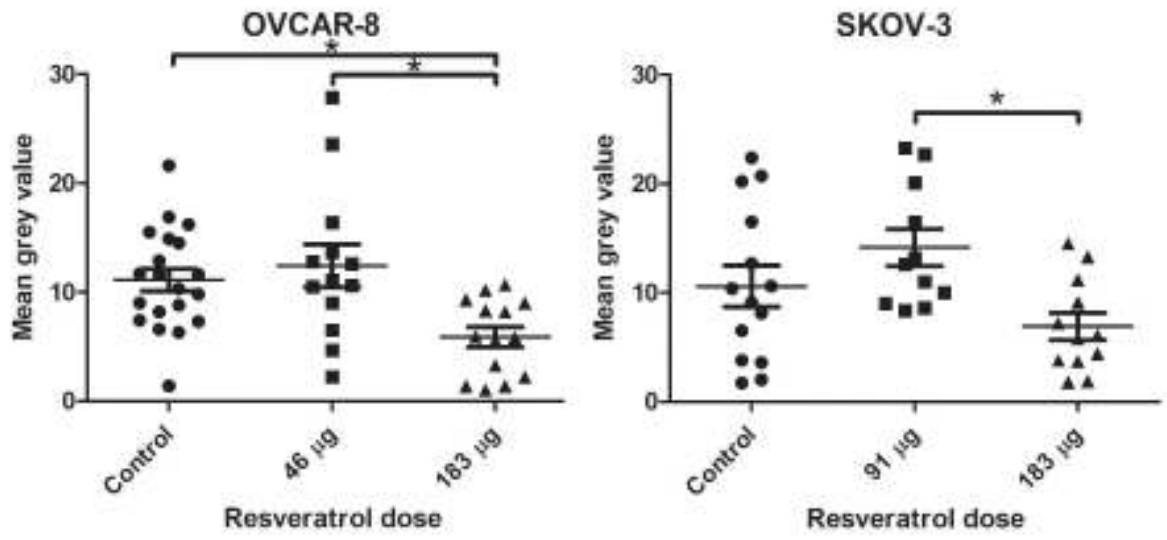

Figure 3.19 Intensity of staining for DNA damage in tumour implants (OVCAR-8 (n = 47) and SKOV-3 (n = 37)) after six days of treatment with varying doses of resveratrol.
Treatment with resveratrol did not lead to a significant increase in DNA damage in tumour implants. Data expressed as means ± SEM. Data considered statistically significantly compared to controls or other doses are indicated as $p < 0.05$ (*).

In OVCAR-8 implants, treatment with 46 µg resveratrol did not lead to a significant increase in the amount of DNA damage present ($p > 0.05$, t-test), although there appears to be a trend for an increase in DNA damage with 46 µg resveratrol, but due to the small sample size and high variability of the results, this was not statistically significant (Fig. 3.19). Somewhat paradoxically, treatment of implants with 183 µg resveratrol led to a significant decrease in DNA degradation compared to control implants ($p = 0.0022$, t-test) and implants treated with 46 µg resveratrol ($p = 0.0039$, t-test).

In SKOV-3 implants, treatment with 91 µg resveratrol did not lead to an increase in DNA damage ($p > 0.05$, t-test) (Fig. 3.19). Again, a trend for an increase in DNA damage with 91 µg resveratrol may be present but this was not statistically significant. Interestingly, compared with implants treated with 91 µg resveratrol, treatment with 183 µg resveratrol led to a significant decrease in DNA damage ($p = 0.0074$, t-test), but there was no statistically significant difference between the DNA damage in control implants compared to those treated with 183 µg resveratrol ($p > 0.05$, t-test).

Existing research suggests that treatment with resveratrol can lead to increased apoptosis, although the extent of this pro-apoptotic effect may vary significantly depending on the cell

line used (Takashina et al., 2017). Evidence suggests that resveratrol is capable of activating the intrinsic, or mitochondrial, apoptotic pathway by depolarising the mitochondrial membrane, thereby facilitating the secretion of cytochrome c into the cytosol and the subsequent activation of caspases 9 and 3 (Sareen et al., 2006). It may also stimulate apoptosis by disturbing the balance of pro- and anti-apoptotic proteins present in cells (Benitez, Pozo-Guisado, Alvarez-Barrientos, Fernandez-Salguero, & Castellon, 2007). Treatment with resveratrol has been shown to lead to downregulation of anti-apoptotic proteins such as Bcl-2 and Bcl-XL, and upregulation of pro-apoptotic proteins such as Bax and Bak (Benitez et al., 2007; Sareen et al., 2006).

Treatment of ovarian cancer cells (PA-1) with 50 or 100 μM resveratrol over twelve, 24, or 48 hours was shown to induce DNA fragmentation, proteolytic activation of caspases 3, 7, and 9, and lead to increased activity of caspase-3 (Lee et al., 2009). A similar study investigating the effects of treatment with 30 or 100 μM resveratrol for 48 hours in ovarian cancer cells (OVCAR-3, Caov-3) showed that resveratrol treatment led to a loss of cell viability and the induction of apoptosis, indicated by increased caspase-3 activity (Lang et al., 2015). In addition, an *in vivo* study involving ovarian cancer (PA-1) xenografts in a mouse model found that treatment with 50 or 100 mg/kg/day resveratrol for 28 days induced apoptosis, as indicated by increased TUNEL positivity and caspase-3 staining (Lee et al., 2009).

Results of TUNEL assays must be interpreted with caution, as cellular processes other than apoptosis, such as necrosis, may also lead to the kind of DNA fragmentation that TUNEL assays label (Takashina et al., 2017). However, other researchers have detected an increase in apoptotic cells in samples treated with resveratrol using different methods in addition to TUNEL assays, such as Annexin V staining, Hoechst staining, accumulation of reactive oxygen species, and activity of caspase proteins (Juan, Wenzel, Daniel, & Planas, 2008; Lang et al., 2015; Takashina et al., 2017). Therefore, it seems logical to conclude that treatment with resveratrol typically induces apoptosis, despite the results of the present study.

4 Conclusions

The high morbidity associated with ovarian cancer is due, in part, to a lack of early detection. This type of cancer is highly metastatic, with a unique mode of spreading throughout the peritoneal cavity. Treatment strategies are harsh, and their efficacy against advanced stage disease is limited, as acquired resistance to chemotherapeutic agents is common in advanced ovarian cancer. The development of more effective treatments for advanced ovarian cancer that offer an alternative to current treatment strategies is therefore an important goal. Resveratrol is a compound that occurs naturally in some foods which has been shown to have some anti-tumour properties.

This study investigated the usefulness of the CAM model as a means of replicating the early stages of ovarian cancer metastasis, in which tumour nodules develop on the surface of the peritoneum. Tumour implants grew well using this model, and this provided a useful platform for investigating the effects of resveratrol on the progression of those tumour implants. This suggests that the CAM model may be useful for investigations into the efficacy of other anti-tumour compounds against advanced ovarian cancer.

This experiment showed that resveratrol treatment may be able to inhibit invasion of tumour cells, and some data indicates that resveratrol may be capable of inhibiting angiogenesis. However, contrary to the majority of previous research, this study did not demonstrate any effect of resveratrol on the proliferation or survival of cancer cells.

4.1 Future research

Resveratrol has been shown to be effective in reducing the growth and progression of various cancers, including ovarian cancer, using both cell culture studies and mammalian models. Previous research has demonstrated that resveratrol can inhibit angiogenesis, invasion, and proliferation, and induce apoptosis in cancer cells. Therefore, further investigation into why resveratrol treatment affected only some of these processes in this experiment is warranted.

One possibility is that the dose of resveratrol used was too low to have any effect. Resveratrol is known to have low bioavailability, so it is possible that a very high dose is required.

Another avenue worth investigating would be the development of a more metabolically stable analogue of resveratrol which exerts similar effects, so that a lower dose is required.

Another possible explanation is that the exposure time used in this experiment was too short for resveratrol treatment to elicit some of its usual effects. The CAM model is limiting in this aspect, as embryonic development of chickens takes approximately three weeks, after which the eggs will hatch.

It is also worth considering the possibility that experimental errors occurred during this study, and time constraints did not permit further investigation into this possibility. For example, it is possible that the Ki67 antibody used needed to be replaced with fresh stock as it was possibly no longer functional.

Finally, as the effects of resveratrol are cell line-specific, testing of resveratrol on a wider range of cell lines is necessary. In this study, resveratrol was tested on one high grade serous ovarian cancer cell line (OVCAR-8) and one ovarian cancer cell line that is now considered unlikely to be of the high-grade serous subtype (Domcke et al., 2013). Investigating the effects of resveratrol on more cell lines that represent the high-grade serous subtype, such as Caov-3 or OVCAR-3, would be beneficial, as this is the most common ovarian cancer subtype (Domcke et al., 2013). It would also be useful to investigate the effects of resveratrol on other subtypes, including the endometrioid (Caov-3, Ishikawa), clear cell (Caki-3, ACC-OV614), and mucinous (MCAS, INT.Ov3) subtypes, as this information would indicate the efficacy of resveratrol treatment in the context of ovarian cancer overall.

References

Adair, T., & Montani, J. (2010). Angiogenesis. San Rafael (CA): Morgan & Claypool Life Sciences; 2010. Chapter 1, Overview of Angiogenesis. In.

Ahmed, N., Thompson, E. W., & Quinn, M. A. (2007). Epithelial–mesenchymal interconversions in normal ovarian surface epithelium and ovarian carcinomas: An exception to the norm. *Journal of Cellular Physiology, 213*(3), 581-588. doi:10.1002/jcp.21240

Alsina-Sanchís, E., Figueras, A., Lahiguera, A., Gil-Martín, M., Pardo, B., Piulats, J. M., . . . Viñals, F. (2017). TGFβ Controls Ovarian Cancer Cell Proliferation. *International Journal of Molecular Sciences, 18*(8), 1658. doi:10.3390/ijms18081658

Ayhan, A., Kurman, R. J., Yemelyanova, A., Vang, R., Logani, S., Seidman, J. D., & Shih, I.-M. (2009). Defining the cut point between low-grade and high-grade ovarian serous carcinomas: a clinicopathologic and molecular genetic analysis. *The American journal of surgical pathology, 33*(8), 1220-1224. doi:10.1097/PAS.0b013e3181a24354

Bai, Y., Mao, Q.-Q., Qin, J., Zheng, X.-Y., Wang, Y.-B., Yang, K., . . . Xie, L.-P. (2010). Resveratrol induces apoptosis and cell cycle arrest of human T24 bladder cancer cells in vitro and inhibits tumor growth in vivo. *Cancer Science, 101*(2), 488-493. doi:10.1111/j.1349-7006.2009.01415.x

Bast Jr, R. C., Hennessy, B., & Mills, G. B. (2009). The biology of ovarian cancer: new opportunities for translation. *Nature Reviews Cancer, 9*, 415. doi:10.1038/nrc2644

Baur, J. A., & Sinclair, D. A. (2006). Therapeutic potential of resveratrol: the in vivo evidence. *Nature Reviews. Drug Discovery, 5*(6), 493-506. doi:http://dx.doi.org/10.1038/nrd2060

Benitez, D. A., Pozo-Guisado, E., Alvarez-Barrientos, A., Fernandez-Salguero, P. M., & Castellon, E. A. (2007). Mechanisms involved in resveratrol-induced apoptosis and cell cycle arrest in prostate cancer-derived cell lines. *J Androl, 28*(2), 282-293. doi:10.2164/jandrol.106.000968

Berman, A. Y., Motechin, R. A., Wiesenfeld, M. Y., & Holz, M. K. (2017). The therapeutic potential of resveratrol: a review of clinical trials. *npj Precision Oncology, 1*(1), 35. doi:10.1038/s41698-017-0038-6

Bishayee, A. (2009). Cancer prevention and treatment with resveratrol: from rodent studies to clinical trials. *Cancer Prevention Research, 2*(5), 409-418.

Bold, R. J., Termuhlen, P. M., & McConkey, D. J. (1997). Apoptosis, cancer and cancer therapy. *Surgical Oncology, 6*(3), 133-142. doi:https://doi.org/10.1016/S0960-7404(97)00015-7

Brakenhielm, E., Cao, R., & Cao, Y. (2001). Suppression of angiogenesis, tumor growth, and wound healing by resveratrol, a natural compound in red wine and grapes. *Faseb j, 15*(10), 1798-1800.

Bray, F., Ferlay, J., Soerjomataram, I., Siegel, R. L., Torre, L. A., & Jemal, A. (2018). Global cancer statistics 2018: GLOBOCAN estimates of incidence and mortality worldwide for 36 cancers in 185 countries. *CA: A Cancer Journal for Clinicians, 68*(6), 394-424.

Bredholt, G., Mannelqvist, M., Stefansson, I. M., Birkeland, E., Bø, T. H., Øyan, A. M., . . . Akslen, L. A. (2015). Tumor necrosis is an important hallmark of aggressive endometrial cancer and associates with hypoxia, angiogenesis and inflammation responses. *Oncotarget, 6*(37), 39676-39691. doi:10.18632/oncotarget.5344

Burri, P. H., Hlushchuk, R., & Djonov, V. (2004). Intussusceptive angiogenesis: Its emergence, its characteristics, and its significance. *Developmental Dynamics, 231*(3), 474-488. doi:doi:10.1002/dvdy.20184

Cannistra, S. A. (2004). Cancer of the ovary. *The New England Journal of Medicine, 351*, 2519-2529.

Cao, Z., Fang, J., Xia, C., Shi, X., & Jiang, B.-H. (2004). trans-3,4,5′-Trihydroxystibene Inhibits Hypoxia-Inducible Factor 1α and Vascular Endothelial Growth Factor Expression in Human Ovarian Cancer Cells. *Clinical Cancer Research, 10*(15), 5253-5263. doi:10.1158/1078-0432.Ccr-03-0588

Carmeliet, P. (2000). Mechanisms of angiogenesis and arteriogenesis. *Nature Medicine, 6*(4), 389-395. doi:http://dx.doi.org/10.1038/74651

Carmeliet, P., & Jain, R. K. (2011). Molecular mechanisms and clinical applications of angiogenesis. *Nature, 473*(7347), 298-307.

Chen, Y., & Tseng, S.-H. (2007). Pro- and Anti-angiogenesis Effects of Resveratrol. *In Vivo, 21*(2), 365-370.

Cho, K. R., & Shih, I.-M. (2009). Ovarian cancer. *Annual Review of Pathology: Mechanisms of Disease, 4*(1), 287-313. doi:10.1146/annurev.pathol.4.110807.092246

Cooper, G. M. (2000). The Eukaryotic Cell Cycle. In *The Cell: A Molecular Approach. 2nd edition*. Sunderland (MA): Sinauer Associates.

de Vries, E. G. E., Gietema, J. A., & de Jong, S. (2006). Tumor Necrosis Factor–Related Apoptosis-Inducing Ligand Pathway and Its Therapeutic Implications. *Clinical Cancer Research, 12*(8), 2390. doi:10.1158/1078-0432.CCR-06-0352

DeLisser, H. M., Christofidou-Solomidou, M., Strieter, R. M., Burdick, M. D., Robinson, C. S., Wexler, R. S., . . . Albelda, S. M. (1997). Involvement of endothelial PECAM-1/CD31 in angiogenesis. *The American journal of pathology, 151*(3), 671-677.

Deryugina, E. I., & Quigley, J. P. (2008). Chick embryo chorioallantoic membrane model systems to study and visualize human tumor cell metastasis. *Histochemistry and Cell Biology, 130*(6), 1119-1130.

Disney, G., McDonald, A., Atkinson, J. and Blakely, T. (2016). New Zealand Census Mortality and Cancer Trends Retrieved from http://www.uow.otago.ac.nz/NZCMS-CT-dataexplorer

Domcke, S., Sinha, R., Levine, D. A., Sander, C., & Schultz, N. (2013). Evaluating cell lines as tumour models by comparison of genomic profiles. *Nature Communications, 4*(1), 2126. doi:10.1038/ncomms3126

Durupt, F., Koppers-Lalic, D., Balme, B., Budel, L., Terrier, O., Lina, B., . . . Rosa-Calatrava, M. (2012). The chicken chorioallantoic membrane tumor assay as model for qualitative testing of oncolytic adenoviruses. *Cancer Gene Therapy, 19*(1), 58-68. doi:10.1038/cgt.2011.68

Durupt, F., Koppes-Lalic, D., Balme, B., Budel, B., Terrier, O., Lina, B., . . . Rosa-Calatrava, M. (2012). The chicken chorioallantoic membrane tumour assay as a model for qualitative testing of oncolytic adenoviruses. *Cancer Gene Therapy, 19*, 58-68.

Dutta, S., Going, J. J., Crumley, A. B. C., Mohammed, Z., Orange, C., Edwards, J., . . . McMillan, D. C. (2012). The relationship between tumour necrosis, tumour proliferation, local and systemic inflammation, microvessel density and survival in patients undergoing potentially curative resection of oesophageal adenocarcinoma. *The British Journal of Cancer, 106*(4), 702-710. doi:http://dx.doi.org/10.1038/bjc.2011.610

El-Azab, M., Hishe, H., Moustafa, Y., & El-Awady, E.-S. (2011). Anti-angiogenic effect of resveratrol or curcumin in Ehrlich ascites carcinoma-bearing mice. *European Journal of Pharmacology, 652*(1), 7-14. doi:https://doi.org/10.1016/j.ejphar.2010.11.008

Elmore, S. (2007). Apoptosis: a review of programmed cell death. *Toxicologic pathology, 35*(4), 495-516. doi:10.1080/01926230701320337

Evan, G. I., & Vousden, K. H. (2001). Proliferation, cell cycle and apoptosis in cancer. *Nature, 411*(6835), 342-348. doi:http://dx.doi.org/10.1038/35077213

Fagotti, A., Gallotta, V., Romano, F., Fanfani, F., Rossitto, C., Naldini, A., . . . Scambia, G. (2010). Peritoneal carcinosis of ovarian origin. *World Journal of Gastrointestinal Oncology, 2*(2), 102-108.

Favaloro, B., Allocati, N., Graziano, V., Di Ilio, C., & De Laurenzi, V. (2012). Role of apoptosis in disease. *Aging, 4*(5), 330-349. doi:10.18632/aging.100459

Folkman, J. (2006). Angiogenesis. *Annual Review of Medicine, 57*(1), 1-18. doi:10.1146/annurev.med.57.121304.131306

Fouad, Y. A., & Aanei, C. (2017). Revisiting the hallmarks of cancer. *American journal of cancer research, 7*(5), 1016-1036.

Glinsky, G. V., Glinsky, V. V., Ivanova, A. B., & Hueser, C. J. (1997). Apoptosis and metastasis: increased apoptosis resistance of metastatic cancer cells is associated with the profound deficiency of apoptosis execution mechanisms. *Cancer Letters, 115*(2), 185-193. doi:https://doi.org/10.1016/S0304-3835(97)04738-1

Goodlett, C. R., & Horn, K. H. (2001). Mechanisms of alcohol-induced damage to the developing nervous system. *Alcohol research and health, 25*(3), 175-184.

Greenlee, R. T., Murray, T., Bolden, S., & Wingo, P. A. (2000). Cancer statistics, 2000. *CA: A Cancer Journal for Clinicians, 50*(1), 7-33. doi:10.3322/canjclin.50.1.7

Hanahan, D., & Weinberg, R. A. (2000). The Hallmarks of Cancer. *Cell, 100*(1), 57-70. doi:10.1016/S0092-8674(00)81683-9

Hanahan, D., & Weinberg, Robert A. (2011). Hallmarks of Cancer: The Next Generation. *Cell, 144*(5), 646-674. doi:https://doi.org/10.1016/j.cell.2011.02.013

Harikumar, K. B., Kunnumakkara, A. B., Sethi, G., Diagaradjane, P., Anand, P., Pandey, M. K., . . . Aggarwal, B. B. (2010). Resveratrol, a multitargeted agent, can enhance antitumor activity of gemcitabine in vitro and in orthotopic mouse model of human pancreatic cancer. *International journal of cancer, 127*(2), 257-268. doi:10.1002/ijc.25041

Hartwell, L. H., & Kastan, M. B. (1994). Cell Cycle Control and Cancer. *Science, 266*(5192), 1821-1828.

Hassan, W., Chitcholtan, K., Sykes, P., & Garrill, A. (2016). A combination of two receptor tyrosine kinase inhibitors, canertinib and PHA665752 compromises ovarian cancer cell growth in 3D cell models. *Oncology and Therapy, 4*(2), 257-274.

Hassan, W., Chitcholtan, K., Sykes, P., & Garrill, A. (2018). Ascitic fluid from advanced ovarian cancer patients compromises the activity of receptor tyrosine kinase inhibitors in 3D cell clusters of ovarian cancer cells. *Cancer Letters, 420*, 168-181.

Hillen, F., & Griffioen, A. W. (2007). Tumour vascularization: sprouting angiogenesis and beyond. *Cancer metastasis reviews, 26*(3-4), 489-502. doi:10.1007/s10555-007-9094-7

Hogg, S. J., Chitcholtan, K., Hassan, W., Sykes, P. H., & Garrill, A. (2015). Resveratrol, acetyl-resveratrol, and polydatin exhibit antigrowth activity against 3D cell aggregates of SKOV-3 and OVCAR-8 ovarian cancer cell lines. *Obstetrics and Gynecology International, 2015*, 1-14.

Hu, W.-H., Duan, R., Xia, Y.-T., Xiong, Q.-P., Wang, H.-Y., Chan, G. K.-L., . . . Tsim, K. W.-K. (2018). Binding of Resveratrol to Vascular Endothelial Growth Factor Suppresses Angiogenesis by Inhibiting the Receptor Signaling. *Journal of Agricultural and Food Chemistry*. doi:10.1021/acs.jafc.8b05977

Huang, H., Li, Y., Liu, J., Zheng, M., Feng, Y., Hu, K., . . . Huang, Q. (2012). Screening and identification of biomarkers in ascites related to intrinsic chemoresistance of serous epithelial ovarian cancers. *PLoS One, 7*(12), e51256.

Jang, M., Cai, L., Udeani, G. O., Slowing, K. V., Thomas, C. F., Beecher, C. W., . . . Pezzuto, J. M. (1997). Cancer chemopreventive activity of resveratrol, a natural product derived from grapes. *Science, 275*(5297), 218-220.

Jayson, G. C. P., Kohn, E. C. M. D., Kitchener, H. C. P., & Ledermann, J. A. P. (2014). Ovarian cancer. *Lancet, The, 384*(9951), 1376-1388. doi:10.1016/S0140-6736(13)62146-7

Jemal, A., Siegel, R., Ward, E., Murray, T., Xu, J., Smigal, C., & Thun, M. J. (2006). Cancer Statistics, 2006. *CA: A Cancer Journal for Clinicians, 56*(2), 106-130. doi:10.3322/canjclin.56.2.106

Ji, Q., Liu, X., Fu, X., Zhang, L., Sui, H., Zhou, L., . . . Li, Q. (2013). Resveratrol inhibits invasion and metastasis of colorectal cancer cells via MALAT1 mediated Wnt/β-catenin signal pathway. *PLOS ONE, 8*(11), e78700-e78700. doi:10.1371/journal.pone.0078700

Juan, M. E., Wenzel, U., Daniel, H., & Planas, J. M. (2008). Resveratrol Induces Apoptosis through ROS-Dependent Mitochondria Pathway in HT-29 Human Colorectal Carcinoma Cells. *Journal of Agricultural and Food Chemistry, 56*(12), 4813-4818. doi:10.1021/jf800175a

Kalluri, R., & Weinberg, R. A. (2009). The basics of epithelial-mesenchymal transition. *The Journal of Clinical Investigation, 119*(6), 1420-1428. doi:10.1172/JCI39104

Karamysheva, A. (2008). Mechanisms of angiogenesis. *Biochemistry (Moscow), 73*(7), 751.

Kerr, J. F. R., Winterford, C. M., & Harmon, B. V. (1994). Apoptosis. Its significance in cancer and cancer Therapy. *Cancer, 73*(8), 2013-2026. doi:10.1002/1097-0142(19940415)73:8<2013::AID-CNCR2820730802>3.0.CO;2-J

Kim, Y. A., Choi, B. T., Lee, Y. T., Park, D. I., Rhee, S. H., Park, K. Y., & Choi, Y. H. (2004). Resveratrol inhibits cell proliferation and induces apoptosis of human breast carcinoma MCF-7 cells. *Oncol Rep, 11*(2), 441-446.

Kim, Y. S., Sull, J. W., & Sung, H. J. (2012). Suppressing effect of resveratrol on the migration and invasion of human metastatic lung and cervical cancer cells. *Mol Biol Rep, 39*(9), 8709-8716. doi:10.1007/s11033-012-1728-3

Kipps, E., Tan, D. S. P., & Kaye, S. B. (2013). Meeting the challenge of ascites in ovarian cancer: new avenues for therapy and research. *Nature Reviews: Cancer, 13*, 273-282.

Kraft, T. E., Parisotto, D., Schempp, C., & Efferth, T. (2009). Fighting Cancer with Red Wine? Molecular Mechanisms of Resveratrol. *Critical Reviews in Food Science and Nutrition, 49*(9), 782-799. doi:10.1080/10408390802248627

Krakhmal, N. V., Zavyalova, M. V., Denisov, E. V., Vtorushin, S. V., & Perelmuter, V. M. (2015). Cancer Invasion: Patterns and Mechanisms. *Acta naturae, 7*(2), 17-28.

Lamouille, S., Xu, J., & Derynck, R. (2014). Molecular mechanisms of epithelial–mesenchymal transition. *Nature Reviews Molecular Cell Biology, 15*, 178. doi:10.1038/nrm3758

Lang, F., Qin, Z., Li, F., Zhang, H., Fang, Z., & Hao, E. (2015). Apoptotic Cell Death Induced by Resveratrol Is Partially Mediated by the Autophagy Pathway in Human Ovarian Cancer Cells. *PLOS ONE, 10*(6), e0129196. doi:10.1371/journal.pone.0129196

Lee, M.-H., Choi, B. Y., Kundu, J. K., Shin, Y. K., Na, H.-K., & Surh, Y.-J. (2009). Resveratrol Suppresses Growth of Human Ovarian Cancer Cells in Culture and in a Murine Xenograft Model: Eukaryotic Elongation Factor 1A2 as a Potential Target. *Cancer research, 69*(18), 7449. doi:10.1158/0008-5472.CAN-09-1266

Lim, S., & Kaldis, P. (2013). Cdks, cyclins and CKIs: roles beyond cell cycle regulation. *Development, 140*(15), 3079. doi:10.1242/dev.091744

Liu, M., Scanlon, C., Banerjee, R., Russo, N., C Inglehart, R., L Willis, A., . . . J D'Silva, N. (2013). *The Histone Methyltransferase EZH2 Mediates Tumor Progression on the*

Chick Chorioallantoic Membrane Assay, a Novel Model of Head and Neck Squamous Cell Carcinoma (Vol. 6).

Liu, Y., Tong, L., Luo, Y., Li, X., Chen, G., & Wang, Y. (2018). Resveratrol inhibits the proliferation and induces the apoptosis in ovarian cancer cells via inhibiting glycolysis and targeting AMPK/mTOR signaling pathway. *Journal of Cellular Biochemistry, 119*(7), 6162-6172. doi:10.1002/jcb.26822

Liu, Z., Li, Y., & Yang, R. (2012). Effects of resveratrol on vascular endothelial growth factor expression in osteosarcoma cells and cell proliferation. *Oncology letters, 4*(4), 837-839. doi:10.3892/ol.2012.824

Lokman, N. A., Elder, A. S. F., Ricciardelli, C., & Oehler, M. K. (2012). Chick chorioallantoic membrane (CAM) assay as an in vivo model to study the effect of newly identified molecules on ovarian cancer invasion and metastasis. *International Journal of Molecular Sciences, 13*, 9959-9970.

Majno, G., & Joris, I. (1995). Apoptosis, oncosis, and necrosis. An overview of cell death. *Am J Pathol, 146*(1), 3-15.

Martinez-Ruiz, G., Maldonado, V., Ceballos-Cancino, G., Grajeda, J. P. R., & Melendez-Zajgla, J. (2008). Role of Smac/DIABLO in cancer progression. *Journal of experimental & clinical cancer research : CR, 27*(1), 48-48. doi:10.1186/1756-9966-27-48

Nagineni, C. N., Raju, R., Nagineni, K. K., Kommineni, V. K., Cherukuri, A., Kutty, R. K., . . . Detrick, B. (2014). Resveratrol Suppresses Expression of VEGF by Human Retinal Pigment Epithelial Cells: Potential Nutraceutical for Age-related Macular Degeneration. *Aging and disease, 5*(2), 88-100. doi:10.14366/AD.2014.050088

Nakayama, K., Nakayama, N., Katagiri, H., & Miyazaki, K. (2012). Mechanisms of ovarian cancer metastasis: biochemical pathways. *International Journal of Molecular Sciences, 13*(9), 11705-11717. doi:10.3390/ijms130911705

Nishida, N., Yano, H., Nishida, T., Kamura, T., & Kojiro, M. (2006). Angiogenesis in cancer. *Vascular health and risk management, 2*(3), 213-219.

Núñez, M. J., Novío, S., Balboa, J., Seoane, J., Suárez, J. A., & Freire-Garabal, M. (2010). Effects of resveratrol on expression of vascular endothelial growth factor in human gingival fibroblasts stimulated by periodontal pathogens. *Acta Odontologica Scandinavica, 68*(4), 239-247. doi:10.3109/00016357.2010.494269

Paku, S., Dezso, K., Bugyik, E., Tóvári, J., Tímár, J., Nagy, P., . . . Döme, B. (2011). A new mechanism for pillar formation during tumor-induced intussusceptive angiogenesis:

inverse sprouting. *The American journal of pathology, 179*(3), 1573-1585. doi:10.1016/j.ajpath.2011.05.033

Panková, K., Rösel, D., Novotný, M., & Brábek, J. (2010). The molecular mechanisms of transition between mesenchymal and amoeboid invasiveness in tumor cells. *Cellular and molecular life sciences : CMLS, 67*(1), 63-71. doi:10.1007/s00018-009-0132-1

Park, S. Y., Jeong, K. J., Lee, J., Yoon, D. S., Choi, W. S., Kim, Y. K., . . . Lee, H. Y. (2007). Hypoxia enhances LPA-induced HIF-1α and VEGF expression: Their inhibition by resveratrol. *Cancer Letters, 258*(1), 63-69. doi:https://doi.org/10.1016/j.canlet.2007.08.011

Pomel, C., Jeyarajah, A., Oram, D., Shepherd, J., Milliken, D., Dauplat, J., & Reynolds, K. (2007). Cytoreductive surgery in ovarian cancer. *Cancer Imaging, 7*(1), 210-215.

Potente, M., Gerhardt, H., & Carmeliet, P. (2011). Basic and Therapeutic Aspects of Angiogenesis. *Cell, 146*(6), 873-887. doi:https://doi.org/10.1016/j.cell.2011.08.039

Prior, B. M., Yang, H., & Terjung, R. L. (2004). What makes vessels grow with exercise training? *Journal of Applied Physiology, 97*(3), 1119-1128.

Provenzano, P. P., Eliceiri, K. W., & Keely, P. J. (2009). Shining new light on 3D cell motility and the metastatic process. *Trends in Cell Biology, 19*(11), 638-648. doi:10.1016/j.tcb.2009.08.009

Ribatti, D. (2010). The chick embryo chorioallantoic membrane as an in vivo assay to study antiangiogenesis. *Pharmaceuticals, 3*, 482-513.

Ribatti, D., & Crivellato, E. (2012). "Sprouting angiogenesis", a reappraisal. *Developmental Biology, 372*(2), 157-165. doi:https://doi.org/10.1016/j.ydbio.2012.09.018

Ribatti, D., & Djonov, V. (2012). Intussusceptive microvascular growth in tumors. *Cancer Letters, 316*(2), 126-131. doi:http://dx.doi.org/10.1016/j.canlet.2011.10.040

Rice, J. J., Gerwins, P., & Kilarski, W. W. (2012). Mechanisms of angiogenesis: Perspectives from antiangiogenic tumor therapies. *Current Angiogenesis, 1*(2), 139-147. doi:10.2174/2211552811201020139

Risau, W. (1997). Mechanisms of angiogenesis. *Nature, 386*, 671. doi:10.1038/386671a0

Sareen, D., van Ginkel, P. R., Takach, J. C., Mohiuddin, A., Darjatmoko, S. R., Albert, D. M., & Polans, A. S. (2006). Mitochondria as the primary target of resveratrol-induced apoptosis in human retinoblastoma cells. *Invest Ophthalmol Vis Sci, 47*(9), 3708-3716. doi:10.1167/iovs.06-0119

Schlüter, A., Weller, P., Kanaan, O., Nel, I., Heusgen, L., Höing, B., . . . Brandau, S. (2018). CD31 and VEGF are prognostic biomarkers in early-stage, but not in late-stage,

laryngeal squamous cell carcinoma. *BMC Cancer, 18*(1), 272. doi:10.1186/s12885-018-4180-5

Schmitt, J., & Matei, D. (2012). Targeting angiogenesis in ovarian cancer. *Cancer Treatment Reviews, 38*(4), 272-283. doi:https://doi.org/10.1016/j.ctrv.2011.06.004

Scholzen, T., & Gerdes, J. (2000). The Ki-67 protein: From the known and the unknown. *Journal of Cellular Physiology, 182*(3), 311-322. doi:10.1002/(SICI)1097-4652(200003)182:3<311::AID-JCP1>3.0.CO;2-9

Semenza, G. L. (2007). Vasculogenesis, angiogenesis, and arteriogenesis: Mechanisms of blood vessel formation and remodeling. *Journal of Cellular Biochemistry, 102*(4), 840-847. doi:doi:10.1002/jcb.21523

Shimizu, S., Eguchi, Y., Kamiike, W., Itoh, Y., Hasegawa, J.-i., Yamabe, K., . . . Tsujimoto, Y. (1996). Induction of apoptosis as well as necrosis by hypoxia and predominant prevention of apoptosis by Bcl-2 and Bcl-XL. *Cancer research, 56*(9), 2161-2166.

Siegel, R. L., Miller, K. D., & Jemal, A. (2016). Cancer statistics. *CA: Cancer Journal for Clinicians, 66*, 7-30.

Siegel, R. L., Miller, K. D., & Jemal, A. (2018). Cancer statistics, 2018. *CA: A Cancer Journal for Clinicians, 68*(1), 7-30. doi:10.3322/caac.21442

Siegel, R. L., Naishadham, D., & Jemal, A. (2012). Cancer statistics, 2012. *CA: A Cancer Journal for Clinicians, 62*(1), 10-29. doi:10.3322/caac.20138

Stakleff, K. S., Sloan, T., Blanco, D., Marcanthony, S., Booth, T. D., & Bishayee, A. (2012). Resveratrol Exerts Differential Effects in Vitro and in Vivo against Ovarian Cancer Cells. *Asian Pacific Journal of Cancer Prevention, 13*(4), 1333-1340. doi:10.7314/APJCP.2012.13.4.1333

Taizi, M., Deutsch, V. R., Leitner, A., Ohana, A., & Goldstein, R. S. (2006). A novel and rapid in vivo system for testing therapeutics on human leukemias. *Experimental Hematology, 34*, 1698-1708.

Takashina, M., Inoue, S., Tomihara, K., Tomita, K., Hattori, K., Zhao, Q.-L., . . . Hattori, Y. (2017). Different effect of resveratrol to induction of apoptosis depending on the type of human cancer cells. *International journal of oncology, 50*(3), 787-797.

The Cancer Genome Atlas Research, N., Bell, D., Berchuck, A., Birrer, M., Chien, J., Cramer, D. W., . . . Thomson, E. (2011). Integrated genomic analyses of ovarian carcinoma. *Nature, 474*, 609. doi:10.1038/nature10166

https://www.nature.com/articles/nature10166#supplementary-information

Tino, A. B., Chitcholtan, K., Sykes, P. H., & Garrill, A. (2016). Resveratrol and acetyl-resveratrol modulate activity of VEGF and IL-8 in ovarian cancer cell aggregates via attenuation of the NF-kappaB protein. *J Ovarian Res, 9*(1), 84. doi:10.1186/s13048-016-0293-0

Torre, L. A., Trabert, B., DeSantis, C. E., Miller, K. D., Samimi, G., Runowicz, C. D., . . . Siegel, R. L. (2018). Ovarian cancer statistics, 2018. *CA Cancer J Clin, 68*(4), 284-296. doi:10.3322/caac.21456

Trapp, V., Parmakhtiar, B., Papazian, V., Willmott, L., & Fruehauf, J. P. (2010). Anti-angiogenic effects of resveratrol mediated by decreased VEGF and increased TSP1 expression in melanoma-endothelial cell co-culture. *Angiogenesis, 13*(4), 305-315. doi:10.1007/s10456-010-9187-8

Tseng, S.-H., Lin, S.-M., Chen, J.-C., Su, Y.-H., Huang, H.-Y., Chen, C.-K., . . . Chen, Y. (2004). Resveratrol suppresses the angiogenesis and tumor growth of gliomas in rats. *Clinical Cancer Research, 10*(6), 2190-2202.

Vakkila, J., & Lotze, M. T. (2004). Inflammation and necrosis promote tumour growth. *Nature Reviews. Immunology, 4*(8), 641-648. doi:http://dx.doi.org/10.1038/nri.2016.107

van Zijl, F., Krupitza, G., & Mikulits, W. (2011). Initial steps of metastasis: cell invasion and endothelial transmigration. *Mutat Res, 728*(1-2), 23-34. doi:10.1016/j.mrrev.2011.05.002

Vande Walle, L., Lamkanfi, M., & Vandenabeele, P. (2008). The mitochondrial serine protease HtrA2/Omi: an overview. *Cell Death And Differentiation, 15*, 453. doi:10.1038/sj.cdd.4402291

Villa-Cuesta, E., Boylan, J. M., Tatar, M., & Gruppuso, P. A. (2011). Resveratrol inhibits protein translation in hepatic cells. *PLoS One, 6*(12), e29513.

Weidle, U. H., Birzele, F., Kollmorgen, G., & Rueger, R. (2016). Mechanisms and targets involved in dissemination of ovarian cancer. *Cancer Genomics and Proteomics, 13*(6), 407-423.

Wong, J. C., & Fiscus, R. R. (2015). Resveratrol at Anti-angiogenesis/Anticancer Concentrations Suppresses Protein Kinase G Signaling and Decreases IAPs Expression in HUVECs. *Anticancer Research, 35*(1), 273-281.

Wong, R. S. Y. (2011). Apoptosis in cancer: from pathogenesis to treatment. *Journal of experimental & clinical cancer research : CR, 30*(1), 87-87. doi:10.1186/1756-9966-30-87

Yang, J., & Weinberg, R. A. (2008). Epithelial-Mesenchymal Transition: At the Crossroads of Development and Tumor Metastasis. *Developmental Cell, 14*(6), 818-829. doi:https://doi.org/10.1016/j.devcel.2008.05.009

Yeung, T.-L., Leung, C. S., Yip, K.-P., Au Yeung, C. L., Wong, S. T. C., & Mok, S. C. (2015). Cellular and molecular processes in ovarian cancer metastasis. A Review in the Theme: Cell and Molecular Processes in Cancer Metastasis. *American journal of physiology. Cell physiology, 309*(7), C444-C456. doi:10.1152/ajpcell.00188.2015

Zhai, X.-X., Ding, J.-C., Tang, Z.-M., Li, J.-G., Li, Y.-C., Yan, Y.-H., . . . Zhang, C.-X. (2016). Effects of resveratrol on the proliferation, apoptosis and telomerase ability of human A431 epidermoid carcinoma cells. *Oncology letters, 11*(5), 3015-3018. doi:10.3892/ol.2016.4351

Zhao, Y., Tang, H., Zeng, X., Ye, D., & Liu, J. (2018). Resveratrol inhibits proliferation, migration and invasion via Akt and ERK1/2 signaling pathways in renal cell carcinoma cells. *Biomed Pharmacother, 98*, 36-44. doi:10.1016/j.biopha.2017.12.029

Ziyad, S., & Iruela-Arispe, M. L. (2011). Molecular mechanisms of tumor angiogenesis. *Genes & cancer, 2*(12), 1085-1096. doi:10.1177/1947601911432334

Appendix

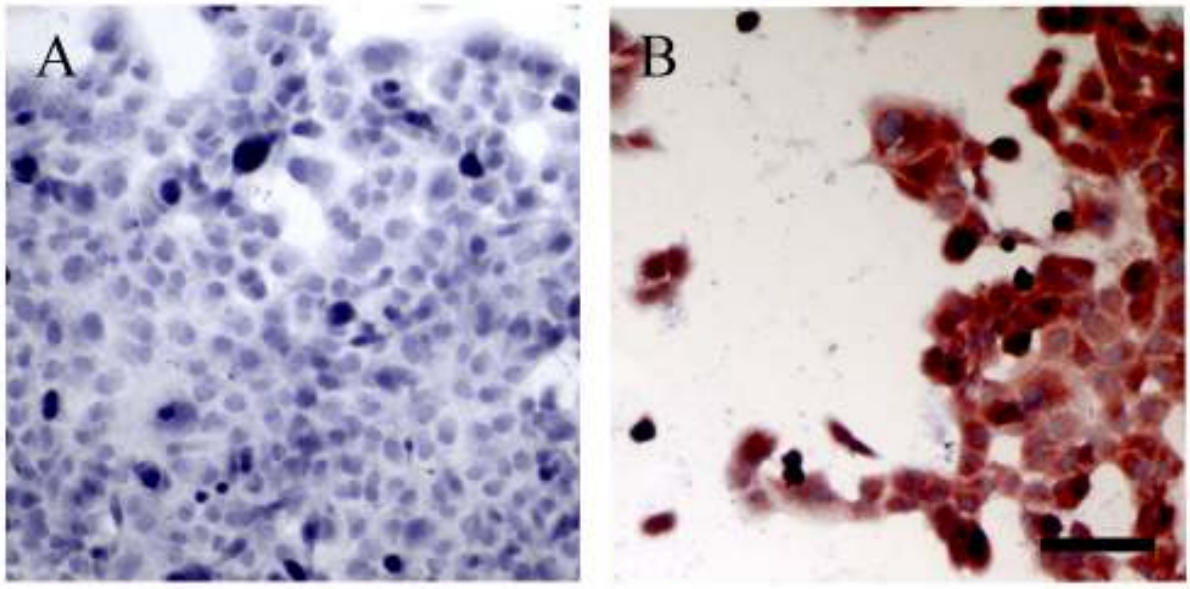

Figure A1. Optimisation of anti-VEGF staining on OVCAR-8 cell monolayers. *Negative control (A), positive control (B). Scale bar, 100 µm.*

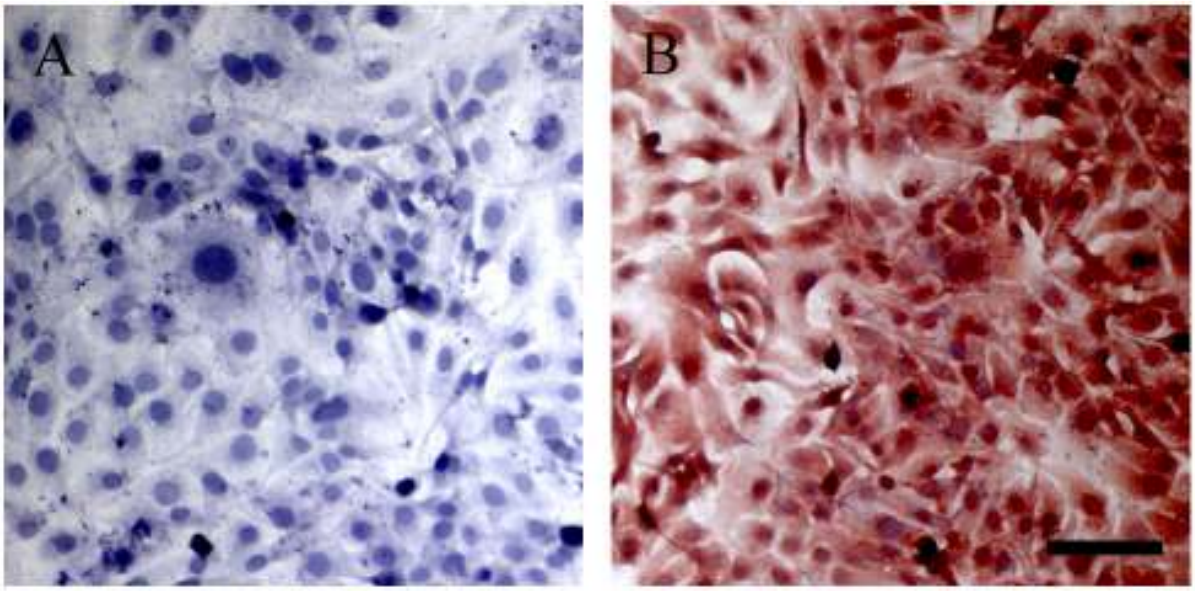

Figure A2. Optimisation of anti-VEGF staining on SKOV-3 cell monolayers. *Negative control (A), positive control (B). Scale bar, 100 µm.*

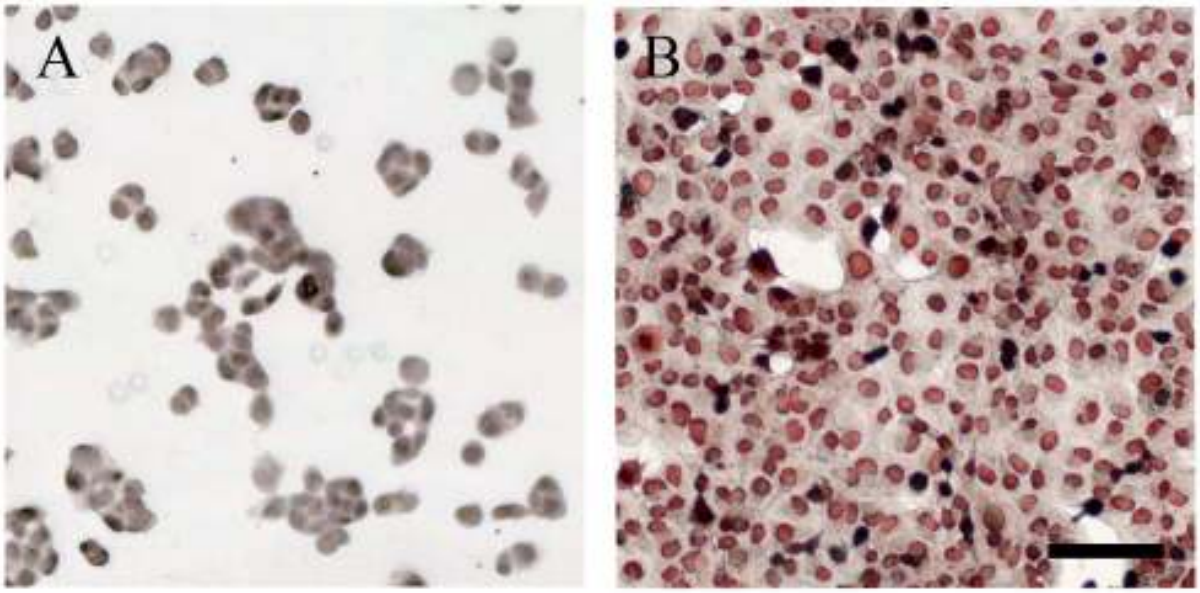

Figure A3. Optimisation of anti-Ki67 staining on OVCAR-8 cell monolayers. *Negative control (A), positive control (B). Scale bar, 100 µm.*

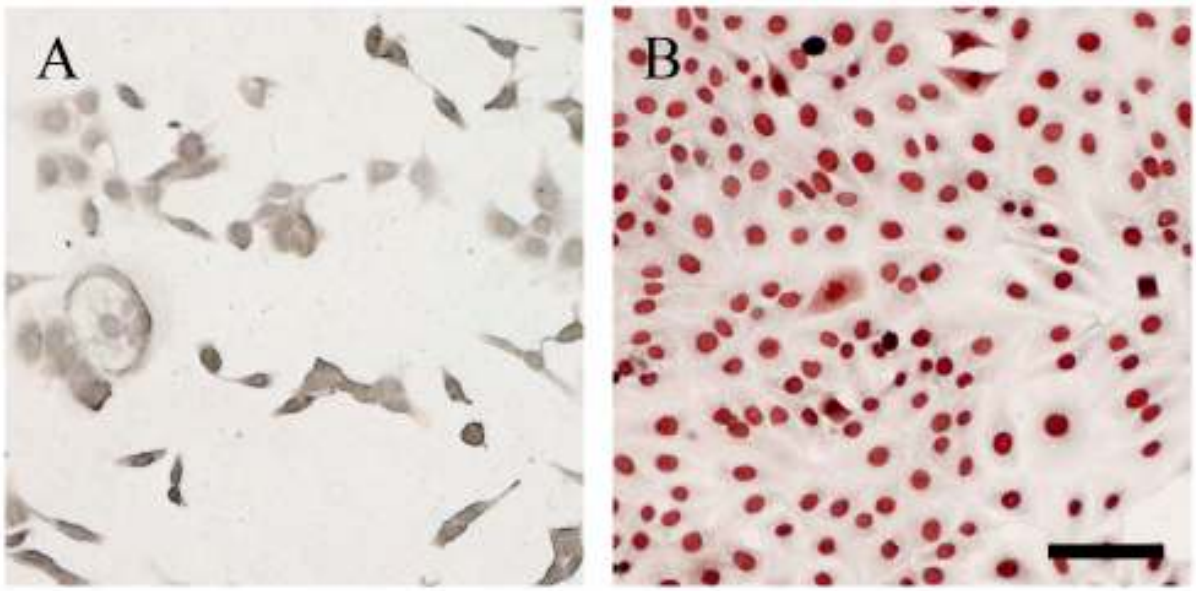

Figure A4. Optimisation of anti-Ki67 staining on SKOV-3 cell monolayers. *Negative control (A), positive control (B). Scale bar, 100 µm.*

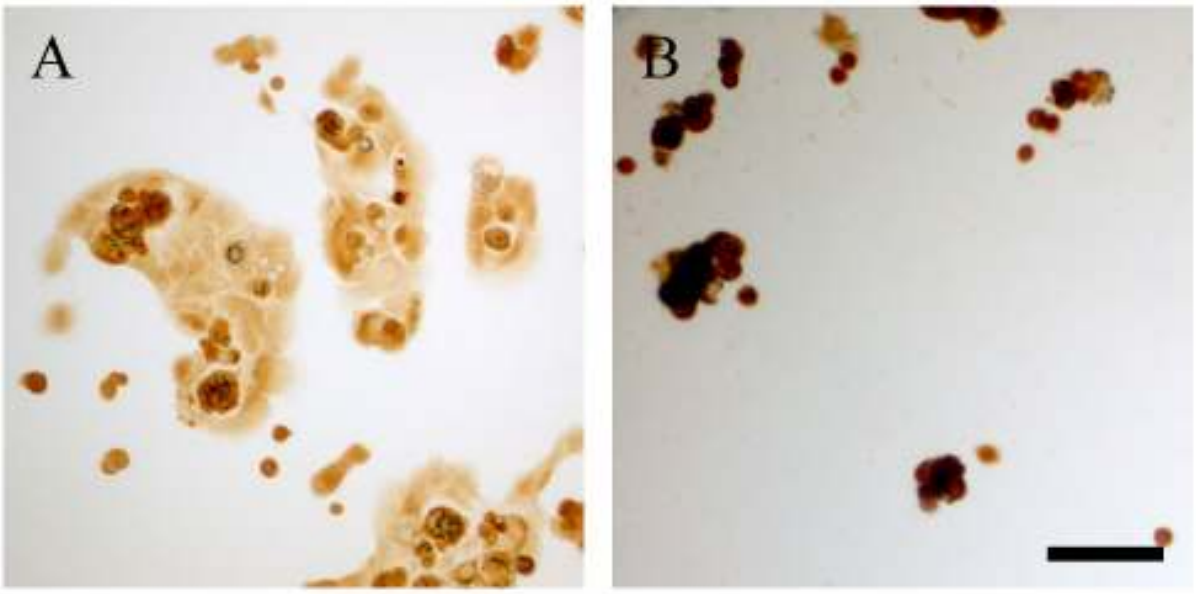

Figure A5. Optimisation of TUNEL assay on OVCAR-8 cell monolayers. *Negative control (A), positive control (B). Scale bar, 100 µm.*

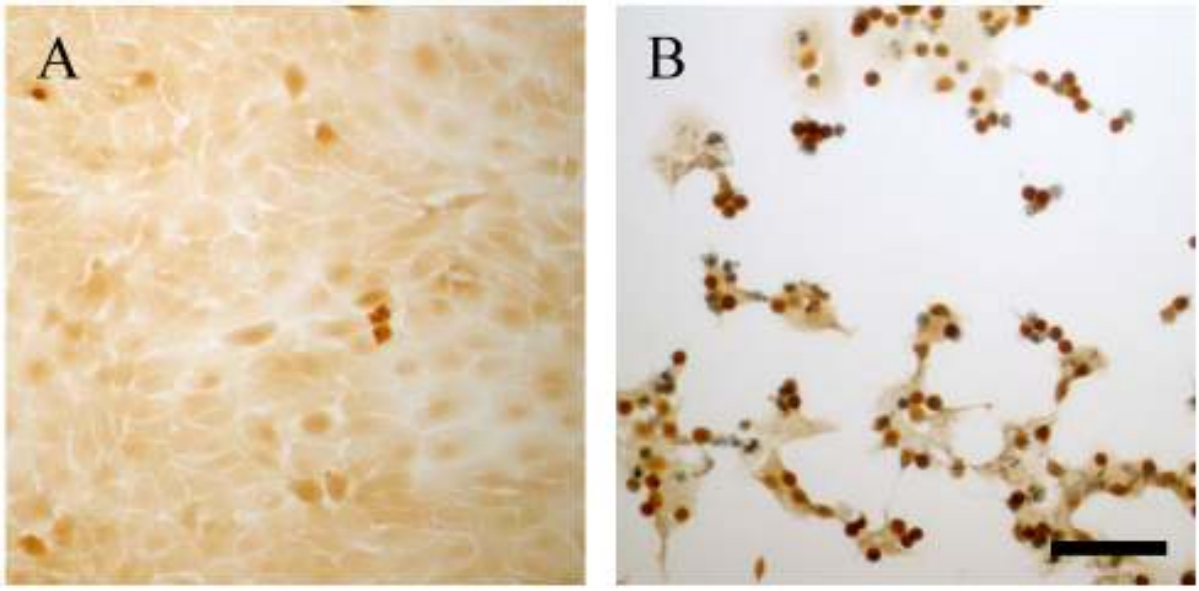

Figure A6. Optimisation of TUNEL assay on SKOV-3 cell monolayers. *Negative control (A), positive control (B). Scale bar, 100 µm.*

Table A1. Raw data for red blood cell counts and invasion of cancer cells into CAM area of OVCAR-8 tumour implants.

Experiment Date	Concentration of resveratrol	Size of implants (μm^2)	Size of implants (mm^2)	Number of blood cells	Number of blood cells per mm^2	Number of cells inside the CAM (whole implant)
04/01/2015	91 µg	649,620	0.6496	11	17	8
04/01/2015	91 µg	1,023,971	1.0240	13	13	5
04/01/2015	Control	813,004	0.8130	33	41	10
01/11/2015	46 µg	973,568	0.9736	23	24	15
01/11/2015	46 µg	950,620	0.9506	9	9	25
01/11/2015	91 µg	585,531	0.5855	22	38	6
01/11/2015	0.5 µg	638,438	0.6384	25	39	45
01/11/2015	0.5 µg	766,206	0.7662	21	27	35
01/11/2015	91 µg	621,291	0.6213	27	43	14
01/11/2015	91 µg	815,950	0.8160	37	45	16
01/11/2015	91 µg	805,003	0.8050	25	31	22
01/11/2015	0.5 µg	597,053	0.5971	97	162	
01/11/2015	0.5 µg	687,664	0.6877	15	22	12
18/01/2016	91 µg	487,423	0.4874	44	90	8
18/01/2016	91 µg	504,499	0.5045	27	54	3
18/01/2016	91 µg	876,856	0.8769	55	63	8
18/01/2016	0.3 µg	388,054	0.3881	33	85	8
18/01/2016	0.3 µg	578,994	0.5790	26	45	10
18/01/2016	Control	171,551	0.1716	12	70	10
18/01/2016	Control	455,706	0.4557	17	37	
18/01/2016	Control	769,307	0.7693	34	44	6
18/01/2016	91 µg	436,628	0.4366	18	41	4
18/01/2016	91 µg	423,878	0.4239	15	35	6
18/01/2016	91 µg	512,449	0.5124	13	25	10

18/01/2016	0.3 µg	236,601	0.2366	4	17	5
18/01/2016	0.3 µg	456,139	0.4561	24	53	10
18/01/2016	0.3 µg	500,237	0.5002	14	28	12
01/12/2017	0.5 µg	1,143,375	1.1434	19	17	14
01/12/2017	0.5 µg	1,069,327	1.0693	42	39	32
01/12/2017	Control	601,937	0.6019	29	48	8
01/12/2017	Control	649,666	0.6497	60	92	10
01/12/2017	Control	849,434	0.8494	35	41	25
01/12/2017	0.5 µg	1,145,960	1.1460	56	49	12
01/12/2017	0.5 µg	1,112,380	1.1124	12	11	10
01/12/2017	0.5 µg	1,152,008	1.1520	34	30	16
01/12/2017	Control	596,714	0.5967	33	55	15
01/12/2017	Control	736,734	0.7367	61	83	25
10/10/2018	183 µg	624,018	0.6240	10	16	20
10/10/2018	183 µg	848,221	0.8482	12	14	25
10/10/2018	Control	347,804	0.3478	50	144	6
10/10/2018	Control	592,402	0.5924	8	14	12
10/10/2018	Control	852,250	0.8523	20	23	15
10/10/2018	183 µg	703,972	0.7040	28	40	10
10/10/2018	183 µg	1,210,532	1.2105	70	58	12
10/10/2018	183 µg	859,006	0.8590	55	64	20
10/10/2018	183 µg	930,978	0.9310	24	26	20
10/10/2018	183 µg	970,759	0.9708	12	12	25
19/10/2018	183 µg	757,241	0.7572	55	73	12
19/10/2018	183 µg	642,405	0.6424	50	78	15
19/10/2018	183 µg	697,070	0.6971	75	108	12
19/10/2018	Control	186,416	0.1864	5	27	26
19/10/2018	Control	578,772	0.5788	24	41	18
19/10/2018	Control	461,602	0.4616	22	48	35
19/10/2018	46 µg	726,779	0.7268	21	29	10
19/10/2018	46 µg	855,489	0.8555	15	18	10
19/10/2018	46 µg	700,268	0.7003	15	21	15

19/10/2018	91 µg	511,046	0.5110	7	14	10
19/10/2018	91 µg	903,341	0.9033	10	11	10
19/10/2018	91 µg	596,707	0.5967	15	25	12
19/10/2018	183 µg	605,695	0.6057	10	17	15
19/10/2018	183 µg	758,666	0.7587	30	40	20
19/10/2018	183 µg	932,667	0.9327	18	19	12
19/10/2018	Control	840,742	0.8407	36	43	5
19/10/2018	Control	748,381	0.7484	45	60	15
19/10/2018	Control	851,143	0.8511	45	53	15
19/10/2018	46 µg	864,338	0.8643	18	21	8
19/10/2018	46 µg	1,102,911	1.1029	12	11	32
19/10/2018	46 µg	1,055,368	1.0554	25	24	35
19/10/2018	91 µg	388,419	0.3884	10	26	12
19/10/2018	91 µg	530,305	0.5303	6	11	10
19/10/2018	91 µg	493,027	0.4930	8	16	16
19/10/2018	183 µg	627,623	0.6276	20	32	15
19/10/2018	183 µg	590,501	0.5905	18	30	25
19/10/2018	183 µg	639,448	0.6394	10	16	10
19/10/2018	Control	719,096	0.7191	42	58	12
19/10/2018	Control	627,131	0.6271	42	67	15
19/10/2018	Control	866,711	0.8667	35	40	20
19/10/2018	Control	645,566	0.6456	8	12	15
19/10/2018	Control	667,319	0.6673	22	33	15
19/10/2018	Control	794,727	0.7947	15	19	25
11/11/2018	46 µg	514,645	0.5146	28	54	8
11/11/2018	46 µg	592,573	0.5926	19	32	11
11/11/2018	46 µg	653,024	0.6530	10	15	7
11/11/2018	46 µg	644,496	0.6445	10	16	9
11/11/2018	46 µg	636,550	0.6365	8	13	6

Table A2. Raw data for red blood cell counts and invasion of cancer cells into CAM area of SKOV-3 tumour implants.

Experiment date	Concentration of resveratrol	Size of implant (μm^2)	Size of implant (mm^2)	Number of blood cells	Number of blood cells per mm^2	Number of cells inside the CAM (whole implant)
30/03/2015	0.3 µg	1,027,044	1.0270	370	360	
30/03/2015	0.3 µg	1,204,253	1.2043	270	224	25
20/04/2015	Control	1,160,161	1.1602	52	45	
20/04/2015	0.5 µg	279,502	0.2795	11	39	
20/04/2015	0.5 µg	773,384	0.7734	175	226	
20/04/2015	0.5 µg	951,407	0.9514	89	94	
10/10/2015	46 µg	757,849	0.7578	56	74	
10/10/2015	46 µg	1,117,754	1.1178	74	66	
10/10/2015	46 µg	1,145,938	1.1459	68	59	
10/10/2015	91 µg	765,109	0.7651	26	34	7
10/10/2015	91 µg	1,046,802	1.0468	38	36	15
10/10/2015	91 µg	1,059,625	1.0596	42	40	15
28/11/2015	46 µg	855,428	0.8554	28	33	15
28/11/2015	46 µg	1,137,474	1.1375	37	33	8
28/11/2015	46 µg	1,207,701	1.2077	97	80	5
28/11/2015	91 µg	653,732	0.6537	29	44	6
28/11/2015	91 µg	1,172,451	1.1725	26	22	12
28/11/2015	0.3 µg	257,659	0.2577	18	70	8
28/11/2015	0.3 µg	535,618	0.5356	14	26	10
28/11/2015	0.3 µg	594,446	0.5944	84	141	9
28/11/2015	Control	768,887	0.7689	28	36	8
28/11/2015	Control	1,224,578	1.2246	73	60	8
28/11/2015	Control	1,242,308	1.2423	51	41	30

19/03/2016	183 µg	823,091	0.8231	38	46	20
19/03/2016	183 µg	1,010,131	1.0101	73	72	30
19/03/2016	183 µg	661,493	0.6615	34	51	15
19/03/2016	Control	419,083	0.4191	14	33	8
19/03/2016	Control	445,002	0.4450	12	27	5
19/03/2016	Control	471,148	0.4711	25	53	10
19/03/2016	183 µg	859,464	0.8595	138	161	15
19/03/2016	183 µg	728,773	0.7288	105	144	20
19/03/2016	183 µg	1,029,516	1.0295	95	92	15
19/03/2016	Control	176,811	0.1768	32	181	
19/03/2016	Control	238,385	0.2384	24	101	
19/03/2016	Control	290,836	0.2908	61	210	
19/03/2016	183 µg	558,163	0.5582	24	43	5
19/03/2016	183 µg	624,782	0.6248	35	56	15
19/03/2016	183 µg	531,482	0.5315	10	19	15
19/03/2016	183 µg	815,179	0.8152	38	47	10
19/03/2016	183 µg	746,354	0.7464	67	90	10
19/03/2016	183 µg	830,501	0.8305	47	57	15
21/08/2017	183 µg	555,740	0.5557	11	20	8
21/08/2017	183 µg	760,877	0.7609	19	25	18
21/08/2017	Control	646,173	0.6462	44	68	6
21/08/2017	Control	741,983	0.7420	34	46	12
21/08/2017	Control	570,121	0.5701	60	105	16
21/08/2017	Control	1,002,637	1.0026	94	94	10
21/08/2017	Control	1,029,171	1.0292	98	95	5
21/08/2017	Control	994,452	0.9945	73	73	12
21/08/2017	183 µg	745,715	0.7457	39	52	25
21/08/2017	183 µg	726,392	0.7264	70	96	25
21/08/2017	183 µg	841,947	0.8419	47	56	30
21/08/2017	183 µg	565,351	0.5654	37	65	12
21/08/2017	183 µg	873,421	0.8734	41	47	15
21/08/2017	183 µg	817,204	0.8172	71	87	25

21/08/2017	183 µg	928,560	0.9286	54	58	24
21/08/2017	183 µg	761,455	0.7615	31	41	20
14/09/2017	0.3 µg	363,146	0.3631	62	171	15
14/09/2017	0.3 µg	625,829	0.6258	47	75	20
14/09/2017	0.3 µg	479,477	0.4795	50	104	30
14/09/2017	0.5 µg	788,884	0.7889	48	61	15
14/09/2017	0.5 µg	1,113,168	1.1132	55	49	20
14/09/2017	0.5 µg	1,210,398	1.2104	49	40	10
14/09/2017	Control	1,148,907	1.1489	58	50	
14/09/2017	Control	1,139,731	1.1397	68	60	15
14/09/2017	Control	891,057	0.8911	64	72	20
14/09/2017	0.5 µg	920,000	0.9200	82	89	8
14/09/2017	0.5 µg	967,346	0.9673	41	42	10
14/09/2017	0.5 µg	1,148,778	1.1488	37	32	15
14/09/2017	0.5 µg	1,203,314	1.2033	85	71	
14/09/2017	0.5 µg	648,899	0.6489	84	129	15
14/09/2017	0.5 µg	1,159,255	1.1593	88	76	10
07/02/2018	183 µg	619,766	0.6198	42	68	7
07/02/2018	183 µg	1,034,832	1.0348	45	43	20
07/02/2018	183 µg	1,053,451	1.0535	41	39	15
07/02/2018	Control	1,213,937	1.2139	8	7	30
07/02/2018	Control	1,057,518	1.0575	98	93	30
07/02/2018	183 µg	271,020	0.2710	28	103	10
07/02/2018	183 µg	401,268	0.4013	37	92	
07/02/2018	183 µg	582,098	0.5821	16	27	
01/09/2018	91 µg	822,599	0.8226	68	83	5
01/09/2018	91 µg	1,115,168	1.1152	50	45	12
01/09/2018	Control	447,431	0.447	125	279	14
01/09/2018	Control	597,131	0.5971	65	109	20
01/09/2018	Control	722,937	0.723	28	39	30
01/09/2018	91 µg	275,747	0.2757	14	51	6
01/09/2018	91 µg	766,644	0.7666	20	26	8

01/09/2018	91 µg	952,232	0.9522	25	26	10
09/09/2018	46 µg	494,013	0.4940	35	71	25
09/09/2018	46 µg	544,979	0.5450	14	26	30
09/09/2018	46 µg	583,271	0.5833	34	58	24
09/09/2018	91 µg	451,731	0.4517	18	40	5
09/09/2018	91 µg	560,127	0.5601	15	27	6
09/09/2018	91 µg	523,491	0.5235	20	38	8
09/09/2018	Control	531,139	0.5311	12	23	10
09/09/2018	Control	794,989	0.7950	10	13	12
09/09/2018	Control	979,203	0.9792	20	20	28
09/09/2018	91 µg	277,799	0.2778	2	7	
09/09/2018	91 µg	477,624	0.4776	5	10	
09/09/2018	91 µg	520,311	0.5203	10	19	2
09/09/2018	Control	477,082	0.4771	35	73	5
09/09/2018	Control	651,562	0.6516	65	100	15
09/09/2018	Control	548,071	0.5481	80	146	30
09/09/2018	91 µg	179,589	0.1796	48	267	2
09/09/2018	91 µg	416,622	0.4166	32	77	8
09/09/2018	91 µg	527,592	0.5276	20	38	6
09/09/2018	Control	547,211	0.5472	44	80	12
09/09/2018	Control	655,292	0.6553	28	43	22
09/09/2018	Control	877,191	0.8772	19	22	25

Table A3. Raw data for mean grey values of OVCAR-8 implants stained for VEGF.

Experiment Date	Treatment	Area (pixel^2)	Integrated density	Mean grey value
01/11/2015	46 µg	5,183,048	211,295,040	40.8
01/11/2015	46 µg	4,308,794	324,826,650	75.4
01/11/2015	46 µg	4,550,611	308,999,565	67.9
01/11/2015	Control	4,614,272	288,981,300	62.6
01/11/2015	Control	4,355,156	340,659,855	78.2
01/11/2015	Control	5,297,577	375,743,010	70.9
18/01/2016	0.3 µg	2,876,410	128,617,665	44.7
18/01/2016	0.3 µg	883,073	145,987,245	165.3
18/01/2016	0.3 µg	3,219,284	391,270,725	121.5
18/01/2016	0.3 µg	2,812,385	88,626,780	31.5
18/01/2016	0.3 µg	4,729,369	360,493,500	76.2
18/01/2016	0.3 µg	2,319,653	172,161,720	74.2
18/01/2016	0.3 µg	3,160,317	121,886,430	38.6
01/12/2017	Control	3,723,786	332,133,930	89.2
01/12/2017	Control	5,215,618	452,358,780	86.7
01/12/2017	Control	5,308,321	425,081,685	80.1
10/10/2018	183 µg	2,196,835	79,609,470	36.2
10/10/2018	183 µg	4,058,568	47,285,415	11.7
10/10/2018	183 µg	4,020,099	228,209,445	56.8
10/10/2018	Control	4,397,809	135,648,525	30.8
10/10/2018	Control	1,619,365	51,770,865	32.0
10/10/2018	183 µg	4,122,368	262,234,095	63.6
10/10/2018	183 µg	4,332,204	229,458,435	53.0
10/10/2018	183 µg	4,465,682	256,434,885	57.4
10/10/2018	183 µg	962,550	41,146,290	42.7
10/10/2018	183 µg	4,276,994	184,493,265	43.1
19/10/2018	183 µg	3,657,160	221,844,900	60.7
19/10/2018	183 µg	3,897,451	304,626,825	78.2
19/10/2018	183 µg	4,383,068	257,296,275	58.7

19/10/2018	Control	3,782,464	139,417,935	36.9
19/10/2018	Control	4,105,156	202,080,360	49.2
19/10/2018	Control	3,728,896	206,961,570	55.5
19/10/2018	46 µg	4,137,498	233,067,960	56.3
19/10/2018	46 µg	3,354,048	134,558,400	40.1
19/10/2018	46 µg	3,051,308	202,563,840	66.4
19/10/2018	183 µg	806,090	142,290,765	176.5
19/10/2018	183 µg	3,612,450	425,048,535	117.7
19/10/2018	183 µg	4,614,080	399,778,035	86.6
19/10/2018	Control	4,107,235	154,017,195	37.5
19/10/2018	Control	4,916,484	258,530,220	52.6
19/10/2018	Control	4,826,125	216,654,885	44.9
19/10/2018	46 µg	3,741,999	174,420,765	46.6
19/10/2018	46 µg	4,000,874	334,227,735	83.5
19/10/2018	46 µg	3,041,482	240,384,165	79.0
19/10/2018	183 µg	2,774,652	289,204,935	104.2
19/10/2018	183 µg	3,291,244	343,559,970	104.4
19/10/2018	183 µg	3,228,384	389,319,210	120.6
19/10/2018	Control	4,509,760	226,599,885	50.2
19/10/2018	Control	3,911,691	214,071,480	54.7
19/10/2018	Control	3,489,908	139,507,695	40.0
19/10/2018	Control	3,385,591	156,437,400	46.2
19/10/2018	Control	4,021,137	236,385,510	58.8
19/10/2018	Control	4,692,477	222,925,080	47.5
11/11/2018	46 µg	3,410,732	133,095,465	39.0
11/11/2018	46 µg	2,218,341	186,084,720	83.9
11/11/2018	46 µg	2,219,961	260,016,105	117.1
11/11/2018	46 µg	2,639,329	74,746,620	28.3
11/11/2018	46 µg	2,156,309	161,229,615	74.8

Table A4. Raw data for mean grey values of SKOV-3 implants stained for VEGF.

Experiment Date	Treatment	Area (pixel^2)	Integrated density	Mean grey value
30/03/2015	0.3 µg	4,177,058	182,394,615	43.7
30/03/2015	0.3 µg	5,507,884	404,078,100	73.4
30/03/2015	0.3 µg	5,033,534	236,318,700	46.9
10/10/2015	91 µg	4,244,898	262,618,890	61.9
10/10/2015	91 µg	3,077,264	148,756,290	48.3
10/10/2015	91 µg	2,114,245	100,818,585	47.7
28/11/2015	91 µg	5,061,978	319,151,625	63.0
28/11/2015	91 µg	6,031,788	304,257,840	50.4
28/11/2015	0.3 µg	1,696,055	88,559,970	52.2
28/11/2015	0.3 µg	3,367,713	255,945,795	76.0
28/11/2015	0.3 µg	3,583,658	220,025,220	61.4
28/11/2015	Control	5,185,974	669,061,860	129.0
28/11/2015	Control	5,834,784	667,243,200	114.4
28/11/2015	Control	5,708,428	632,859,255	110.9
21/08/2017	183 µg	1,988,652	122,454,825	61.6
21/08/2017	183 µg	3,772,664	244,964,985	64.9
21/08/2017	183 µg	4,104,482	235,902,285	57.5
21/08/2017	Control	2,838,632	111,020,880	39.1
21/08/2017	Control	2,646,956	143,558,625	54.2
21/08/2017	Control	4,010,331	172,798,455	43.1
21/08/2017	183 µg	4,071,246	410,351,865	100.8
21/08/2017	183 µg	3,484,444	366,846,570	105.3
21/08/2017	183 µg	4,446,311	385,178,520	86.6
21/08/2017	Control	5,933,854	352,193,505	59.4
21/08/2017	Control	3,871,513	266,402,325	68.8
21/08/2017	Control	5,859,881	385,318,770	65.8
14/09/2017	0.3 µg	2,948,834	151,423,335	51.4
14/09/2017	0.3 µg	2,087,200	165,978,225	79.5
14/09/2017	0.3 µg	3,673,947	134,116,230	36.5

14/09/2017	Control	5,960,007	174,477,120	29.3
14/09/2017	Control	3,306,601	135,795,150	41.1
14/09/2017	Control	4,844,427	176,911,095	36.5
07/02/2018	183 µg	4,453,929	168,146,745	37.8
07/02/2018	183 µg	4,244,919	222,271,515	52.4
07/02/2018	183 µg	4,555,311	162,143,535	35.6
07/02/2018	Control	5,682,300	117,996,405	20.8
07/02/2018	Control	5,128,871	242,277,030	47.2
07/02/2018	Control	5,966,942	145,359,435	24.4
01/09/2018	91 µg	3,196,808	247,994,385	77.6
01/09/2018	91 µg	5,295,070	464,446,545	87.7
01/09/2018	91 µg	5,371,628	411,864,525	76.7
09/09/2018	91 µg	2,660,184	202,636,515	76.2
09/09/2018	91 µg	2,786,221	217,353,075	78.0
09/09/2018	91 µg	2,641,414	191,889,615	72.6
09/09/2018	Control	4,162,536	323,192,100	77.6
09/09/2018	Control	4,244,012	327,341,715	77.1
09/09/2018	Control	4,645,258	366,221,310	78.8
09/09/2018	91 µg	2,467,177	187,811,580	76.1
09/09/2018	91 µg	2,766,797	372,889,050	134.8
09/09/2018	91 µg	3,382,822	326,275,560	96.5
09/09/2018	Control	4,654,492	343,789,215	73.9
09/09/2018	Control	804,425	64,472,925	80.1
09/09/2018	Control	3,374,568	240,793,440	71.4
09/09/2018	91 µg	1,612,691	107,726,025	66.8
09/09/2018	91 µg	1,898,188	144,812,460	76.3
09/09/2018	91 µg	3,067,249	130,843,560	42.7

Table A5. Raw data for mean grey values of OVCAR-8 implants stained for Ki67.

Experiment Date	Treatment	Area (pixel^2)	Integrated density	Mean grey value
01/11/2015	46 µg	433.1	687.0	1.6
01/11/2015	46 µg	320.3	4,909.9	15.3
01/11/2015	46 µg	442.0	332.7	0.8
01/11/2015	Control	299.7	81.5	0.3
01/11/2015	Control	587.7	151.8	0.3
01/11/2015	Control	446.4	8,328.5	18.7
11/11/2015	46 µg	308.5	50.2	0.2
11/11/2015	46 µg	277.1	3,664.9	13.2
11/11/2015	46 µg	285.0	7,912.2	27.8
11/11/2015	46 µg	308.0	18,846.8	61.2
11/11/2015	46 µg	384.4	9,045.4	23.5
18/01/2016	0.3 µg	155.3	7,646.7	49.2
18/01/2016	0.3 µg	159.6	6,851.7	42.9
18/01/2016	0.3 µg	349.2	115.9	0.3
18/01/2016	0.3 µg	293.5	3,183.6	10.8
18/01/2016	0.3 µg	307.9	632.3	2.1
18/01/2016	0.3 µg	284.2	30.6	0.1
18/01/2016	0.3 µg	354.7	181.0	0.5
18/01/2016	0.3 µg	273.4	6,005.3	22.0
01/12/2017	Control	373.3	779.5	2.1
01/12/2017	Control	448.4	210.0	0.5
01/12/2017	Control	425.3	26,035.4	61.2
10/10/2018	183 µg	260.3	313.3	1.2
10/10/2018	183 µg	389.0	518.0	1.3
10/10/2018	183 µg	459.6	159.1	0.3
10/10/2018	Control	304.4	1,216.8	4.0
10/10/2018	Control	381.0	25,757.3	67.6
10/10/2018	Control	218.8	10,904.5	49.8
10/10/2018	183 µg	227.5	1,041.7	4.6

10/10/2018	183 µg	427.2	11,219.5	26.3
10/10/2018	183 µg	231.8	1,087.1	4.7
10/10/2018	183 µg	457.4	18,904.2	41.3
10/10/2018	183 µg	339.9	1,626.2	4.8
19/10/2018	183 µg	152.0	3,523.2	23.2
19/10/2018	183 µg	421.3	91.9	0.2
19/10/2018	183 µg	385.8	16,357.4	42.4
19/10/2018	Control	363.9	5,807.3	16.0
19/10/2018	Control	351.1	15,945.1	45.4
19/10/2018	Control	392.6	251.5	0.6
19/10/2018	46 µg	316.6	20,987.8	66.3
19/10/2018	46 µg	340.9	20,160.8	59.1
19/10/2018	46 µg	401.1	8,654.4	21.6
19/10/2018	183 µg	376.2	145.4	0.4
19/10/2018	183 µg	269.6	13,052.6	48.4
19/10/2018	183 µg	433.8	283.5	0.7
19/10/2018	Control	288.4	4,681.9	16.2
19/10/2018	Control	429.5	20,834.8	48.5
19/10/2018	Control	391.6	1,416.5	3.6
19/10/2018	46 µg	344.7	55.7	0.2
19/10/2018	46 µg	432.4	15,360.3	35.5
19/10/2018	46 µg	323.5	70.3	0.2
19/10/2018	183 µg	225.3	21,487.0	95.4
19/10/2018	183 µg	296.7	17,922.9	60.4
19/10/2018	183 µg	336.6	164.9	0.5
19/10/2018	Control	224.7	5,365.2	23.9
19/10/2018	Control	384.8	25,135.2	65.3
19/10/2018	Control	379.4	301.2	0.8
19/10/2018	Control	326.2	12,192.7	37.4
19/10/2018	Control	226.2	17,886.8	79.1
19/10/2018	Control	484.9	161.8	0.3

Table A6. Raw data for mean grey values of SKOV-3 implants stained for Ki67.

Experiment Date	Treatment	Area (pixel^2)	Integrated density	Mean grey value
30/03/2015	0.3 µg	234.7	154.2	0.7
30/03/2015	0.3 µg	431.8	13,652.8	31.6
30/03/2015	0.3 µg	610.3	16,300.3	26.7
30/03/2015	0.3 µg	481.8	19,479.9	40.4
30/03/2015	0.3 µg	599.9	57.6	0.1
20/04/2015	Control	459.6	7,245.8	15.8
20/04/2015	Control	566.9	8,851.2	15.6
20/04/2015	Control	572.5	14,331.7	25.0
10/10/2015	91 µg	353.8	6,080.3	17.2
10/10/2015	91 µg	361.1	15.5	0.0
28/11/2015	91 µg	112.1	7,278.8	64.9
28/11/2015	91 µg	476.1	18,704.0	39.3
28/11/2015	0.3 µg	153.4	0.9	0.0
28/11/2015	0.3 µg	361.4	27,868.1	77.1
28/11/2015	0.3 µg	328.9	3.8	0.0
28/11/2015	Control	570.4	22,016.3	38.6
28/11/2015	Control	629.9	45,514.5	72.3
28/11/2015	Control	592.5	32,470.0	54.8
21/08/2017	183 µg	458.7	13,279.8	28.9
21/08/2017	183 µg	443.2	4,944.3	11.2
21/08/2017	Control	506.1	26,532.4	52.4
21/08/2017	Control	569.7	23,147.2	40.6
21/08/2017	Control	353.3	85.6	0.2
21/08/2017	183 µg	480.2	511.7	1.1
21/08/2017	183 µg	269.5	2,889.6	10.7
21/08/2017	183 µg	385.3	6,483.2	16.8
14/09/2017	0.3 µg	182.3	15,717.9	86.2
14/09/2017	0.3 µg	412.5	29,386.5	71.2
14/09/2017	0.3 µg	422.1	1,298.5	3.1

14/09/2017	Control	265.6	17.4	0.1
14/09/2017	Control	205.7	8,361.6	40.6
14/09/2017	Control	595.0	14,480.0	24.3
07/02/2018	183 µg	376.8	6,944.9	18.4
07/02/2018	183 µg	567.5	31,972.6	56.3
07/02/2018	Control	383.5	1,315.4	3.4
07/02/2018	Control	546.9	12,535.4	22.9
07/02/2018	Control	568.8	22,558.8	39.7
01/09/2018	91 µg	332.6	6.4	0.0
01/09/2018	91 µg	504.1	20,846.1	41.4
01/09/2018	91 µg	455.8	14,760.5	32.4
09/09/2018	91 µg	260.7	8,872.4	34.0
09/09/2018	91 µg	292.0	9,432.7	32.3
09/09/2018	91 µg	158.1	3,964.6	25.1
09/09/2018	91 µg	152.5	5,429.7	35.6
09/09/2018	91 µg	137.4	5,389.6	39.2
09/09/2018	91 µg	537.0	555.5	1.0
09/09/2018	Control	145.6	3,739.3	25.7
09/09/2018	Control	334.8	822.2	2.5
09/09/2018	Control	399.0	798.1	2.0
09/09/2018	91 µg	159.5	4,029.6	25.3
09/09/2018	91 µg	282.4	3,279.0	11.6
09/09/2018	91 µg	267.2	1,717.4	6.4
09/09/2018	Control	476.2	12,421.0	26.1
09/09/2018	Control	426.6	17,122.9	40.1
09/09/2018	Control	376.2	11,752.3	31.2

Table A7. Raw data for mean grey values of OVCAR-8 implants stained using a TUNEL assay.

Experiment Date	Treatment	Area (pixel^2)	Integrated density	Mean grey value
01/11/2015	46 µg	4,973,759	62,629,020	12.6
01/11/2015	46 µg	4,890,090	54,168,120	11.1
01/12/2017	Control	2,502,931	42,191,025	16.9
01/12/2017	Control	3,617,262	78,283,725	21.6
01/12/2017	Control	3,617,154	35,548,785	9.8
10/10/2018	Control	2,719,681	39,433,965	14.5
10/10/2018	Control	2,905,619	21,645,675	7.4
10/10/2018	Control	4,739,455	54,894,105	11.6
18/01/2016	Control	1,824,068	27,208,500	14.9
18/01/2016	Control	2,072,849	26,654,895	12.9
19/10/2018	46 µg	2,710,430	17,521,815	6.5
19/10/2018	46 µg	3,932,814	92,677,965	23.6
19/10/2018	46 µg	4,134,591	115,344,150	27.9
19/10/2018	46 µg	3,278,443	15,331,875	4.7
19/10/2018	46 µg	4,716,035	50,129,940	10.6
19/10/2018	46 µg	5,443,955	49,076,535	9.0
19/10/2018	Control	3,152,760	22,940,055	7.3
19/10/2018	Control	3,813,793	5,473,620	1.4
19/10/2018	Control	3,937,129	32,128,910	8.2
19/10/2018	Control	3,778,880	38,816,610	10.3
19/10/2018	Control	2,819,814	32,712,930	11.6
19/10/2018	Control	4,330,253	28,485,540	6.6
19/10/2018	Control	2,587,889	23,386,305	9.0
19/10/2018	Control	3,040,025	26,629,905	8.8
19/10/2018	Control	4,581,971	28,944,030	6.3
19/10/2018	Control	2,572,926	39,773,115	15.5
19/10/2018	Control	3,253,738	52,673,055	16.2
19/10/2018	Control	4,028,640	47,093,655	11.7

10/10/2018	183 µg	2,080,719	17,213,520	8.3
10/10/2018	183 µg	3,386,860	30,359,280	9.0
10/10/2018	183 µg	4,354,451	25,156,515	5.8
10/10/2018	183 µg	1,225,342	13,134,540	10.7
10/10/2018	183 µg	1,490,458	1,514,445	1.0
10/10/2018	183 µg	2,887,418	6,421,155	2.2
10/10/2018	183 µg	3,393,232	18,908,760	5.6
10/10/2018	183 µg	3,522,119	32,645,100	9.3
11/11/2018	46 µg	2,616,659	5,636,265	2.2
11/11/2018	46 µg	3,538,631	58,129,290	16.4
11/11/2018	46 µg	3,819,174	40,047,240	10.5
11/11/2018	46 µg	3,361,691	42,955,770	12.8
11/11/2018	46 µg	3,589,154	49,047,720	13.7
19/10/2018	183 µg	2,143,295	3,102,840	1.4
19/10/2018	183 µg	2,261,112	13,294,935	5.9
19/10/2018	183 µg	3,964,831	40,260,930	10.2
19/10/2018	183 µg	2,268,440	7,372,815	3.3
19/10/2018	183 µg	3,372,332	4,670,580	1.4
19/10/2018	183 µg	2,043,140	16,661,190	8.2

Table A8. Raw data for mean grey values of SKOV-3 implants stained using a TUNEL assay.

Experiment Date	Treatment	Area (pixel^2)	Integrated density	Mean grey value
10/10/2015	91 µg	4,452,434	37,260,345	8.4
10/10/2015	91 µg	4,243,635	36,389,265	8.6
28/11/2015	91 µg	5,452,711	109,505,415	20.1
28/11/2015	91 µg	4,776,545	111,192,495	23.3
28/11/2015	Control	2,766,174	61,931,595	22.4
28/11/2015	Control	5,720,609	115,400,250	20.2
28/11/2015	Control	5,491,457	113,631,825	20.7
21/08/2017	Control	3,295,259	54,266,040	16.5
21/08/2017	Control	3,190,435	20,667,750	6.5
21/08/2017	Control	3,393,352	12,840,780	3.8
21/08/2017	Control	5,620,718	59,736,045	10.6
21/08/2017	Control	5,842,160	53,051,985	9.1
21/08/2017	Control	5,382,241	11,022,885	2.0
21/08/2017	183 µg	2,903,278	21,026,025	7.2
21/08/2017	183 µg	3,519,325	13,022,340	3.7
21/08/2017	183 µg	3,021,493	43,953,585	14.5
21/08/2017	183 µg	3,625,888	13,653,210	3.8
21/08/2017	183 µg	3,625,204	7,066,305	1.9
21/08/2017	183 µg	4,131,436	23,760,900	5.8
14/09/2017	Control	5,161,024	41,847,795	8.1
14/09/2017	Control	4,017,193	41,613,450	10.4
07/02/2018	183 µg	4,846,075	21,153,270	4.4
07/02/2018	183 µg	4,681,315	28,728,045	6.1
07/02/2018	183 µg	4,330,002	7,631,130	1.8
07/02/2018	183 µg	2,644,180	35,137,725	13.3
07/02/2018	183 µg	3,033,986	34,030,260	11.2
07/02/2018	183 µg	3,344,333	30,453,885	9.1
01/09/2018	91 µg	1,991,817	19,973,640	10.0

01/09/2018	91 µg	3,265,892	41,037,150	12.6
01/09/2018	91 µg	4,984,383	65,767,305	13.2
01/09/2018	Control	1,903,797	24,200,010	12.7
01/09/2018	Control	1,848,003	3,231,360	1.7
01/09/2018	Control	3,153,880	11,402,070	3.6
01/09/2018	91 µg	3,581,692	39,219,765	11.0
01/09/2018	91 µg	5,161,610	46,217,435	9.0
09/09/2018	91 µg	2,255,002	51,257,040	22.7
09/09/2018	91 µg	2,679,088	44,333,790	16.5